MSC INTERNAL NOTE NO. 68-FM-70

MANNED EXPLORATION OF MARS: A MINIMUM-ENERGY MISSION PLAN FOR MAXIMUM SCIENTIFIC RETURN

By Jack Funk, James J. Taylor, Joseph R. Thibodeau III,
Flora B. Lowes, and John T. McNeely
Advanced Mission Design Branch

April 1, 1968

MISSION PLANNING AND ANALYSIS DIVISION
NATIONAL AERONAUTICS AND SPACE ADMINISTRATION
MANNED SPACECRAFT CENTER
HOUSTON, TEXAS

Approved: Jack Funk
Jack Funk, Chief
Advanced Mission Design Branch

Approved:
John P. Mayer, Chief
Mission Planning and Analysis Division

CONTENTS

TABLES

FIGURES

MANNED EXPLORATION OF MARS: A MINIMUM-ENERGY MISSION PLAN FOR MAXIMUM SCIENTIFIC RETURN

By Jack Funk, James J. Taylor, Joseph R. Thibodeau III, Flora B. Lowes, and John T. McNeely

1.0 SUMMARY AND INTRODUCTION

This report describes a mission plan and a systems model based on chemical propulsion which can be used to fly a manned landing mission to Mars after assembling four uprated Saturn-class launch vehicles in earth orbit. The primary objective of the report is to demonstrate that manned landings on Mars are possible with the existing space flight technology and can be competitive in schedule and cost with less ambitious missions, such as the multiplanet-flyby missions which have received extensive consideration. The scientific yield of a landing mission or an orbiting mission using the same system will be many magnitudes greater than the flyby mission.

Whenever possible the spacecraft flight plan used minimum-energy trajectories even at the expense of increasing the flight time. Such a flight plan, of course, requires conjunction class (i.e., near-Hohmann transfer) trajectories on outbound and return legs and highly elliptical orbits about the planet.

The mission objectives, however, have not been minimized but have been increased over those in previous mission studies. The following mission objectives were considered in the mission plan and flight systems model:

1. Photograph Martian surface during half a season.
2. Map the entire surface of Mars.
3. Research the Mars atmosphere using unmanned probes.
4. Research the Mars surface with unmanned soft-landers.

5. Research the Martian moons using manned rendezvous with either or both of the moons.

6. Land a man on Mars for 30 days.

In addition to demonstrating the feasibility of Mars orbital and landing missions at an early date, this study is intended as a yardstick for comparing the effects of future technological advancements.

2.0 NOMINAL MISSION PROFILE

2.1 Introduction

The velocity requirements for a Mars landing mission vary greatly according to the type of trajectory profile selected for the heliocentric phase of the mission. The trade-off of velocity with total mission duration is not a continuous function. There are classes of missions plans within which the velocity requirement and mission duration vary continuously, but there is a large jump in energy requirements between these classes. The minimum-energy Mars orbiting (and landing) mission is in the so-called "conjunction" class of missions, which has a total duration of 950 to 1000 days. The next mission in the energy spectrum is the Venus-flyby - Mars-orbiting mission, which has a duration of 600 to 680 days. The Venus flyby energy requirements (ref. 1) are about 30 percent higher than the minimum-energy mission, and the Mars orbital stay capability is about 10 percent of the minimum-energy mission. A 450-day mission, i.e., opposition class, to Mars and return-to-Earth is possible with an increase in energy requirements of 60 to 75 percent relative to the minimum-energy mission. (See refs. 2 and 3.)

A low energy flyby mission (ref. 4) is possible by using multiple heliocentric orbits. A short-duration stopover at Mars using this technique results in mission energy requirements in the conjunction class. However, the total mission is about 1300 days and there appears to be no advantage for this mission except as an alternate.

The minimum-energy trajectory was selected for the nominal mission profile for several reasons:

1. The energy requirements for the next class of trajectories in the energy spectrum is at least 30 percent greater, which results in increased costs and loss of mission opportunities. (The energy increases 50 percent without reducing mission opportunities.)

2. The Mars orbital stay times for all other mission classes are only about 10 percent of that available with the minimum-energy mission. The longer stay time allows observation of Mars during seasonal changes and allows time for more detailed exploration, such as a visit of one of the Martian moons.

3. The minimum-energy trajectory profile is contained between the orbits of the Earth and Mars. This is desirable since a close approach to the Sun (as in the Venus flyby mode) increases concern over radiation and temperature and since large heliocentric distances increase the possibility of penetrating the asteroid belt and require increasing the area of the solar panels if they are used as a power source.

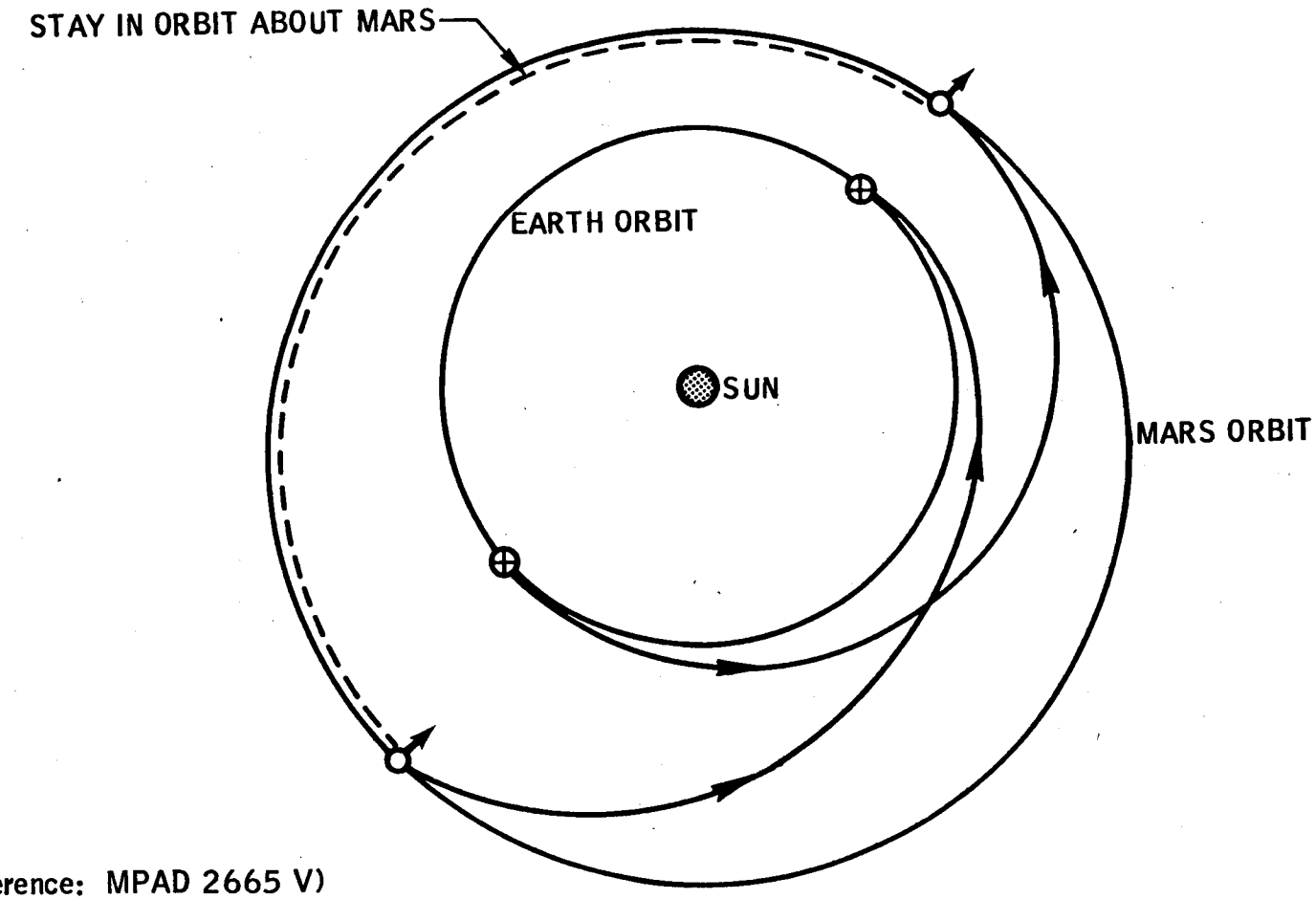

(Reference: MPAD 2665 V)

Figure 1.- Heliocentric phase of the nominal minimum-energy Mars landing mission profile.

The nominal mission profile is discussed in the following sections except for the Mars orbit operations phase which is the subject of section 3.

2.2 Mission Plan

The heliocentric phase of the mission plan is illustrated in figure 1 and consists of three separate parts:

1. The Earth-to-Mars phase.

2. The Mars orbit phase (dashed lines).

3. The Mars-to-Earth return.

The primary requirement for the mission design is to minimize the propulsion requirements without compromising the mission objectives. A secondary requirement is to maintain the Earth entry velocities on return within Apollo entry technology. To meet these requirements, conjunction class trajectories are used for outbound and return-to-Earth trajectories. Elliptical orbits are used about Mars.

The conjunction class trajectories use near-180°, or Hohmann, transfers between the two orbits of the planets. Two impulses are used on the trajectories - one to depart Earth orbit and one to establish Mars orbit. On the return trip, one impulse is used to leave Mars orbit and the second impulse is the aerodynamic entry into the Earth's atmosphere. A limited analysis of two- and three-impulse trajectories (ref. 5) indicates that the minimum-energy transfer to Mars is a two-impulse trajectory and that a large launch window is available before three-impulse trajectories would appreciably reduce the velocity requirements. The conjunction class trajectories do not pass into the asteroid belt or into the high radiation region near the Sun.

The technique for trans-Mars injection (TMI) from Earth orbit is illustrated in figure 2. TMI is accomplished with a series of thrusting maneuvers and coast in an intermediate elliptical orbit between each burn to reduce gravity losses. Each thrusting period is near perigee of the elliptical orbits, except thrustings for plane-change maneuvers which are applied at apogee of the largest orbit. The actual sizes of the intermediate orbits depend on the characteristics of the orbital launch vehicle and operational constraints. The three (or four) burn maneuvers for TMI allow time for orbit operations such as booster staging, orbit determination, and spacecraft systems checkout prior to the final thrust to hyperbolic speed.

The mission operations within the Martian SOI are shown schematically in figure 3. The hyperbolic approach to Mars (labeled "arrive" in fig. 3) is from the leading limb of the SOI. The trajectory can be visualized as

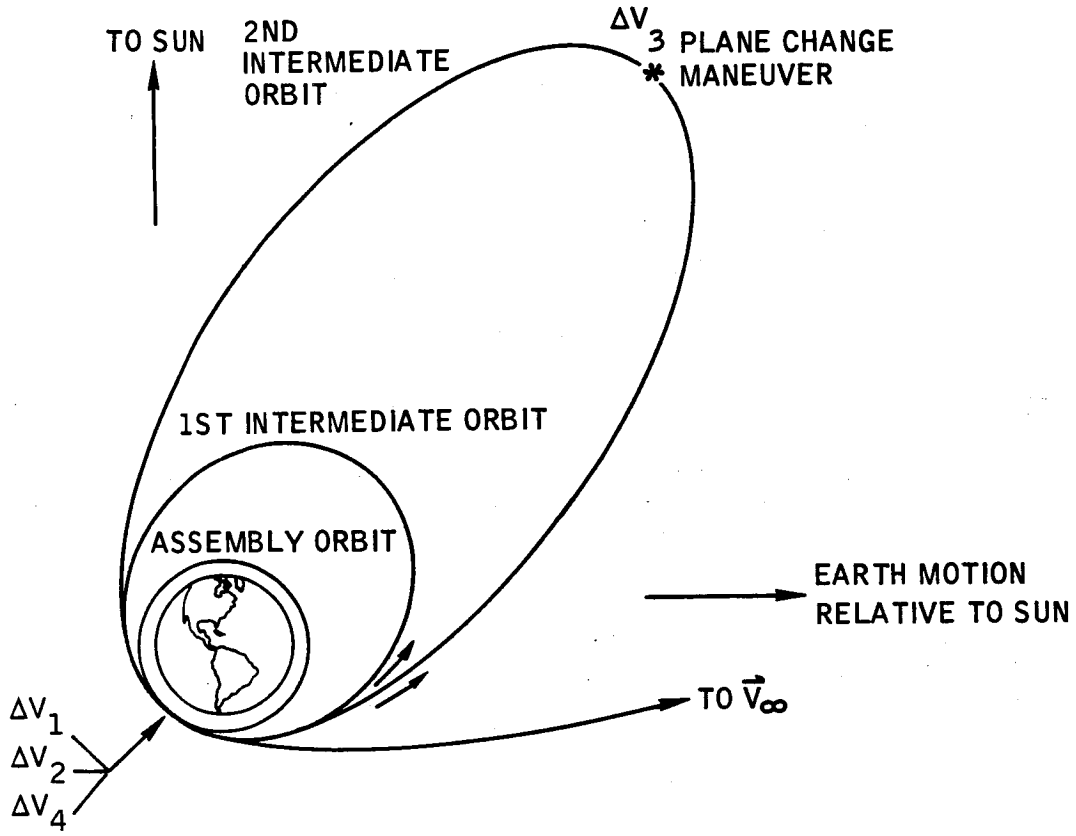

ΔV_1 = TRANSFER FROM ASSEMBLY ORBIT TO 1ST INTERMEDIATE ORBIT

ΔV_2 = TRANSFER FROM 1ST INTERMEDIATE ORBIT TO 2ND INTERMEDIATE ORBIT

ΔV_3 = PLANE CHANGE MANEUVER IF REQUIRED

ΔV_4 = TRANSFER FROM 2ND INTERMEDIATE ORBIT TO $\vec{V}_\infty$

Figure 2.- Earth orbit operations for trans-Mars injection.

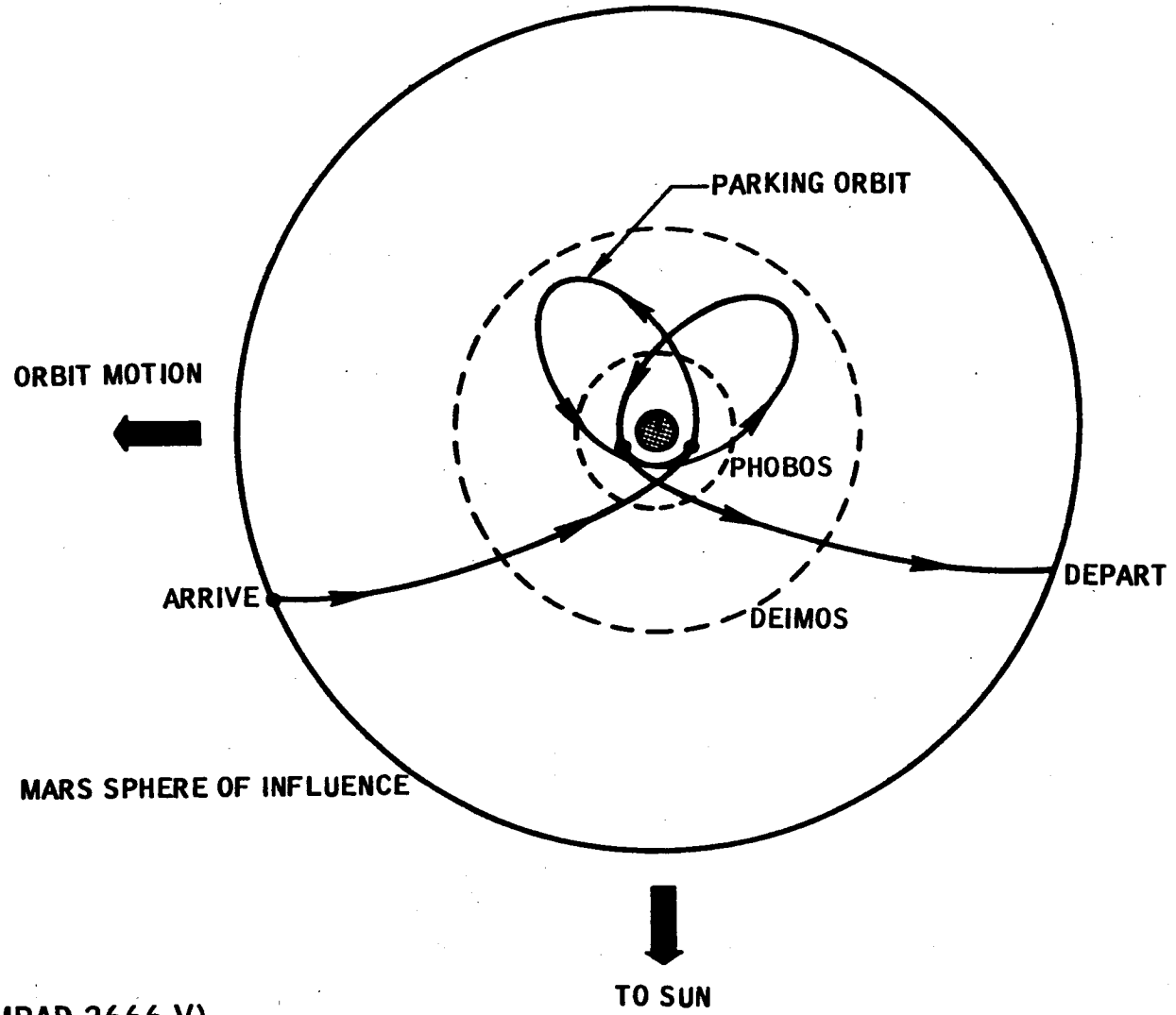

(Reference: MPAD 2666 V)

Figure 3.- Nominal mission profile for Mars orbit operations.

the Martian SOI running into the spacecraft. The orientation of the approach hyperbola is critical (section 3.0), and the approach is restricted to low, posigrade inclinations. The approach periapsis is on the sunlighted side of Mars.

To further reduce the propulsion requirements, the Mars landing module (sometimes called the Mars excursion module) is staged from the main spacecraft near the SOI and targeted for entry into the Martian atmosphere for aerodynamic braking to orbit. The landing module is unmanned during this portion of the trajectory. Atmospheric probes will be launched and targeted to arrive at Mars sufficiently ahead of the landing module so that the atmospheric data from them can be used in adjusting the targeting for the braking maneuver. The unmanned landing module and the spacecraft will arrive at periapsis at approximately the same time. The landing module will enter the atmosphere, perform a skip-out maneuver, and, at apoapsis of the skip, apply a posigrade ΔV to raise periapsis clear of the Martian atmosphere. The spacecraft performs a retrograde maneuver and enters an orbit as close to that of the landing module as possible. The spacecraft or the landing module, or both, is then maneuvered for rendezvous and docking.

The parking orbit about Mars is elliptical and has an apoapsis altitude of approximately 10 000 n. mi. and a periapsis altitude of 200 n. mi. The exact apoapsis altitude is a function of the orbital inclination and stay time. The orbit is designed so that the perturbations of the Mars oblate gravitational field assist in reducing the velocity required for trans-Earth injection (TEI, labeled "depart" in fig. 3).

The orbits of the Martian moons, Phobos and Deimos, are indicated in figure 3 by the dashed circles, which are drawn approximately to scale. The apoapsis of the parking orbit is near the orbit of Deimos but the parking orbit is inclined to the orbit of Deimos. The apoapsis of the parking orbit is perturbed through the plane of Deimos during the orbit stay. At this time, rendezvous maneuvers with either Deimos or Phobos are made using a small orbit excursion module. The perturbations that Deimos and Phobos cause on the spacecraft parking orbit are negligible because of the small size of the moons.

The stay time in Mars orbit is long enough that at least half a Martian season can be observed. Atmospheric research probes and unmanned soft landers will be launched periodically from the main spacecraft. Photographic orbiters may be placed in polar orbits. The time of the manned landing will be determined after sufficient research (mapping, studying surface characters, etc.) has been accomplished to select a landing site. The stay time on the Martian surface will be approximately 30 days. The orbiting spacecraft is manned at all times and, if the lander is unable to rendezvous with the spacecraft, the Martian moon rendezvous module (MMRM) may be used for rescue.

2.3 Mission Opportunities

An analysis was made of the characteristics of conjunction class missions using data similar to that presented in reference 6. A considerable number of plots were required so the data were recomputed and plotted automatically by the computer. The analysis was for 1977 through 1985. The 1983 missions require maximum energy for the conjunction class trajectories. A typical plot of velocity requirements for the 1983 launch window is shown in figure 4. Plots were made of the velocity requirements for flight times of 160 to 400 days from which the mission trajectories were selected. The velocity data shown in figure 4 are for transfers from a 262-n. mi. circular orbit at Earth to a 200-n. mi. circular orbit at Mars. The velocity increments for other parking orbits are obtained by adding or subtracting a constant increment from the data shown.

Minimum velocities for the Earth-to-Mars trajectories were observed on October 8, 1977, October 29, 1979, November 16, 1981, and December 21, 1983 for the outbound leg at trip times of 340, 320, 300, and 280 days, respectively. Minimum velocities for return from Mars orbit were observed on July 5, 1979, July 14, 1981, August 3, 1983, and December 15, 1985. Thus, a typical minimum-energy mission would leave Earth orbit on October 8, 1977 with an outbound flight time of 340 days and would arrive in Mars orbit on September 7, 1978. The next minimum-energy return after arrival is on July 5, 1979. The stay in Mars orbit, therefore, will be 295 days if the velocity increments for the mission are to be minimized.

A typical mission flight plan is shown in table I for the 1977 launch window. The elliptical orbit selection of the mission is discussed in section 3. In addition to the incremental velocity requirements of the transfer trajectories, a nonmission-dependent velocity budget (table II) was added to account for gravity losses due to finite thrust, midcourse guidance correction requirements, spacecraft attitude control and spin requirements. The guidance velocity requirements and delivery accuracies are discussed in section 4 and the spacecraft spin requirements, in section 5.

The TMI gravity and steering losses (table II) are low (325 fps) because multiple-revolution injection procedures are used. The Earth orbit operations phase is discussed in detail in section 2.4. The midcourse correction and artificial gravity spin-up velocity requirements are combined into a single budget of 500 fps for trans-Mars and 500 fps for trans-Earth. The gravity and steering losses for Mars orbit insertion (MOI) and TEI are low for two reasons: (1) The Mars parking orbit is elliptical, which reduces the magnitude of the required velocity change, and (2) the orbit is oriented to take advantage of the oblateness of the planet so that the nominal burns are coplanar. The 500 fps allotted for Mars orbital

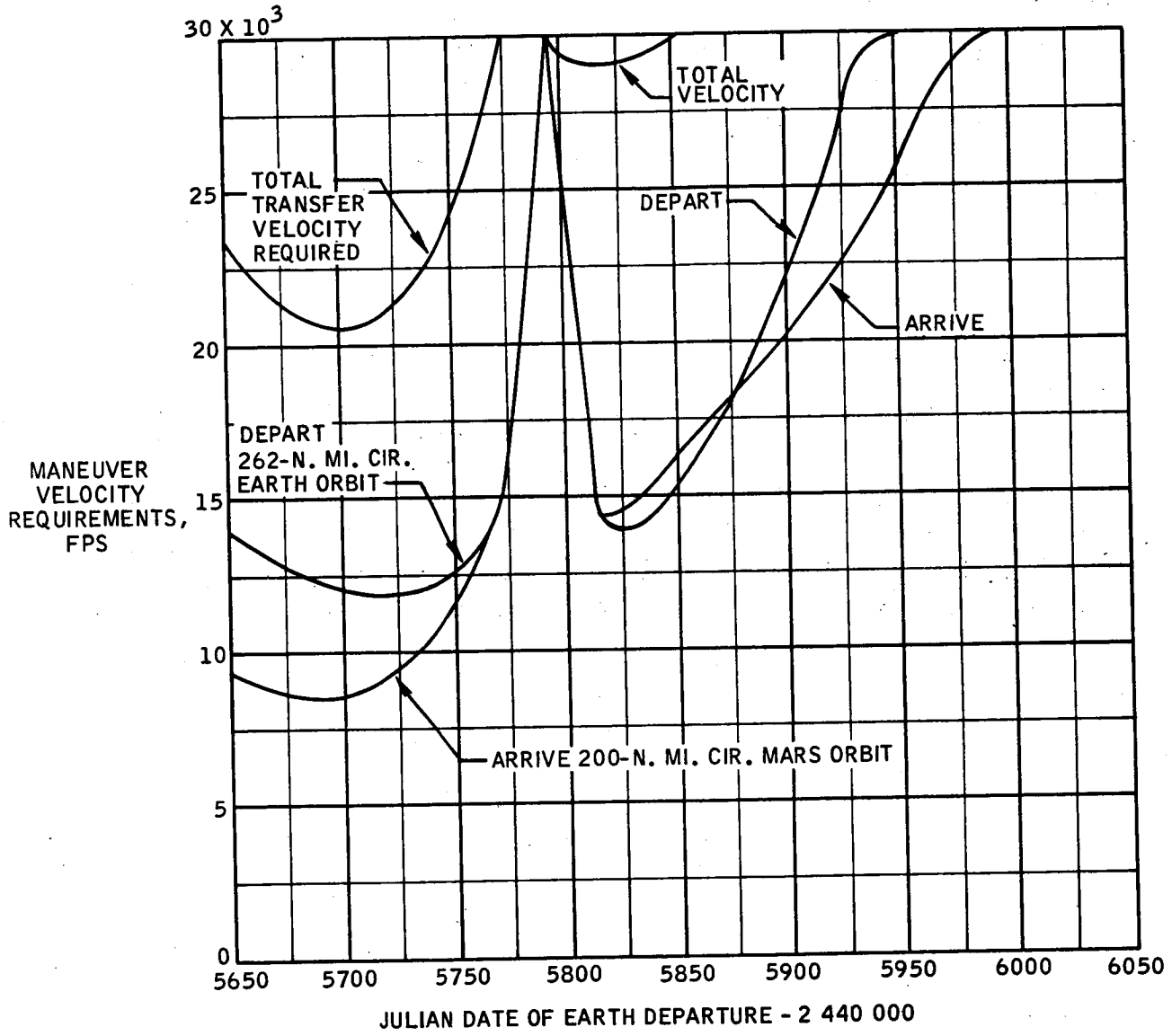

Figure 4.- Velocity requirements for transfer from Earth to Mars in 1983 with a total trip time of 280 days.

TABLE I.- TYPICAL PARAMETERS FOR A MINIMUM-ENERGY MARS LANDING MISSION IN THE 1977 OPPORTUNITY

Earth to Mars	
TMI, Julian date - 2 440 000	3 425
Calendar date	October 8, 1977
Flight time, days	340
ΔV for TMI from 262-n. mi. circular orbit, fps	11 827
Mars periapsis velocity, fps	17 630
Mars orbit	
Periapsis altitude, n. mi.	200
Apoapsis altitude, n. mi.	9 302
Equatorial inclination, deg	21.1
Orbit period, hr	11.4
Orbit stay time, days	295
Periapsis velocity, fps	14 371
ΔV for MOI, fps	3 257
Mars to Earth	
TEI, Julian date - 2 440 000	4 060
Calendar date	July 6, 1979
Flight time, days	320
ΔV for TEI, fps	4 023
Earth entry, fps	38 463
Arrive at Earth	May 20, 1980

TABLE II.- NONMISSION-DEPENDENT VELOCITY BUDGET

Maneuver	Velocity, fps
Trans-Mars injection gravity and steering losses	325
Trans-Mars midcourse corrections and artificial gravity	500
Mars orbit insertion gravity and steering losses	100
Mars orbit maneuvers and artificial gravity spin-ups	500
Trans-Earth injection gravity and steering losses	50
Trans-Earth midcourse corrections and artificial gravity spin-ups	500

adjustments to correct for uncertainties in the Mars gravitational potential. A total of 1650 fps is added to the spacecraft propulsion requirements and 325 fps is added to the Earth departure propulsion requirements, as determined by impulsive velocity calculations.

The nominal TMI windows from 1977 through 1985 are shown in figure 5. Although the velocity requirements are plotted as a function of Earth departure date, the windows are actually discrete events occurring at approximately 2-year intervals - the dashed lines are drawn to show trends. The mission opportunities are indicated by the vertical bars and the year of Earth departure (e.g., 1977, 1979, ...). The minimum-energy requirements are indicated by the "bottom" of the bar and the requirements for a 50-day Earth departure window is shown at the "top" of the bar. All velocities include the nonmission-dependent velocity budget.

The MOI and TEI velocity requirements are shown as a total since the total represents the velocity capability required onboard the spacecraft. The maximum spacecraft velocity requirements (11 000 fps) occur in the 1983 TMI window. However, the increase in spacecraft velocity requirements for a 50-day window is nearly constant at 300 fps. The TMI requirements are much more sensitive to departure time. The 50-day TMI window costs from 600 to 1100 fps, depending on the particular TMI window. The maximum TMI requirements occur in the 1983 mission window.

The Earth entry velocity is indicated by a point rather than a vertical bar because the Mars orbit stay time is adjusted to minimize the ΔV required for TEI and the trans-Earth trip is then fixed (i.e., the dates to depart Mars and arrive at Earth are fixed) for the TMI window. The entry velocity is constant for a given window, and the orbit stay time is variable. The Earth entry velocity does not exceed 40 000 fps and is maximum in the 1983 window. The Earth entry velocity is computed at an altitude of 400 000 ft.

The total mission time varies about 50 days for a 50-day departure window. The maximum mission duration (1028 days) occurs in the 1981 mission opportunity.

The 1977, 1979, 1981, and 1983 mission parameters are tabulated in table III for the beginning, middle, and end of the 50-day TMI window. Note that a 5-day reduction in the 1983 TMI window reduces the injection velocity requirements from 14 075 fps to 13 145 fps. Therefore, a small reduction in the 1983 window seems advisable.

The 1983 TMI opportunity establishes the maximum propulsion requirements; the reason for this is shown in figure 6. Figure 6 is a plot of Mars ephemeris parameters as a function of time. The date of TMI is indicated by a solid dot near the time scale and arrival at Mars is shown by a vertical line on each parameter curve. The Earth-Mars phase angle is

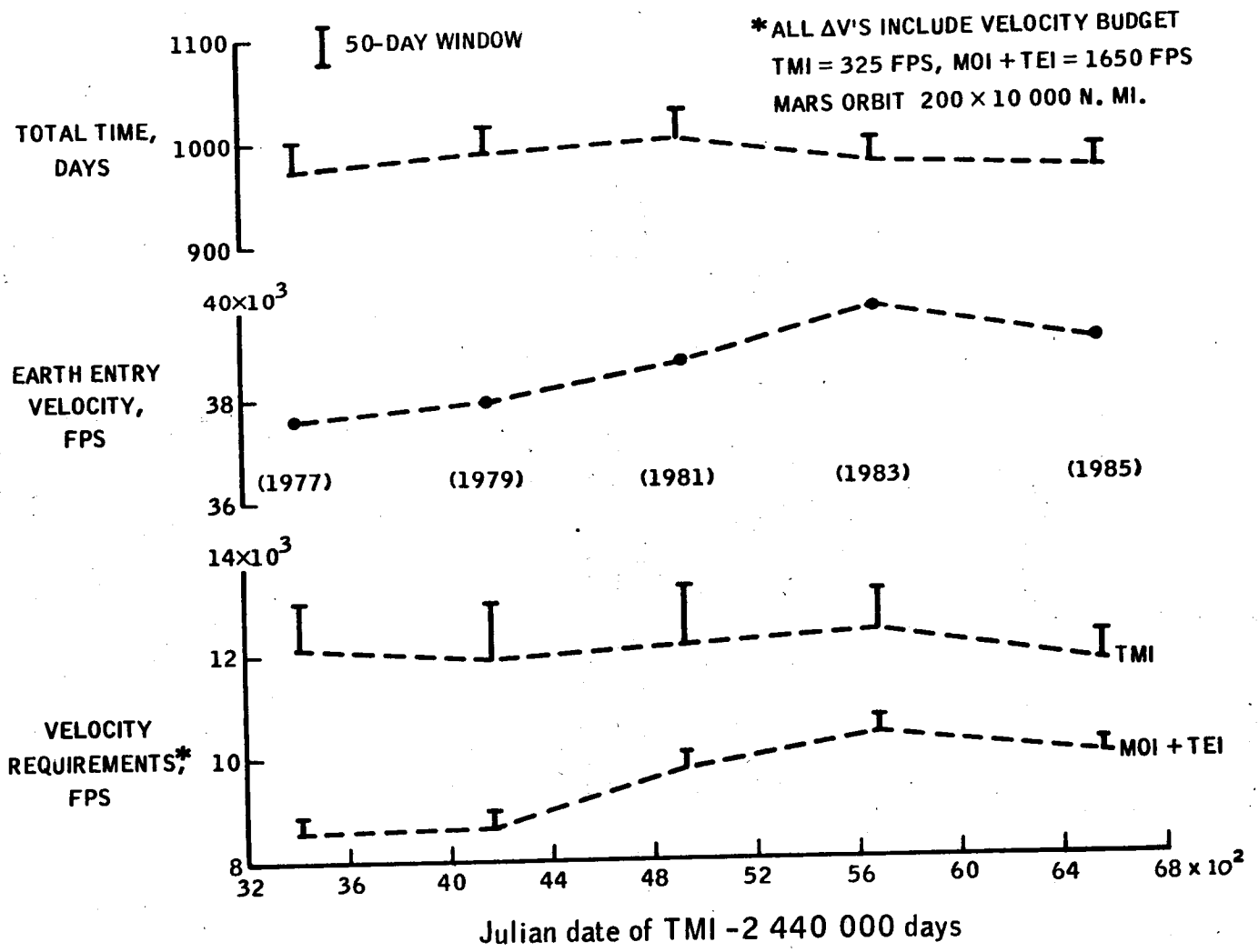

(Reference: MPAD 2672 V)

Figure 5.- Minimum-energy Mars landing mission opportunities.

TABLE III.- OPPORTUNITIES FOR A MINIMUM ENERGY MARS LANDING MISSION[a]

[262-n. mi. circular Earth departure orbit]

Calendar date of TMI for the minimum energy mission	Julian date of TMI minus 2 440 000 days	Outbound time, days	Stay time, days	Inbound time, days	Total trip time, days	TMI ΔV, fps	MOI[b] ΔV, days	TEI ΔV, days	MOI ΔV + TEI ΔV, fps	Total ΔV, fps	Entry V, fps
--	3400	360	300	338	998	12 968	4459	4364	8 823	21 791	37 637
October 8, 1977	3425	340	295	338	973	12 159	4295	4364	8 659	20 818	37 637
--	3450	320	290	338	948	12 951	4535	4364	8 899	21 850	37 637
--	4150	340	310	365	1015	12 969	4738	4239	8 977	21 946	38 000
October 29, 1979	4175	320	305	365	990	11 961	4503	4239	8 742	20 703	38 000
--	4200	300	300	365	965	12 564	4669	4239	8 908	21 472	38 000
--	4900	320	330	378	1028	13 317	5346	4454	9 800	23 117	38 550
November 16, 1981	4925	300	325	378	1003	12 125	5204	4454	9 658	21 783	38 550
--	4950	280	320	378	978	12 410	5599	4454	10 053	22 463	38 550
--	5665	280	469	251	1000	14 075	6599	4376	10 975	25 050	39 760
--	5670	280	465	251	996	13 145	6324	4376	10 700	23 845	39 760
December 21, 1983	5690	280	445	251	976	12 440	5067	4376	9 543	21 883	39 760
--	5710	280	425	251	956	12 120	6392	4376	10 768	22 888	39 760
--	5715	280	419	251	950	12 100	6599	4376	10 975	23 075	39 760

[a]All ΔV's include the velocity budget: 352 fps for TMI, 1100 fps for MOI, and 550 fps for TEI.

[b]200- by 10 000-n. mi. Mars parking orbit.

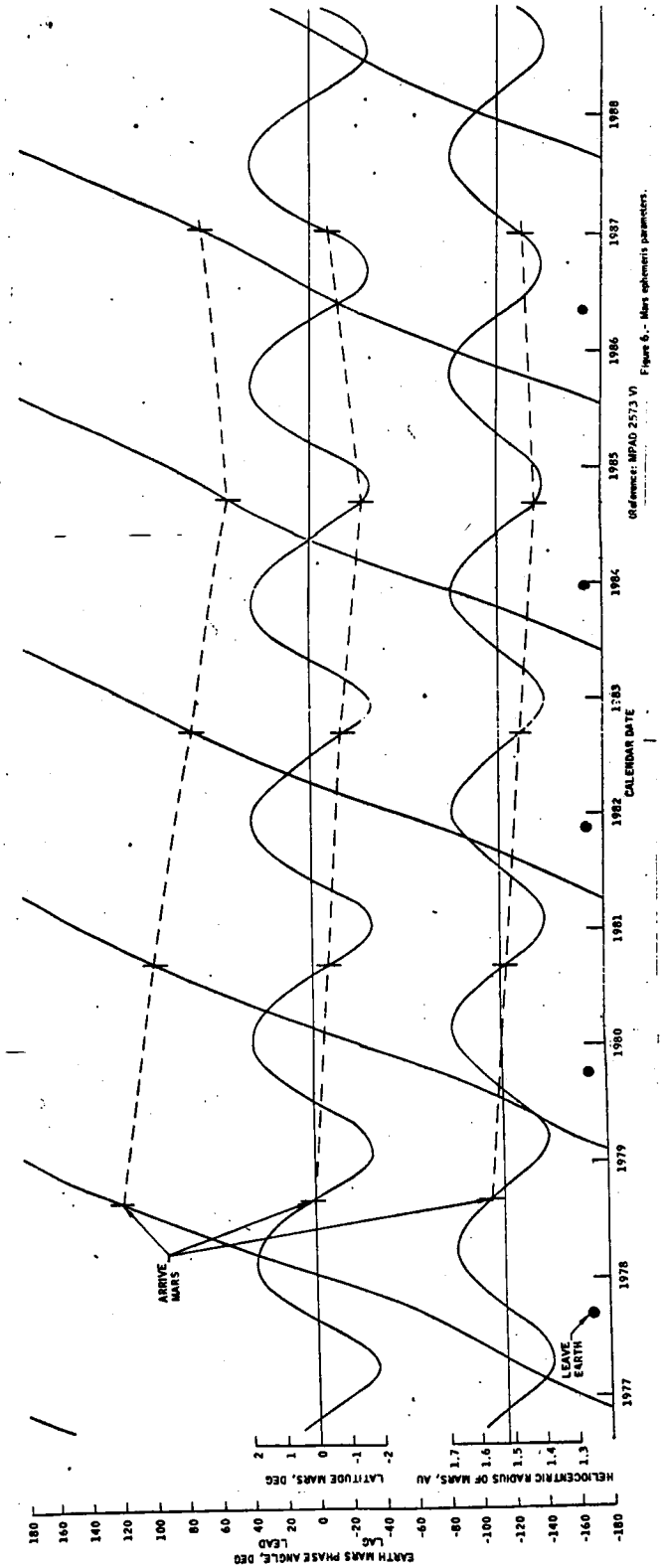

Reference: MPAD 2573 VI

Figure 6. - Mars ephemeris parameters.

positive when Mars is leading the Earth. Note that the heliocentric latitude of Mars relative to the ecliptic plane is "in phase" with the Mars-to-Sun distance. Mars is at aphelion when the latitude is maximum south. The minimum spacecraft velocity requirements would occur when Mars arrival is at its mean distance from the Sun if the Earth and Mars orbits were coplanar. However, they are not coplanar and the required phase angle forces arrival to occur closer to perihelion which corresponds to the maximum latitude of Mars thus causing an increase in the out-of-plane velocity requirements.

After 1983, the latitude of Mars at arrival begins to move north again and the velocity requirements are reduced. The minimum-velocity requirements are represented by the 1977 opportunity.

2.4 Trans-Mars Injection Windows

The Earth orbit operations (fig. 2) result in a spacecraft assembled in a low Earth orbit and injected toward Mars with a series of four burns. The first launch establishes the orientation of the parking orbit, which is then perturbed by gravitational forces until the actual injection is accomplished.

The time between first launch and final injection is expected to be between 30 and 45 days. The 50-day TMI window discussed in the previous section assumes that TMI occurs on time for a coplanar burn. However, TMI may not occur on time and, therefore, the parking orbit is designed to maximize the TMI window for a total velocity injection capability of 13 500 fps.

The injection windows for the 1977, 1979, 1981, and 1983 mission opportunities are shown in figures 7 through 10. The basic energy requirement is the impulsive velocity required for injection from the assembly orbit with a single impulse. The difference between the basic energy requirement and the actual injection requirement is caused by a combination of gravity losses and plane-change requirements. The maximum parking orbit period is arbitrarily set at 48 hours and establishes the apogee altitude for the plane-change maneuver. The plane-change maneuver is accomplished so that the perigee altitude of the parking orbit is constant throughout the burn. The injection window for a 13 500-fps injection capability is 27 days in 1977, 1979, and 1981. The window is reduced to 20 days in 1983.

The injection window decreases after the first burn is completed, but studies indicate that 75 percent of the remaining window is still available. For example, if the first burn occurs at the beginning of a 27-day window, the final injection must occur within the next 20 days. A typical injection sequence for the 1977 opportunity is listed in table IV. Reference 7 is a more detailed discussion of the trans-Mars injection window for low-energy missions.

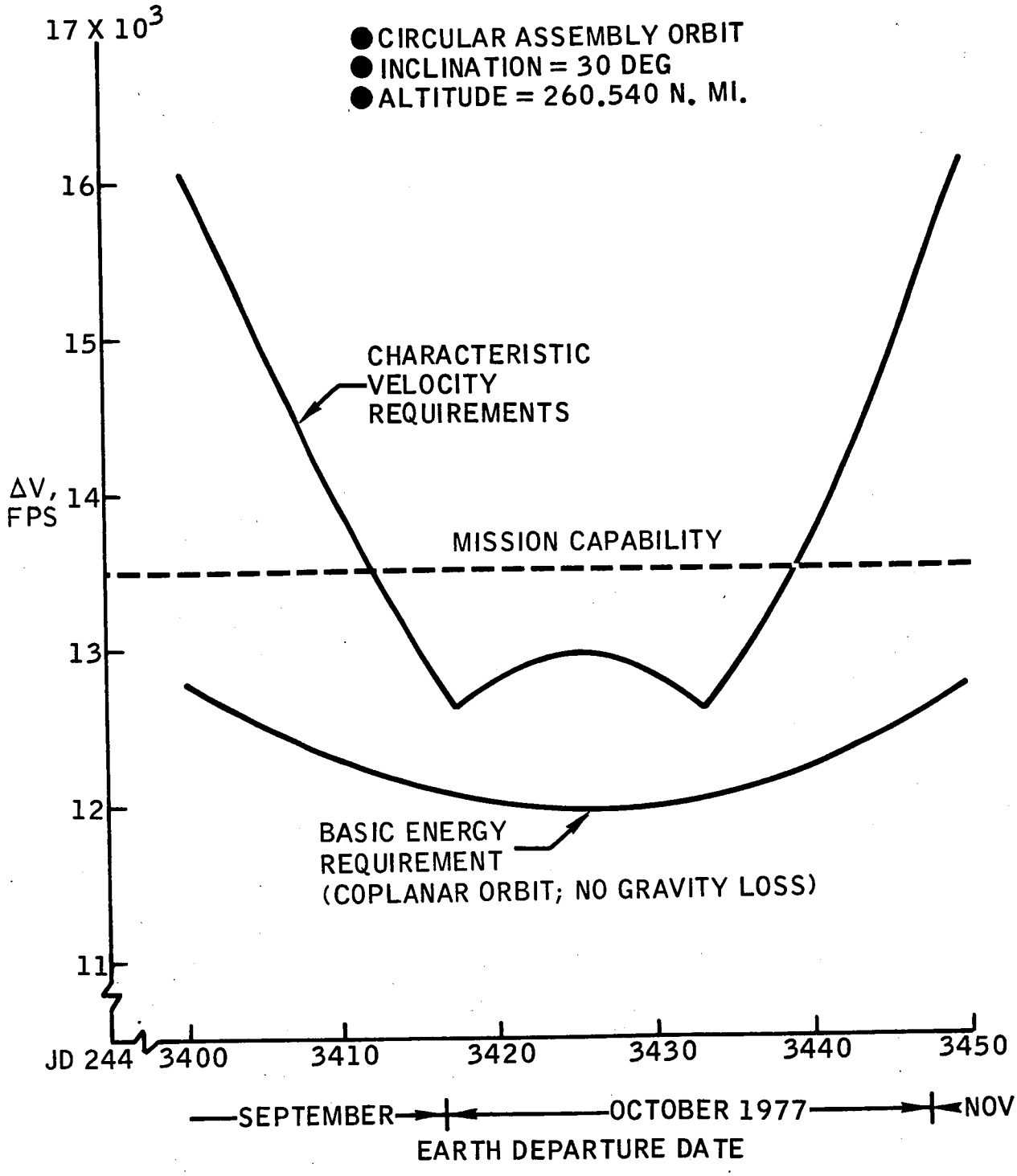

Figure 7.- Trans-Mars injection window for the 1977 minimum-energy mission opportunity.

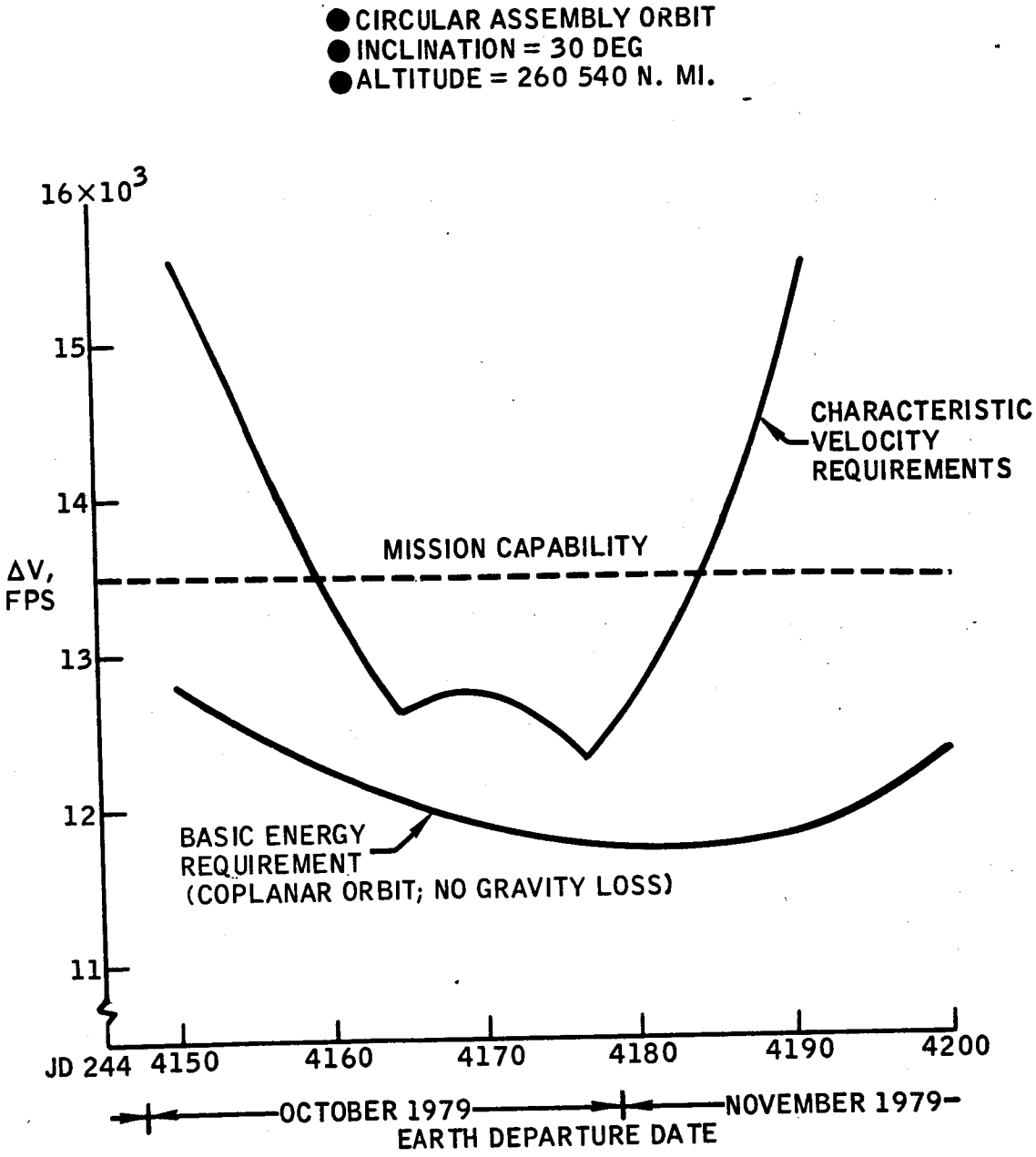

Figure 8.- Trans-Mars injection window for the 1979 minimum-energy mission opportunity.

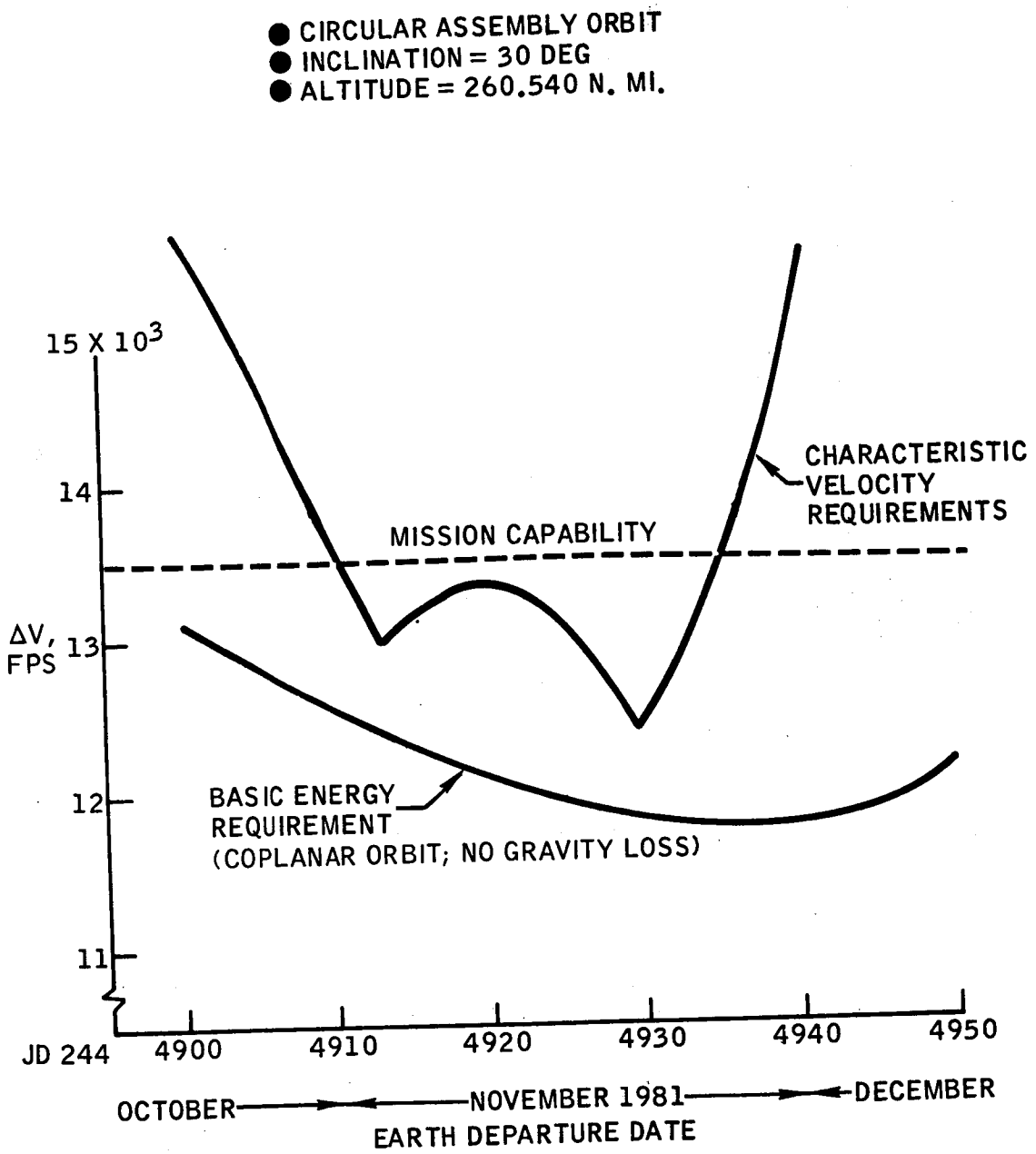

Figure 9.- Trans-Mars injection window for the 1981 minimum-energy mission opportunity.

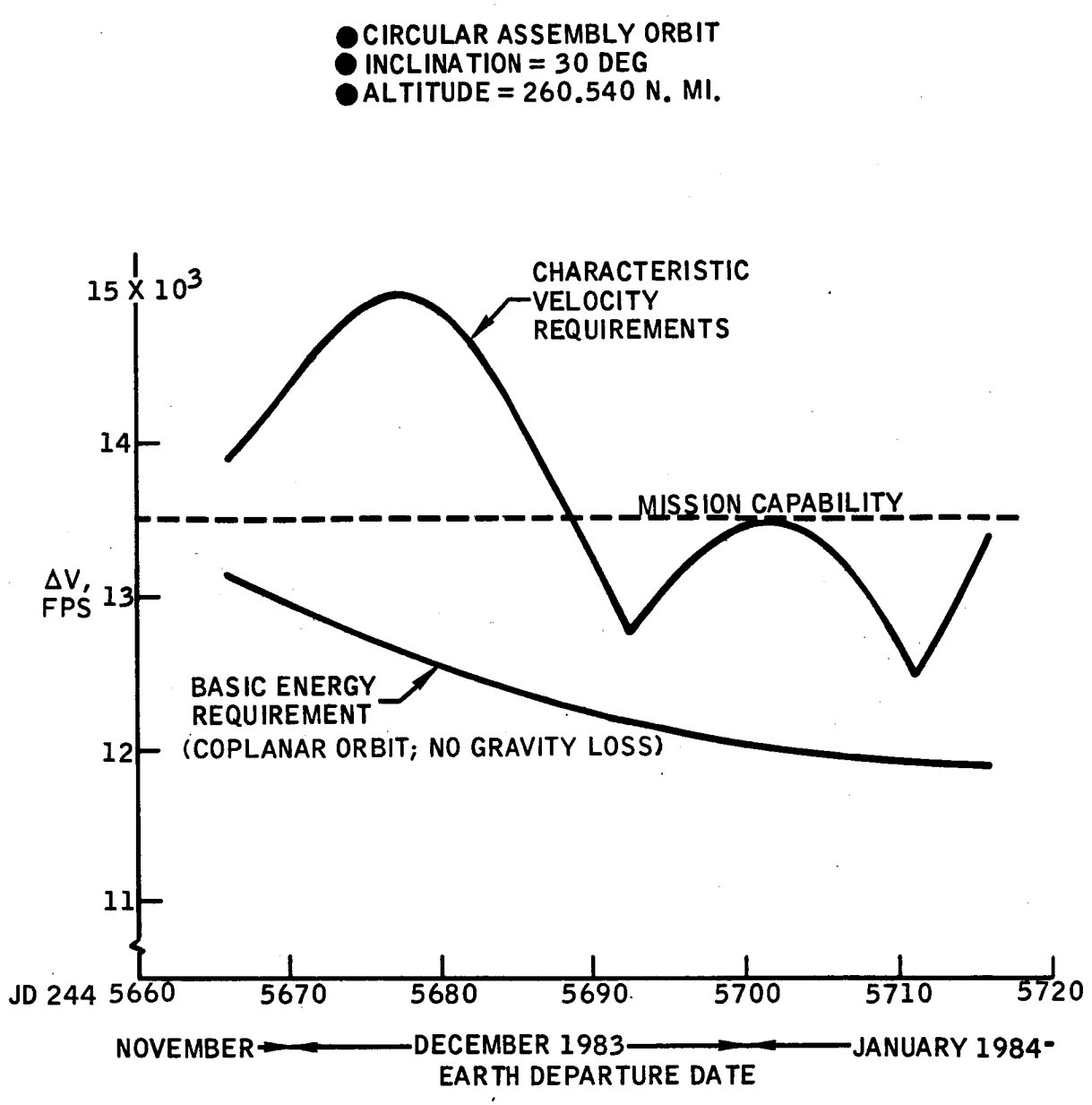

Figure 10.- Trans-Mars injection window for the 1983 minimum-energy mission opportunity.

TABLE IV.- NOMINAL TMI SEQUENCE FOR AN OCTOBER 7, 1977 DEPARTURE

Time from nominal TMI, hr	-62.45	-59.90	-49.22	-16.59	0.0
Orbit before impulse					
Perigee altitude, n. mi.	260.54	260.54	260.54	260.54	260.54
Apogee altitude, n. mi.	260.54	3 097.5	19 455.	65 264.	65 264.
Inclination, deg	30.0	30.	30.	30.	26.15
Inertial period, hr	1.57	2.55	10.69	48.0	48.00
Nodal regression rate, deg/day	-6.71	-2.55	-0.33	-0.06	-0.06
Apsidal regression rate, deg/day	--	4.01	0.53	0.10	0.11
Impulse					
Characteristic velocity increment, fps	3475.	4 867.	1 645.	431.	2 534.
Wedge angle between orbit planes, deg	0.	0.	0.	12.15	0.
SC true anomaly before impulse, deg	0.	0.	0.	-171.6	0.
SC true anomaly after impulse, deg	0.	0.	0.	-171.6	0.
Accumulated velocity increments, fps	3475.	8 342.	9 987.	10 418.	12 952.
Orbit after impulse					
Perigee altitude, n. mi.	260.54	260.54	260.54	260.54	260.54
Apogee altitude, n. mi.	3097.5	19 455.	65 264.	65 264.	∞
Inclination, deg	30.	30.	30.	26.15	26.15
Inertial period, hr	2.55	10.69	48.0	48.00	∞
Nodal regression rate, deg/day	-2.53	-0.33	-0.06	-0.06	0.
Apsidal regression rate, deg/day	4.01	0.53	0.10	0.11	0.

2.5 Conclusions

The minimum-energy Mars landing mission requirements (assuming a 50-day departure window) for the 1977 through 1985 time period are:

TMI (includes 325-fps mission velocity budget), fps	13 500
MOI (includes 1100-fps mission velocity budget), fps. . . .	5 500
TEI (includes 550-fps mission velocity budget), fps	5 500
Earth entry velocity, fps	40 000
Total mission duration, days.	1 028

The minimum-energy mission profile has several desirable characteristics in addition to the obviously low spacecraft ΔV requirements. The Earth entry velocity is less than 40 000 fps and entry can be accomplished within current Apollo technology. The maximum spacecraft distance from the Sun is 1.7 A.U.'s when Mars is at aphelion; this distance avoids penetration of the asteroid belt and limits the size of the solar electric panels. The spacecraft does not approach the Sun closer than 1.0 A.U., which reduces solar radiation intensity.

The long time to observe the planet increases the scientific return by allowing time to make good use of the payload gained by using the minimum-energy mission profile.

3.0 MARS PARKING ORBIT OPERATIONS

3.1 Introduction

The determination of a nominal Mars parking orbit presents several fundamental and conflicting problems in mission analysis and trajectory design. The basic problem is to find a parking orbit which not only satisfies mission objectives, but also provides for efficient planetary capture and escape, and, at the same time, allows flexibility for alternate mission modes.

The following discussion evaluates a class of regressing elliptical orbits in terms of a few of these criteria, specifically (1) efficient planetary capture and escape maneuvers, and (2) satisfying mission objectives (mapping and surveying, manned landing, and Martian moon rendezvous). The analysis assumes an oblate planet and employs a technique which relies on the effects of the gravitational harmonics to assist in parking orbit alignment.

3.2 Spacecraft Parking Orbit Design for Minimum ΔV

Performance of the spacecraft hardware, parking orbit lifetime, and overall mission objectives define several characteristics of the nominal Mars parking orbit. The manned landing and Martian moon rendezvous both dictate a posigrade parking orbit since both Mars spin axis and the moon orbital motion are posigrade. It is also desirable that the parking orbit periapsis remain in the sunlight both prior to the time of landing for landing site reconnaissance and at the time of landing. Periapsis altitude must be greater than some minimum value (for this study, greater than 200 n. mi.) to avoid orbital decay due to drag and long-period gravitational perturbation. The apoapsis altitude should be high enough tc minimize total mission ΔV yet not so high that the ΔV requirements for Mars landing become prohibitive.

Prior to a Mars landing, one of the primary crew objectives is the selection of an appropriate landing site. To insure adequate coverage and satisfactory evaluation of possible landing sites, it is desirable that the spacecraft make frequent passes over candidate landing sites. Thus it may be desirable to restrict the orbital period (apoapsis altitude) to insure periapsis passages on a once- or twice-daily basis.

A significant amount of fuel can be saved by using a parking orbit with a moderate eccentricity. As shown in figure 11, MOI ΔV first decreases rapidly with increasing apoapsis altitude, but, because of the asymptotic nature of the curve, there is a point where large increases in apoapsis altitude do not significantly reduce the MOI ΔV requirement. In the region

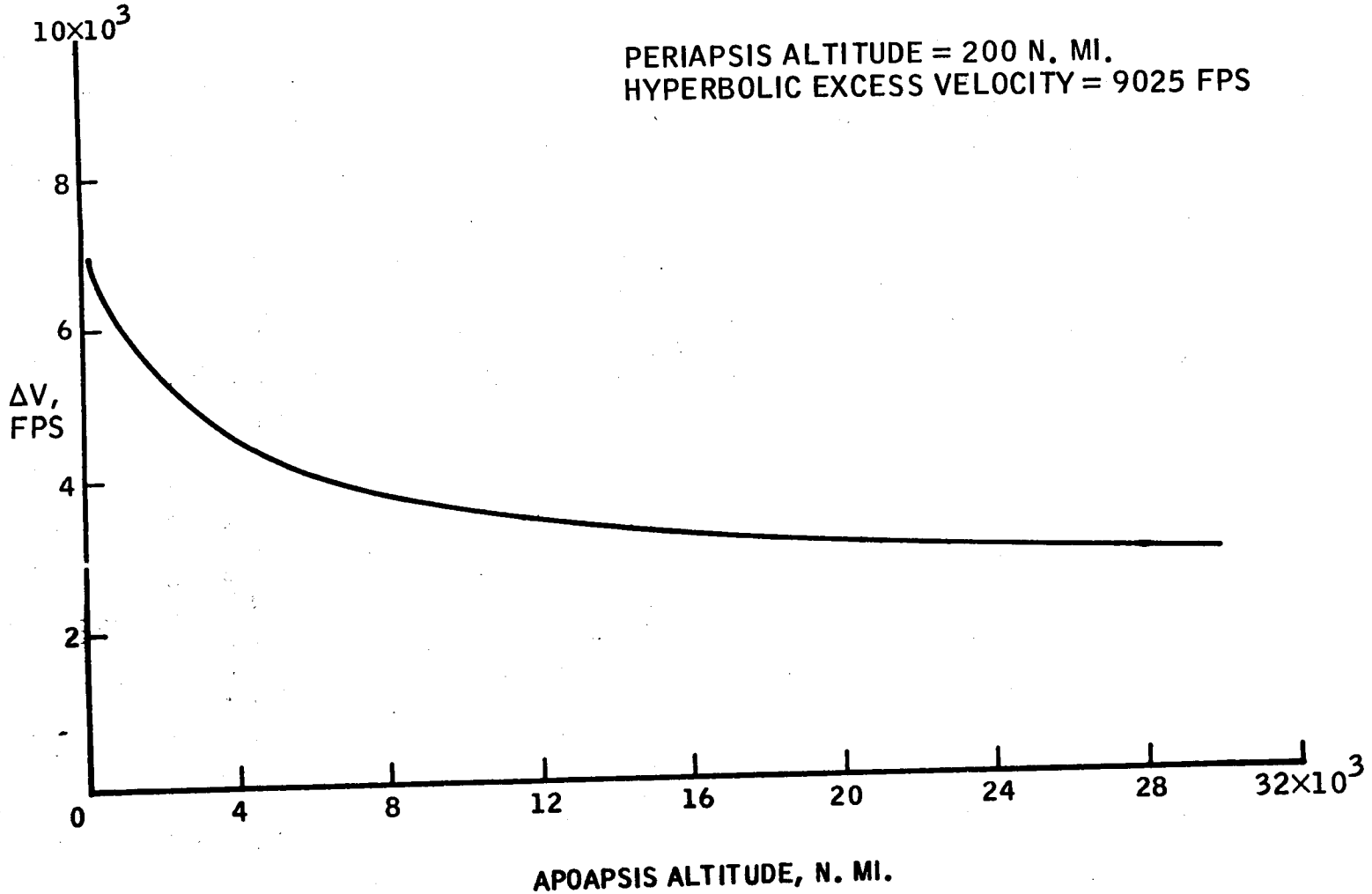

(Reference: MPAD 2677 V)

Figure 11.- Mars orbit insertion velocity requirements for elliptical parking orbits.

of 8000 n. mi. and above, the apoapsis can be adjusted to meet mission constraints without significantly affecting ΔV.

The hyperbolic excess velocity (V_∞) shown is typical of the Mars arrival V_∞ for a near-minimum-energy trajectory. Note that the MOI costs nearly 7000 fps for a 200-n. mi. circular orbit. For a 200- by 10 000-n. mi. ellipse, the MOI is reduced to half that much, or 3500 fps, but does not become significantly less than 3000 fps for any parking orbit. (Braking the spacecraft to parabolic speed requires 2400 fps.) Thus, a parking orbit having a 10 000-n. mi. apoapsis altitude (which corresponds to an eccentricity of about 0.7) appears to be a reasonable choice for the nominal parking orbit considering the ΔV cost for MOI. As will be seen later, this orbit will become more advantageous in terms of landing site selection, moon rendezvous, solar lighting, and efficiency of the planetary escape maneuver.

The analysis employs a technique which relies on the effects of the gravitational harmonics for parking orbit alignment. This technique is discussed in references 8, 9, and 10. The basic approach is to choose the orbital characteristics so that the resulting nodal and apsidal motion will shift the original parking orbit into proper alignment for departure on the intended date. This technique was developed to consider (1) the orientation and motion of the hyperbolic departure asymptote, and (2) the motion of the parking orbit resulting from the asphericity of the planet's gravitational field. Employing this technique allows the use of impulses at periapsis for both the capture and escape maneuvers (see fig. 12), thus insuring maximum efficiency for the MOI and TEI maneuvers. Of course, orbits that satisfy this technique may not necessarily satisfy other mission requirements, and, in that case, the efficiency of MOI and TEI would have to be compromised and propulsive maneuvers made for orbital alignment. This becomes apparent in the 1979 and 1981 mission windows, which are discussed below.

The technique was used to determine the characteristics of regressing parking orbits which require no discrete propulsive maneuvers for orbital alignment. Although there are a large number of possible parking orbits which shift into proper alignment for departure and require no discrete propulsive maneuvers, many of these possible orbits are low-energy or nearly circular and, therefore, require high MOI and TEI ΔV. Figure 13, therefore, considers only the two highest energy parking orbits which occurred most frequently during the analysis. The highest energy regressing orbit was selected as the nominal parking orbit for the base-line analysis.

Three 50-day launch opportunities - in 1977, 1979, and 1981 - are considered in figure 14 to show the feasibility of using regressing elliptical orbits for the nominal Mars parking orbit. The solid curves show the characteristics of parking orbits which require a combination of oblateness perturbations and auxiliary propulsive maneuvers (see ref. 11) for

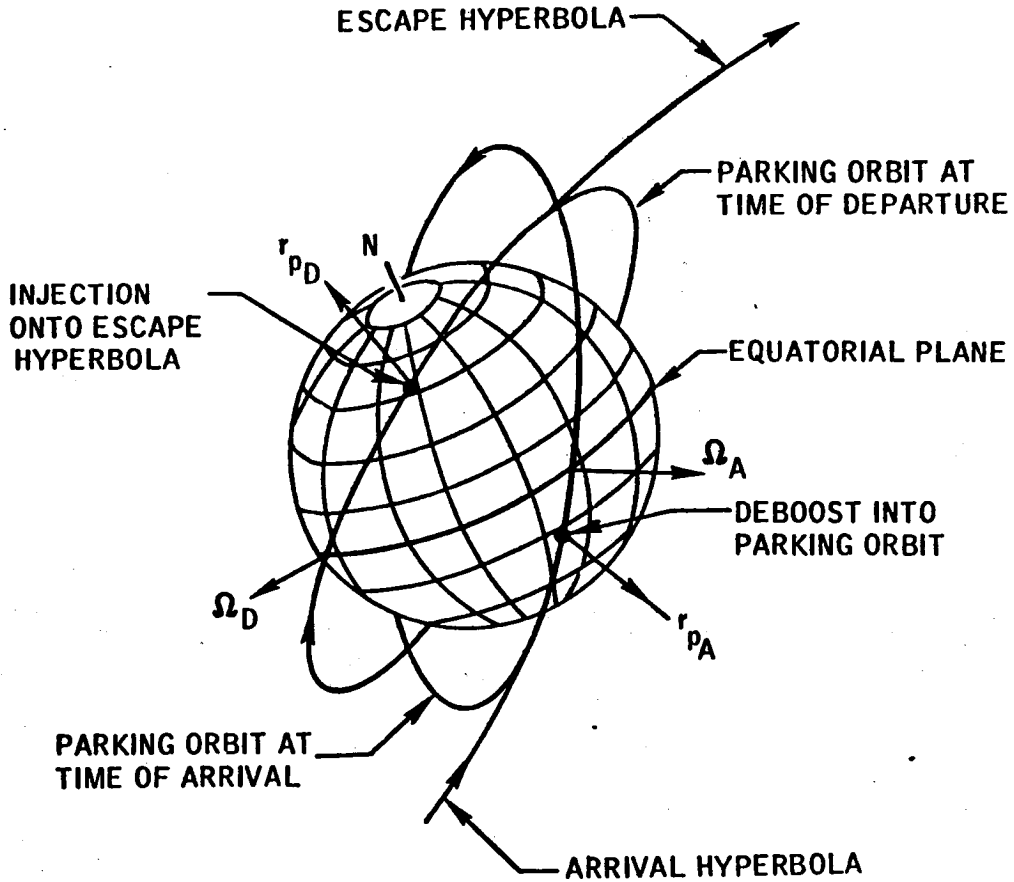

(Reference: MPAD 2678 V)

Figure 12.- Geometry of the parking orbit at the time of arrival and departure.

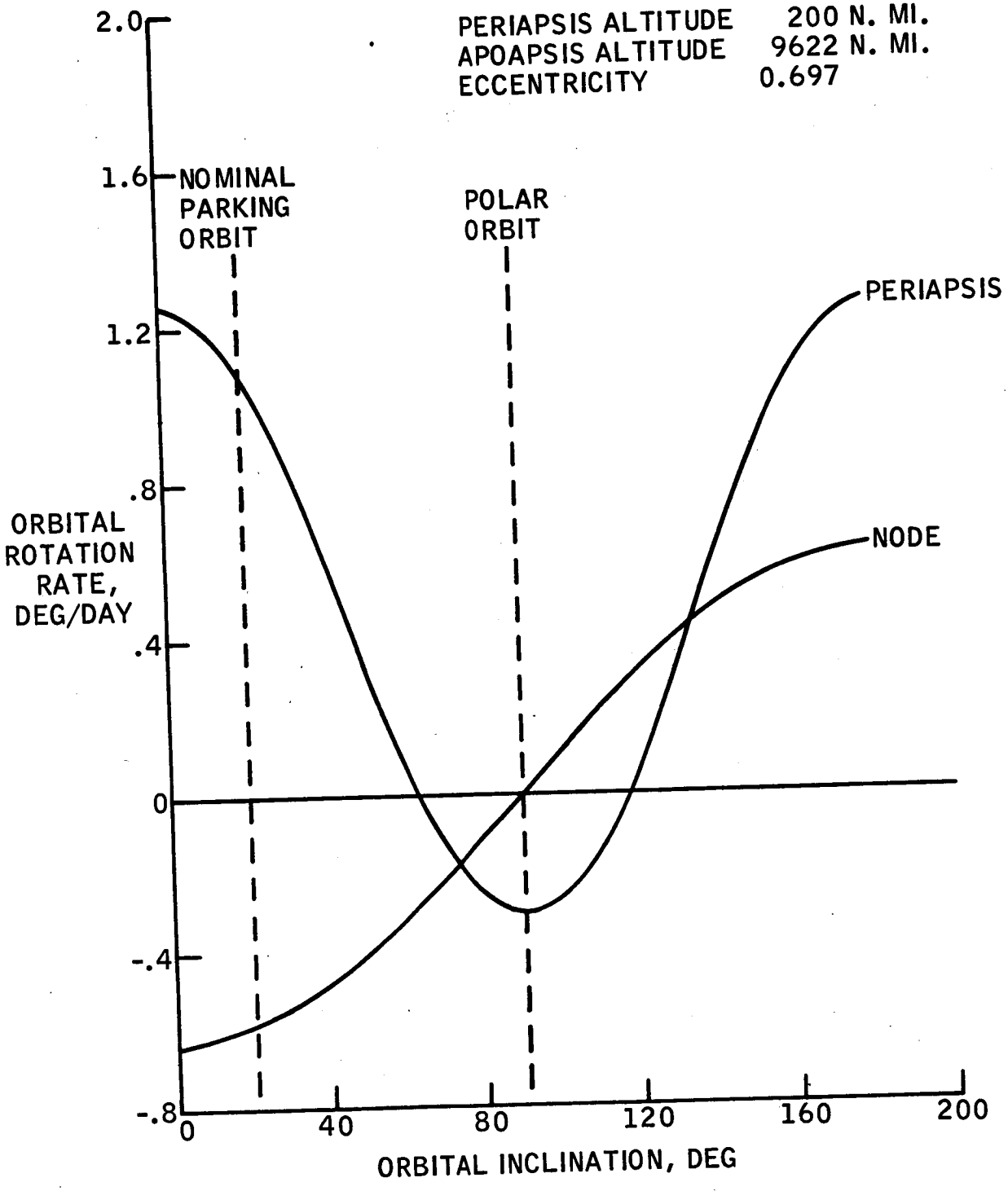

Figure 13 .- Secular rotation rate of parking orbit node and periapsis vectors due to Mars oblateness.

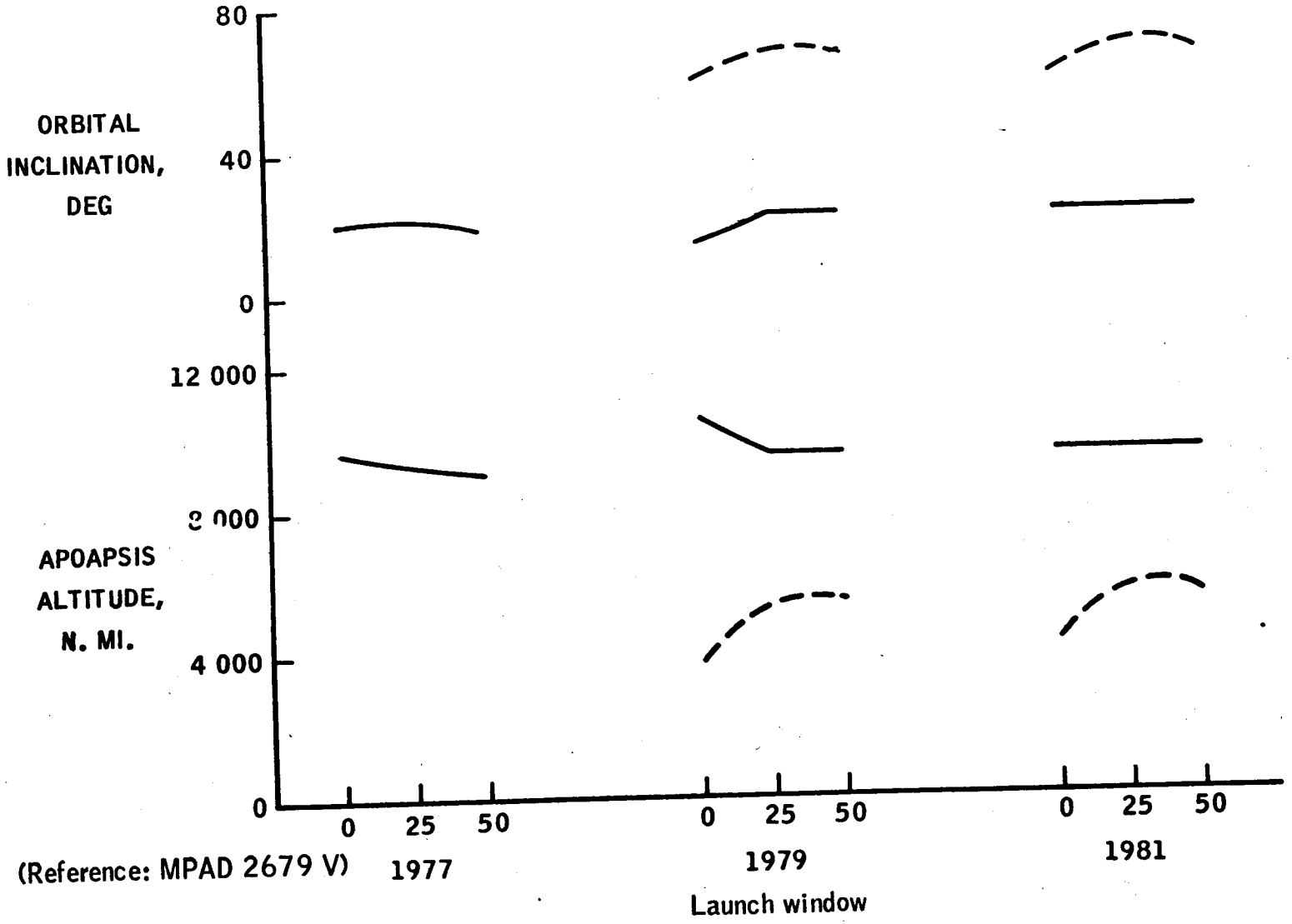

(Reference: MPAD 2679 V)

Figure 14.- Variation of the characteristics of the nominal Mars parking orbit during the mission window.

orbital realignment to reduce the ΔV cost for orbiting the planet, moon rendezvous, and Mars landing. The dashed curves indicate the characteristics of those parking orbits which shift into proper alignment for departure. The discontinuities in the 1979 curves indicate failure of the gravitational perturbations to shift the nominal parking orbit into proper alignment for departure. The 1977 injection window is the only window where the nominal regressing parking orbit requires no plane change of line-of-apsides corrections for alignment. For the 1979 and 1981 windows, the highest energy regressing orbit has an inclination between 60° and 70°, and requires a prohibitive ΔV budget for Martian moon rendezvous.

Figure 15 shows the velocity requirements for MOI and TEI throughout the same three launch windows. The MOI ΔV remains near 3500 fps throughout the 1977 window, but increases in the 1979 and 1981 windows because of a growing plane-change requirement later in the window. This is due to the increasing declination of the Mars hyperbolic arrival asymptote which is higher than the nominal orbital inclination. The nominal TEI ΔV remains essentially constant at 4000 fps because the time of TEI is held constant throughout each window. Again, the dashed lines show the MOI and TEI ΔV for the next highest energy orbit which does shift into proper alignment for departure.

3.3 Operational Characteristics of the Spacecraft Parking Orbit

The parking orbit is primarily designed to reduce the ΔV cost for orbiting the planet, moon rendezvous, and landing on Mars. The relation of the spacecraft parking orbit to the Sun and Mars is important to the operation of the mission. Location of the parking orbit periapsis affects the choice of landing sites and visibility constraints for landing. Parking orbit inclination affects the ΔV budget for moon rendezvous and Mars landing.

The dashed lines of figure 16 are inertial traces of the parking orbit ground track for the first revolution after MOI and the final revolution prior to TEI 300 days later. The solid bell-shaped curve shows the positions of periapsis at the time of MOI and TEI and at 50-day intervals during the orbital stay time. Also, the apparent path of the Sun around Mars is shown at 50-day intervals between MOI and TEI. This figure illustrates several features important to the Mars orbit operations during the 1977 mission window.

1. The spacecraft has an opportunity for close photography of Mars through two seasonal variations in each of both hemispheres.

2. The parking periapsis sweeps through a wide range in latitude, from -12° to 20°, thus providing flexibility in landing site selection with the lander deorbit maneuver occurring at periapsis.

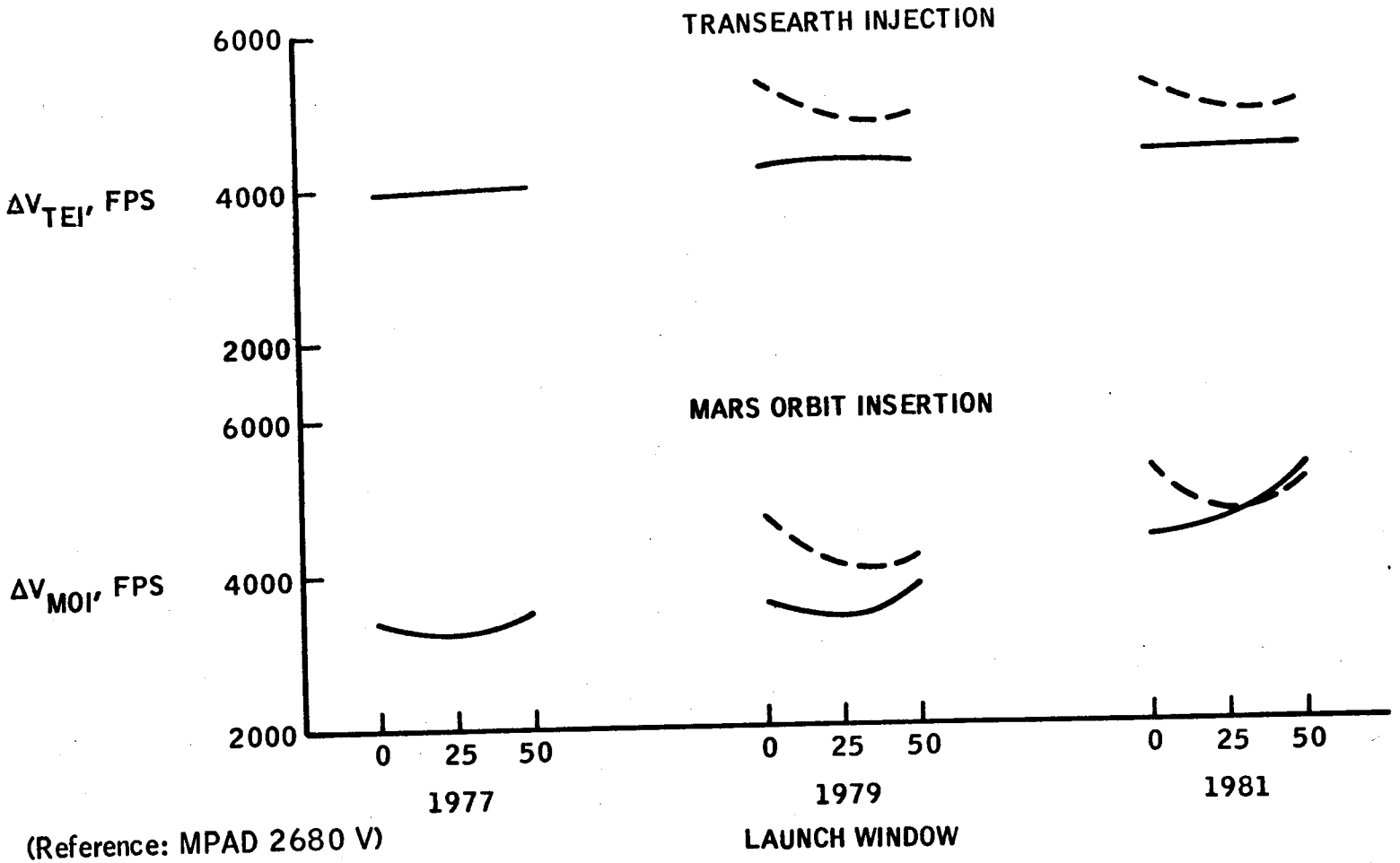

(Reference: MPAD 2680 V)

Figure 15.- Variation of velocity requirements for Mars orbit insertion and transearth injection during the mission window.

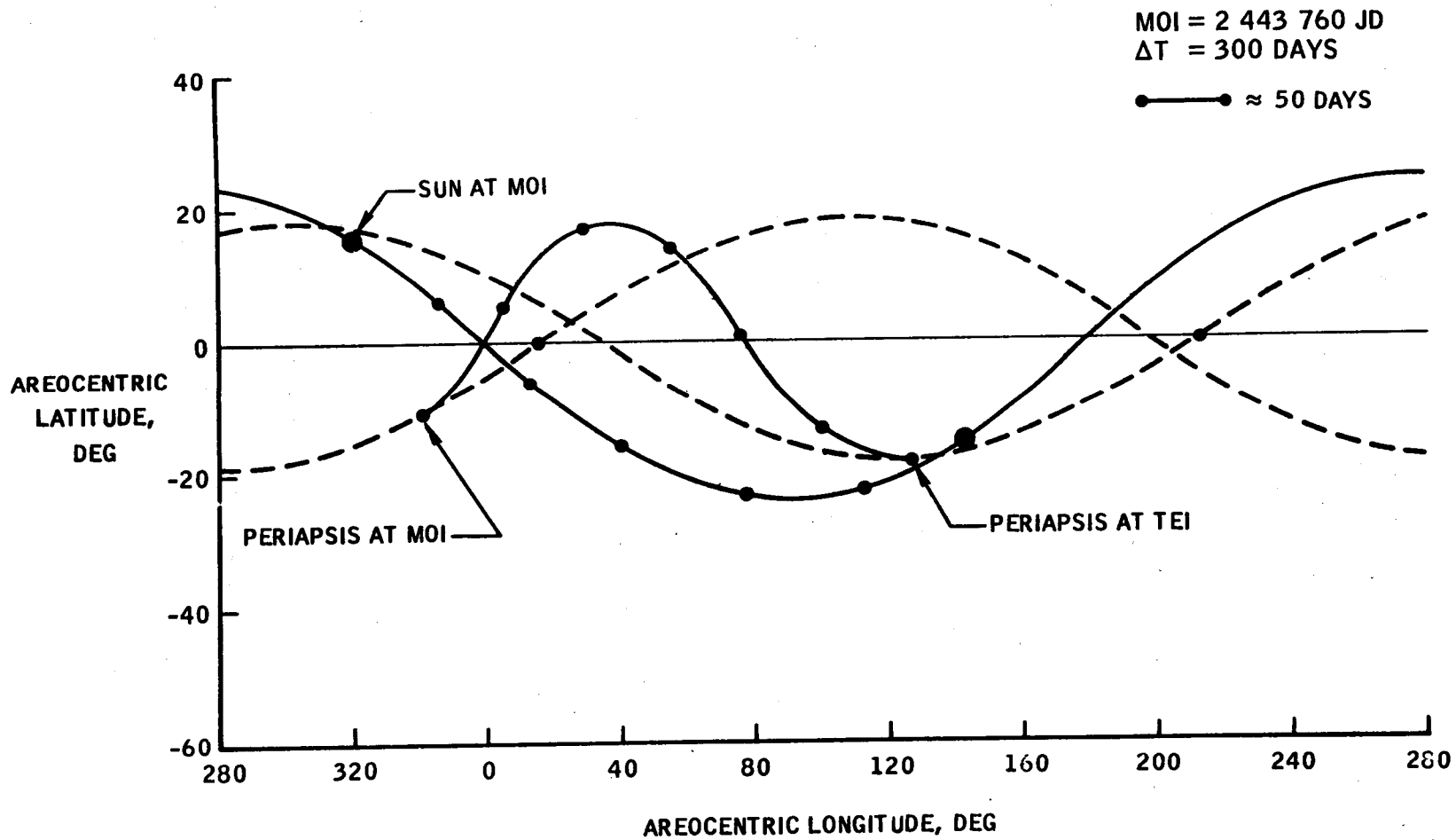

(Reference: MPAD 2681 V)

Figure 16.- The planetocentric position of the parking orbit periapsis and the subsolar point during Mars orbit stay in 1977.

3. The periapsis crosses Mars equator twice, about 40 days after MOI and again at 200 days after MOI. This fact is crucial to minimize plane-change requirements for moon rendezvous.

4. The periapsis "chases" the Sun. Thus the position of periapsis remains in full sunlight for the entire duration of the planetary visit.

These features are also characteristic of parking orbits available during the 1979 and 1981 mission opportunities as shown in figures 17 and 18.

Figure 19 shows the position of orbital periapsis relative to the subsolar point for three nominal parking orbits corresponding to the beginning of each of three launch windows. The curves show the motion of periapsis relative to the Sun during the orbital stay. For the greatest portion of the planetary visit, the high disparity between the declination of the Sun and periapsis insures that the apoapsis will also be in sunlight, and the spacecraft will pass through Mars shadow for only very short periods of each revolution - an important consideration since solar cells may be the spacecraft's primary power source. When the relative declination is near zero (which occurs twice during each sample mission), apoapsis will be in darkness. Thus, the spacecraft will be without solar power for no more than 20 percent of each revolution, which represents time in shadow for the worst case illustrated in figure 20.

3.4 Martian Moon Rendezvous

One of the primary objectives of a long-stay-time Mars orbital mission could be a manned visit to one of the Martian moons, Phobos or Deimos. Their orbital and physical characteristics are summarized in table V. The moons have nearly circular equatorial orbits, and their small sizes indicate the necessity for regarding a moon landing as a rendezvous problem. A preliminary moon rendezvous profile and ΔV budget are presented in figure 21 and table VI in order to demonstrate the feasibility of using an Apollo LM ascent stage for the moon rendezvous spacecraft.

For the moon rendezvous profile shown in figure 21, it is assumed that correct orbital phasing is maintained throughout the rendezvous maneuver sequence. Orbital phasing could significantly increase the total trip time required for a moon rendezvous and subsequent return to the spacecraft. It is possible to indicante the minimum total trip time by considering the periods of the moons' orbits and the required transfer orbits. The respective periods of revolution of the near and far moons are 7.6 and 30.3 hours. The periods of the transfer orbits to a direct moon rendezvous from the parking orbit are 20 hours for the near moon and 30 hours for the far moon. Assuming the rendezvous craft station-keeps for one moon orbital revolution, the minimum possible total trip time is about 30 hours for the near moon

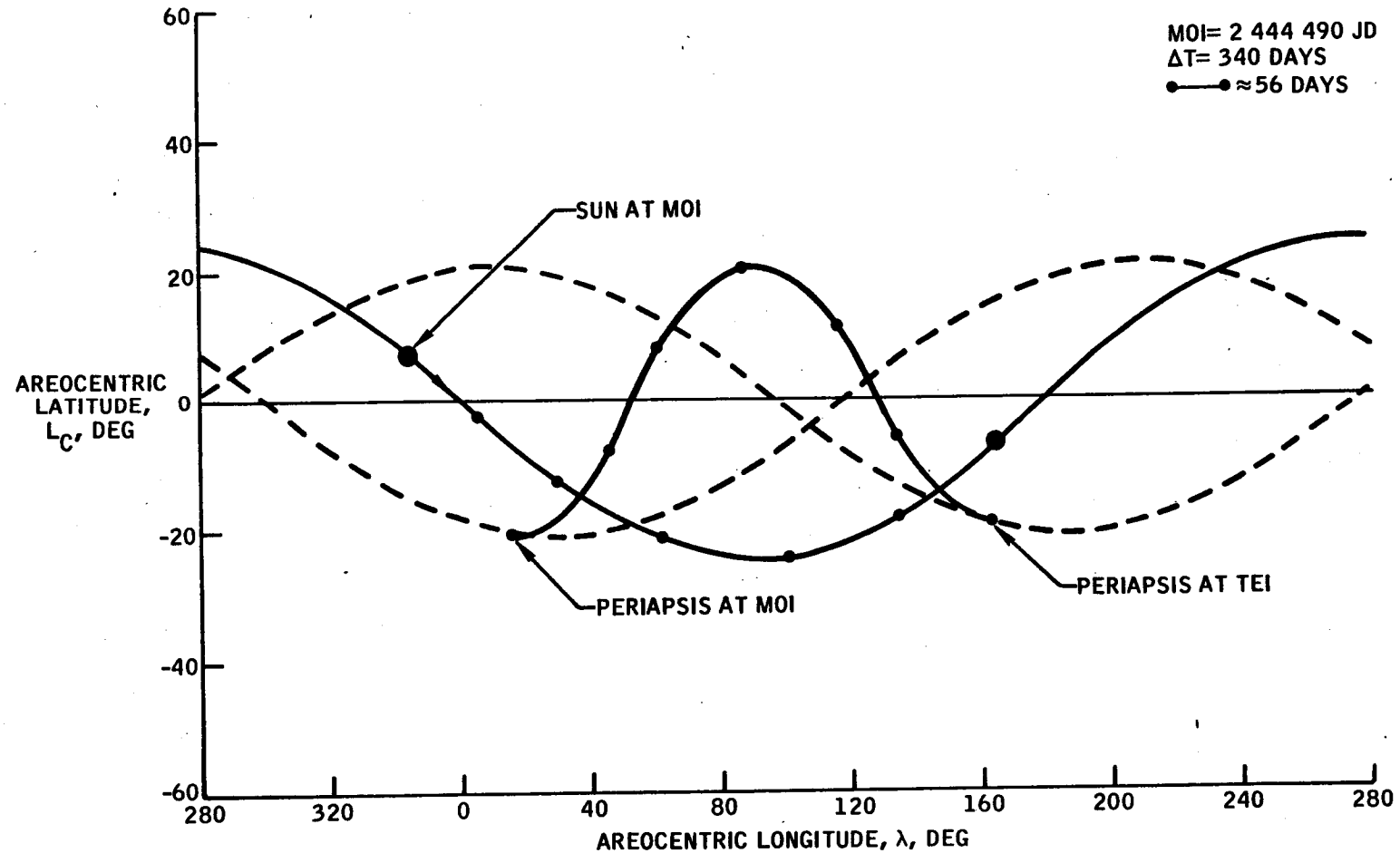

Figure 17.- The planetocentric position of periapsis and the subsolar point during Mars orbit stay in 1979.

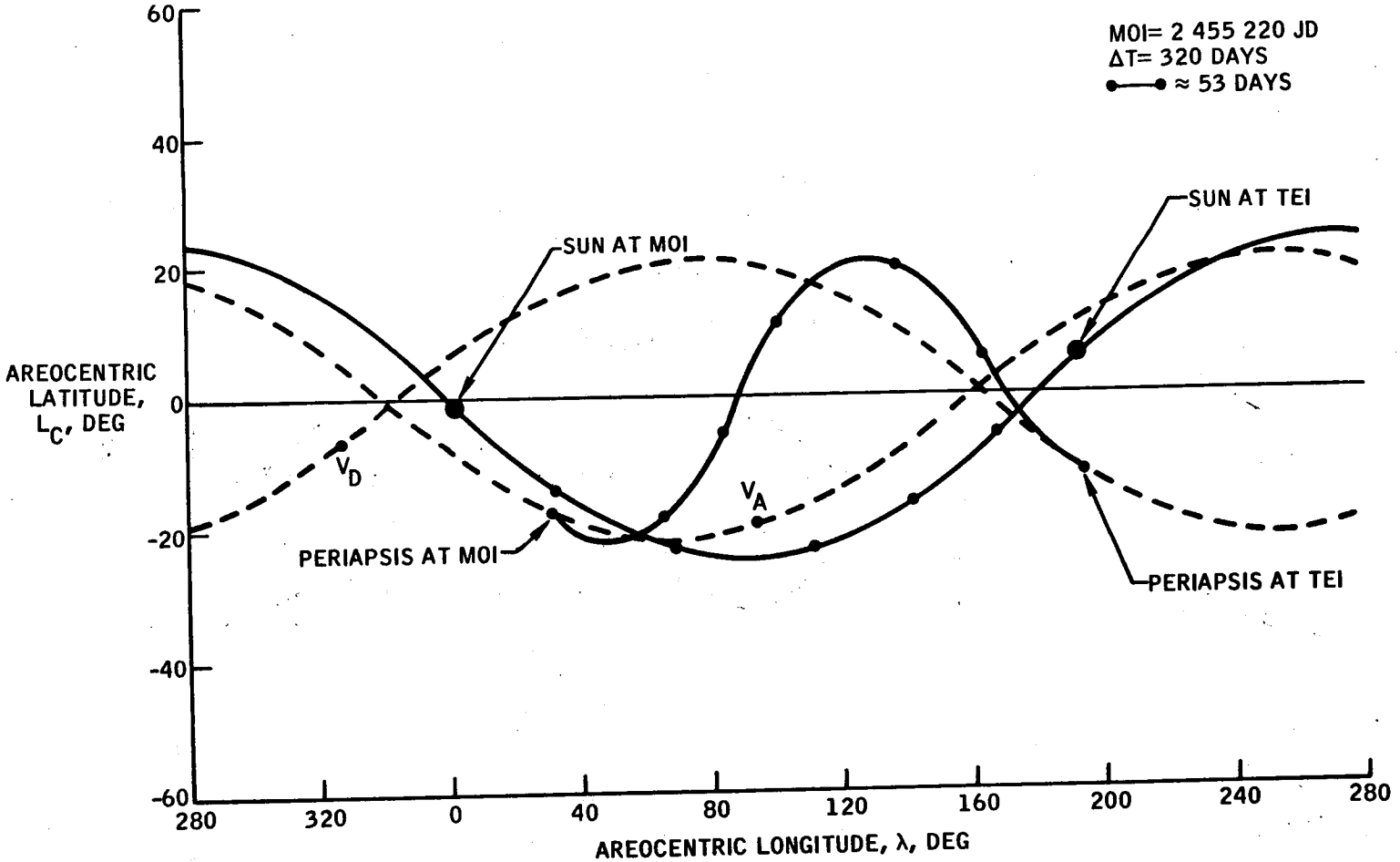

Figure18.- The planetocentric position of periapsis and the subsolar point during Mars orbit stay in 1981.

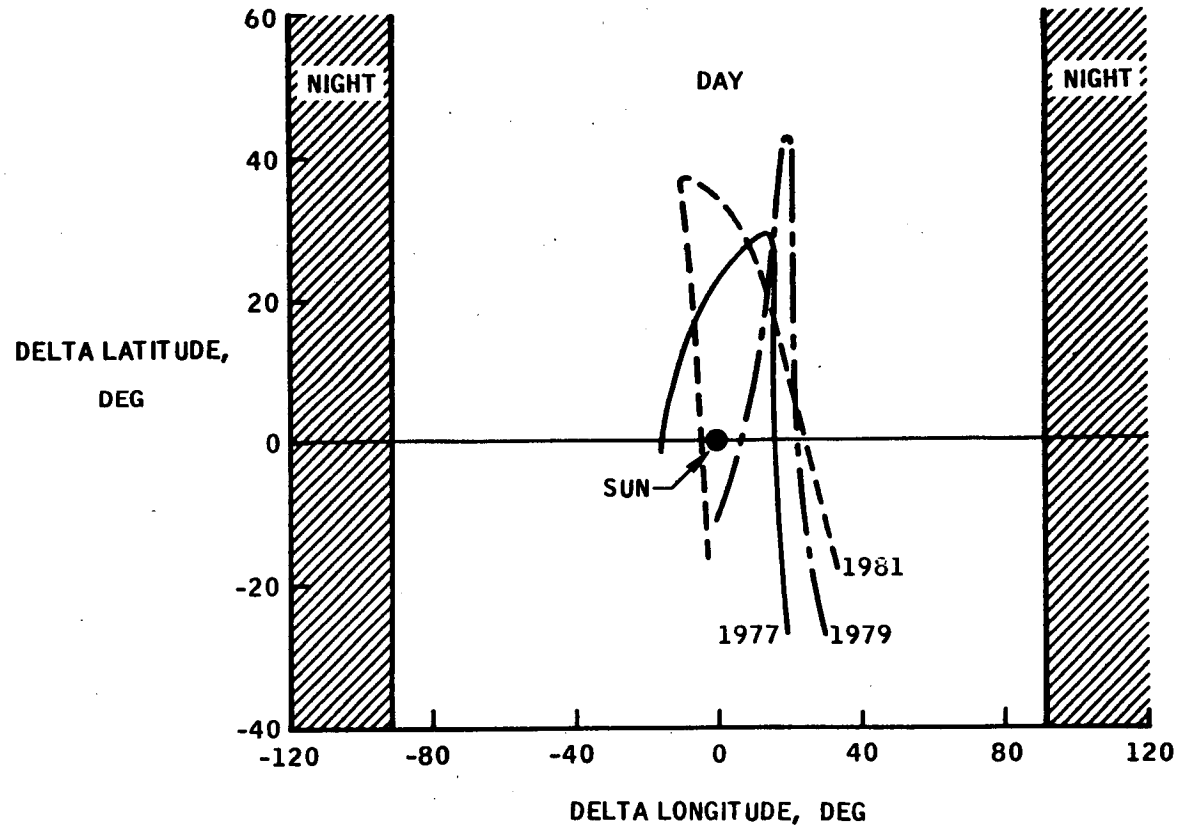

(Reference: MPAD 2682 V)

Figure 19.- The position of orbital periapsis relative to the subsolar point.

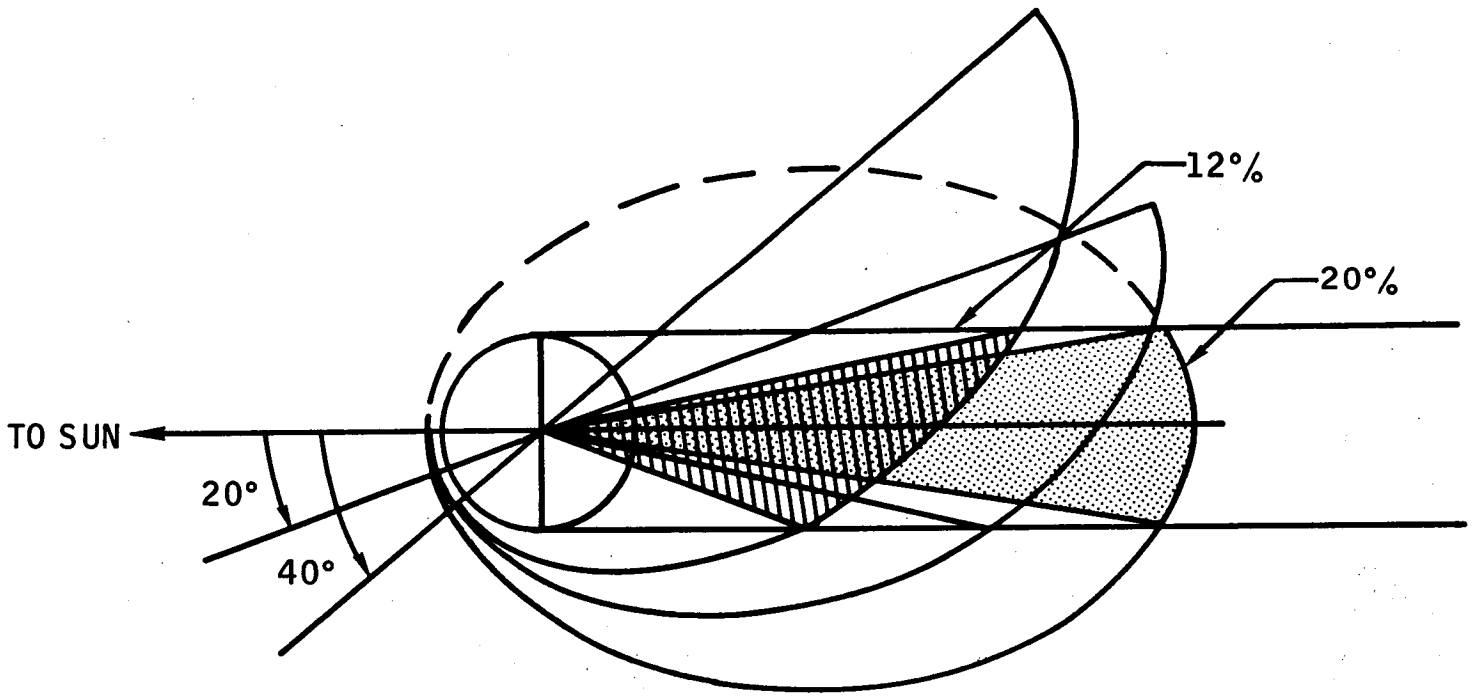

Figure 20.- Time in Mars shadow for zero relative declination between periapsis and the subsolar point.

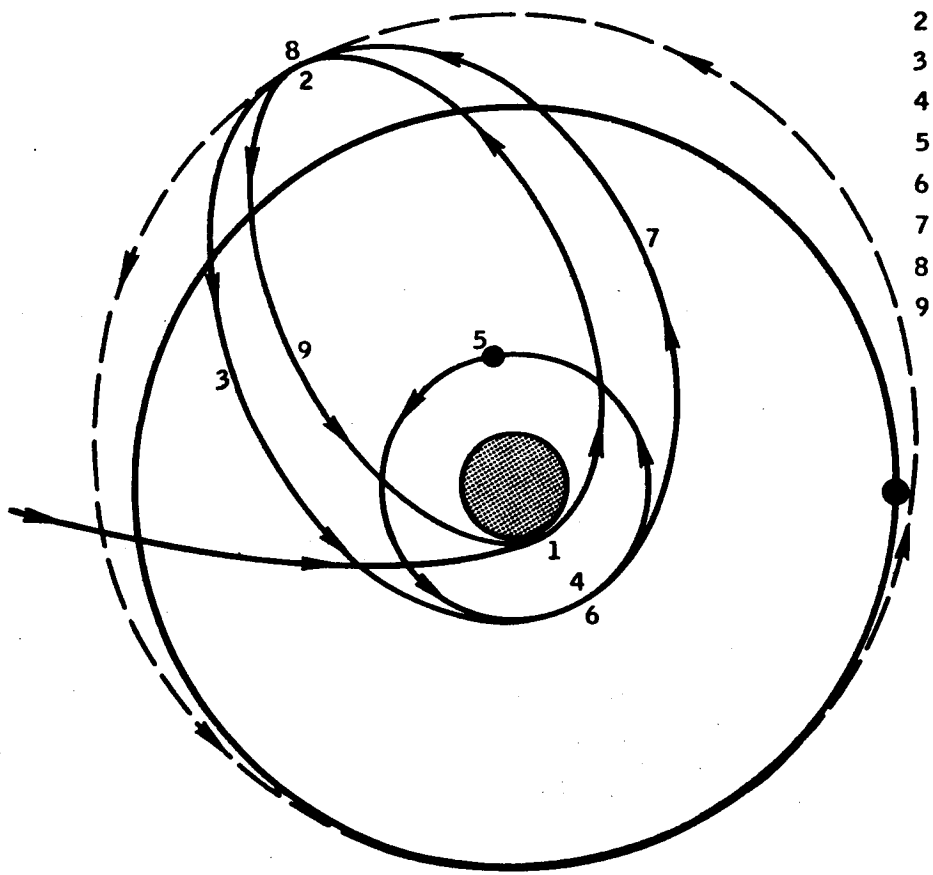

1. PARKING ORBIT INSERTION
2. LM/SC SEPARATION
3. MIDCOURSE
4. LM CIRCULARIZATION
5. LM/MOON RENDEZVOUS
6. LM INJECTION
7. MIDCOURSE
8. LM TRANSFER TO PARKING ORBIT
9. LM/SC RENDEZVOUS

(Reference: MPAD 2685 V)

Figure 21.- Maneuver sequence for Martian moon rendezvous.

TABLE V.- CHARACTERISTICS OF THE SATELLITES OF MARS

Physical characteristics

Parameter	Phobos	Deimos
Radius, n. mi.	5048	12 689
Altitude, n. mi.	3204	10 845
Period, hr	7.65	30.32
Speed, fps	7034	4436
Inclination, deg:min	1:08	1:46
Eccentricity	0.021	0.003

Orbital characteristics

Parameter	Phobos	Deimos
Diameter, n. mi.	8	5.3
Surface gravity[a], ft/sec^2	.037	.025
Circular velocity[b], fps	30	20
Escape velocity[a,b], fps	42	28

TABLE VI.- ΔV BUDGET FOR THE MARTIAN MOON RENDEZVOUS

Event	Near moon, Phobos				Far moon, Deimos			
	Apoapsis altitude of parking orbit[c], n. mi.				Apoapsis altitude of parking orbit[c], n. mi.			
	9000	10 845	12 400	30 000	9000	10 845	12 400	30 000
LM/SC separation, fps	1122	1 010	931	492	169	2 100	1 967	1 142
LM/Moon midcourse, fps	50	50	50	50	50	50	50	50
LM/Moon circularization, fps	1183	1 380	1 514	2 208	2100	0	126	869
LM/Moon rendezvous, fps	100	100	100	100	100	100	100	100
LM/Moon separation, fps	1183	1 380	1 514	2 208	2100	0	126	869
LM/SC midcourse, fps	50	50	50	50	50	50	50	50
LM/SC transfer, fps	1122	1 010	931	492	169	2 100	1 967	1 142
LM/SC rendezvous, fps								
Total ΔV, fps	4810	4 980	5 090	5 600	[d]4738	4 400	4 386	4 222

[a]Density assumed to be same as Earth.

[b]At surface.

[c]Periapsis is 200 n. mi.

[d]LM/SC separation at periapsis of Mars parking orbit.

and 60 hours for the far moon. It thus appears that a moon rendezvous would require 2 to 5 days total trip time.

The ΔV budget presented in table VI shows the impulsive ΔV cost to perform a moon rendezvous and subsequent return to the spacecraft. Three different parking orbits were used to assess the effect of parking orbit apoapsis altitude on the moon rendezvous ΔV budget. Table VI does not include the ΔV cost to make the plane change between the parking orbit and the moon orbit. The ΔV budget indicates a LM/moon rendezvous can be performed from the nominal parking orbit for about 5000 fps for the near moon, Phobos, and 4500 fps for the far moon, Deimos, if the nominal parking orbit is equatorial.

Figure 22 shows the plane-change ΔV requirement as a function of parking orbit inclination and the declination of the line of apsides. The solid curves marked with a 20° out-of-plane angle represent the nominal parking orbit. The periapsis of the nominal parking orbit crosses Mars equator twice during the orbital stay, after 40 days into the orbital phase and again after 200 days. At these time, the declination of the line of apsides is zero, and the plane change requires about 750 fps. Since the LM must return to the spacecraft, the total plane-change ΔV would be about 1500 fps. The total required ΔV for moon rendezvous then would be 6000 fps for the far moon and 6500 fps for the near moon.

Since the LM ascent stage has a ΔV capability of 7000 fps, it appears feasible that a vehicle of this size could be used to rendezvous with either Martian moon from the nominal parking orbit. Life support and crew quarters would be required for periods on the order of 5 days.

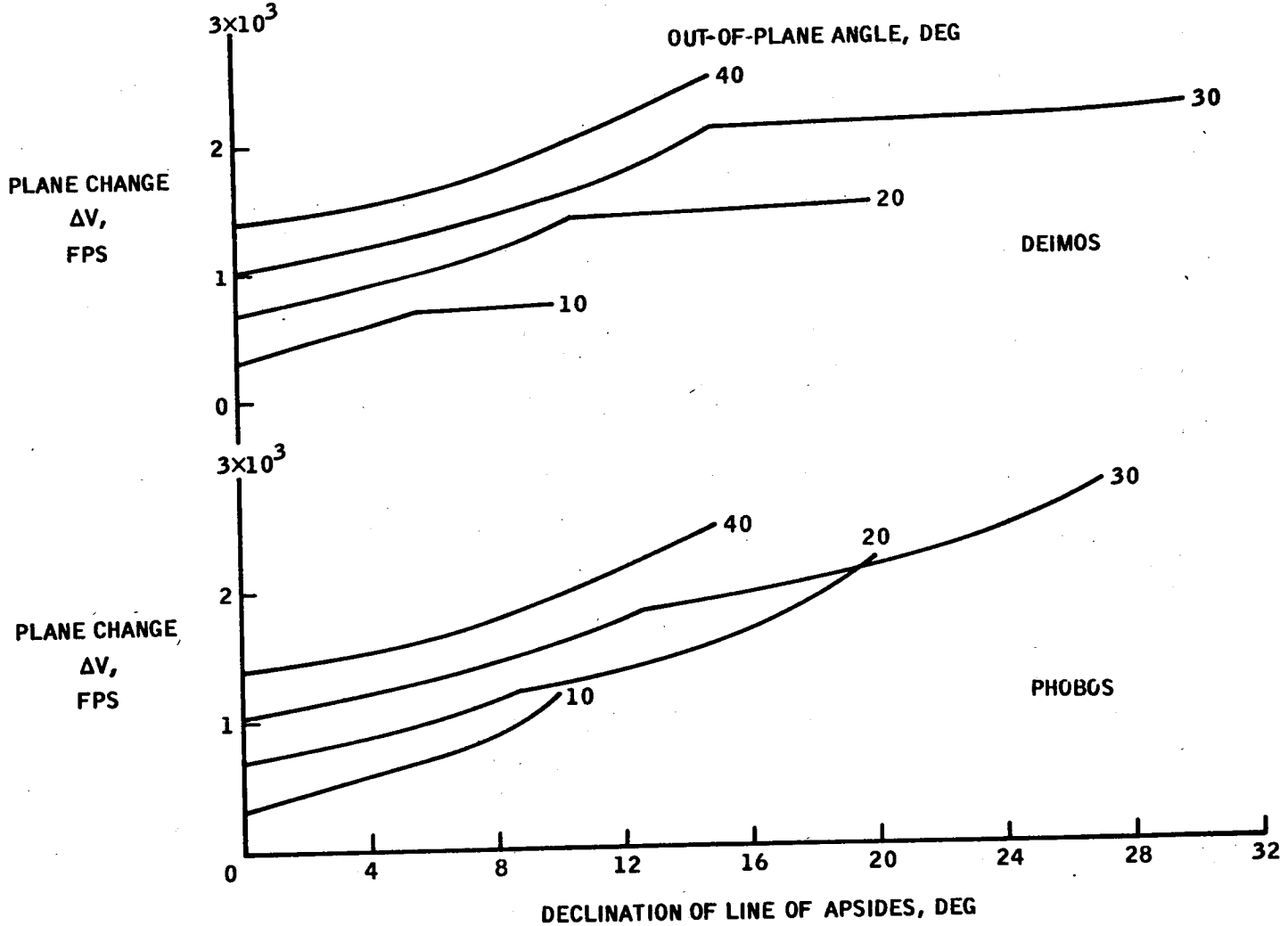

(Reference: MPAD 2682 V)

Figure 22.- Plane change ΔV requirements for Martian moon rendezvous.

4.0 NAVIGATION AND GUIDANCE

4.1 Introduction

When considering interplanetary missions involving long-time durations and a planet stopover, it is necessary to analyze the effectiveness of current navigation and guidance techniques for such missions. Looking at the Mars stopover mission as three principal phases - the outbound, orbital, and return phases - a complete navigation and guidance analysis can be performed. From this analysis, delivery accuracies can be determined and a midcourse velocity budget established. The principal questions which need answering are "what navigational accuracy can be obtained?" and "what is the fuel cost for guidance maneuvers in each mission phase?"

The 1977 Mars stopover mission was chosen as the reference mission for the navigation and guidance study. This mission consists of a 360-day outbound phase, a 300-day stay time in orbit about Mars, and a 320-day return phase. A schematic drawing of the midcourse navigation and guidance profile of this mission is presented in figure 23. The orbits of Earth and Mars about the Sun are represented by the inner and outer circles, respectively, and the trajectory of the spacecraft is represented by the dashed lines. The respective dates of departure and arrival at both planets are noted. The shaded areas around Earth and Mars represent the sphere of influence (SOI); the radius of the Earth's sphere of influence (ESOI) is about 500 000 n. mi., and the radius of Mars' sphere of influence (MSOI) is about 300 000 n. mi.

In the analysis, a combination of Earth-based tracking and onboard sextant measurements was assumed for navigating the spacecraft; a radar system onboard the spacecraft was assumed for tracking of any unmanned landers or probes which are deployed from the spacecraft during the approach to Mars. All navigation data were processed by a Kalman filter to reduce the uncertainties in position and velocity of the spacecraft and the lander. Fixed- and variable-time-of-arrival guidance were used to compute the velocity corrections and appropriate target dispersions.

The pertinent navigation and guidance system equations can be found in references 13, 14, 15, and 16. Reference 16 also contains additional information about the navigation and guidance systems performance for a 1977 Mars stopover mission.

4.2 System Errors

The navigation and guidance system errors assumed for the analysis are listed in table VII. Only errors in range and range-rate were

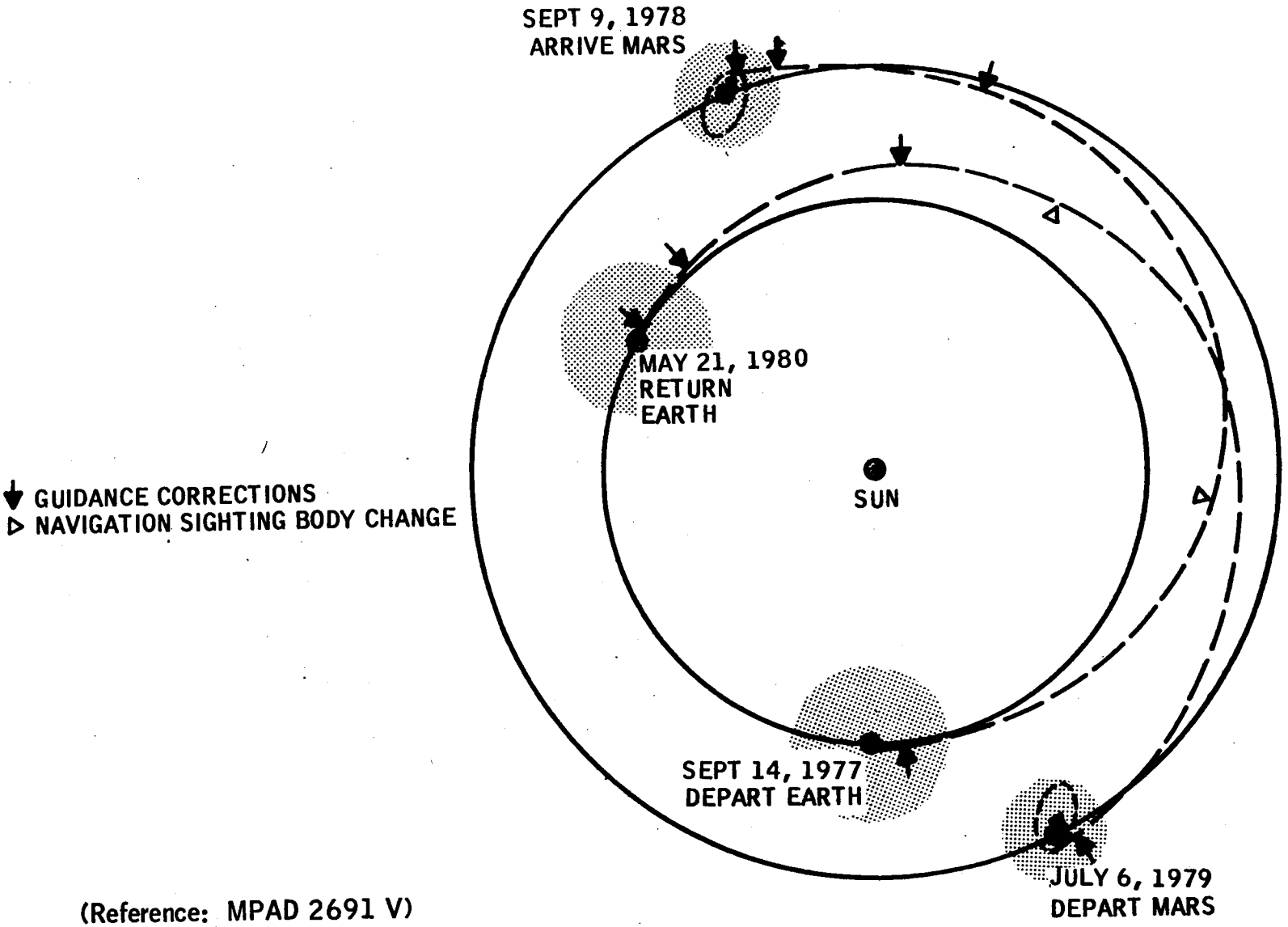

(Reference: MPAD 2691 V)

Figure 23.- Midcourse navigation and guidance profile.

TABLE VII.- 1σ RMS ERROR SOURCES OF THE NAVIGATION AND GUIDANCE SYSTEMS

Earth-based navigation system	
Range, ft	$20 \leq \sigma_\rho \leq 200$
Range-rate, fps	$0.5 \leq \sigma_{\dot{\rho}} \leq 2$
Station location	0
Astronomical constants	0
Onboard navigation system	
Sextant, arc sec	10
Radar, ft, fps	20, 0.5
Astronomical constants	
Ephemeris, n. mi.	100
Earth radius, n. mi.	4
Mars radius, n. mi.	10
Guidance system	
Proportional, percent	1
Pointing, deg	1
Cutoff, fps	1/2

assumed in the Earth-based navigation system. These error components were assigned rather conservative nominal values in order to partly compensate for not including errors in other components of this system at the present time. The lower values listed for both range and range-rate errors represent the initially assigned values. The higher values represent the maximum obtained by computing range and range-rate errors as a function of time.

For the onboard system, a 10-arc second sextant was assumed for all optical measurements in order to consider the effects of not only readout error but also other possible contributing errors in the use of the sextant. The error values assigned to the onboard radar were arbitrarily chosen to be the same as those for the lower bound of the Earth-based tracking range and range-rate errors. The ephemeris error assumed relates directly to a lack of knowledge of the position of a celestial body when sighting to it during the heliocentric phase of an interplanetary mission. The Earth and Mars radius errors relate to the inability to determine the center of the planet when making optical sightings to the planet.

The nominal errors for the guidance system are also listed in table VII. These proportional, pointing, and cutoff errors are directly related to accelerometer bias and scale factor errors, gyro drift and platform misalignment, and engine tailoff errors, respectively.

4.3 Outbound Phase (Spacecraft)

The outbound phase is the portion of the mission from injection at Earth to arrival at Mars periapsis. For this phase, an Earth-based tracking system was assumed for navigation within the ESOI. Outside the ESOI, navigation by an onboard system was assumed so that errors in the ephemerides of the planets could be included. During the heliocentric part of the trajectory (i.e., the portion between the ESOI and the MSOI when the Sun is the central body of the conic), star-planet included angle measurements were processed at 12-hour intervals. Star selection was random; sighting planet choice was semi-optimum based on range to the planet and optical sighting variances. The Earth was the sighting planet until 140 days into the mission; Mars was the sighting body for the remainder of the outbound phase. With the MSOI, measurement intervals were reduced to 30 minutes, and the type of measurement changed to the star-horizon included angle.

A total of four guidance corrections was implemented. The corrections are shown in figure 23, denoted by arrows spaced on the trajectory according to the times they were instigated in the analysis.

Navigation accuracy data for the outbound phase are shown in figure 24. This figure shows the RMS uncertainty in radius of periapsis

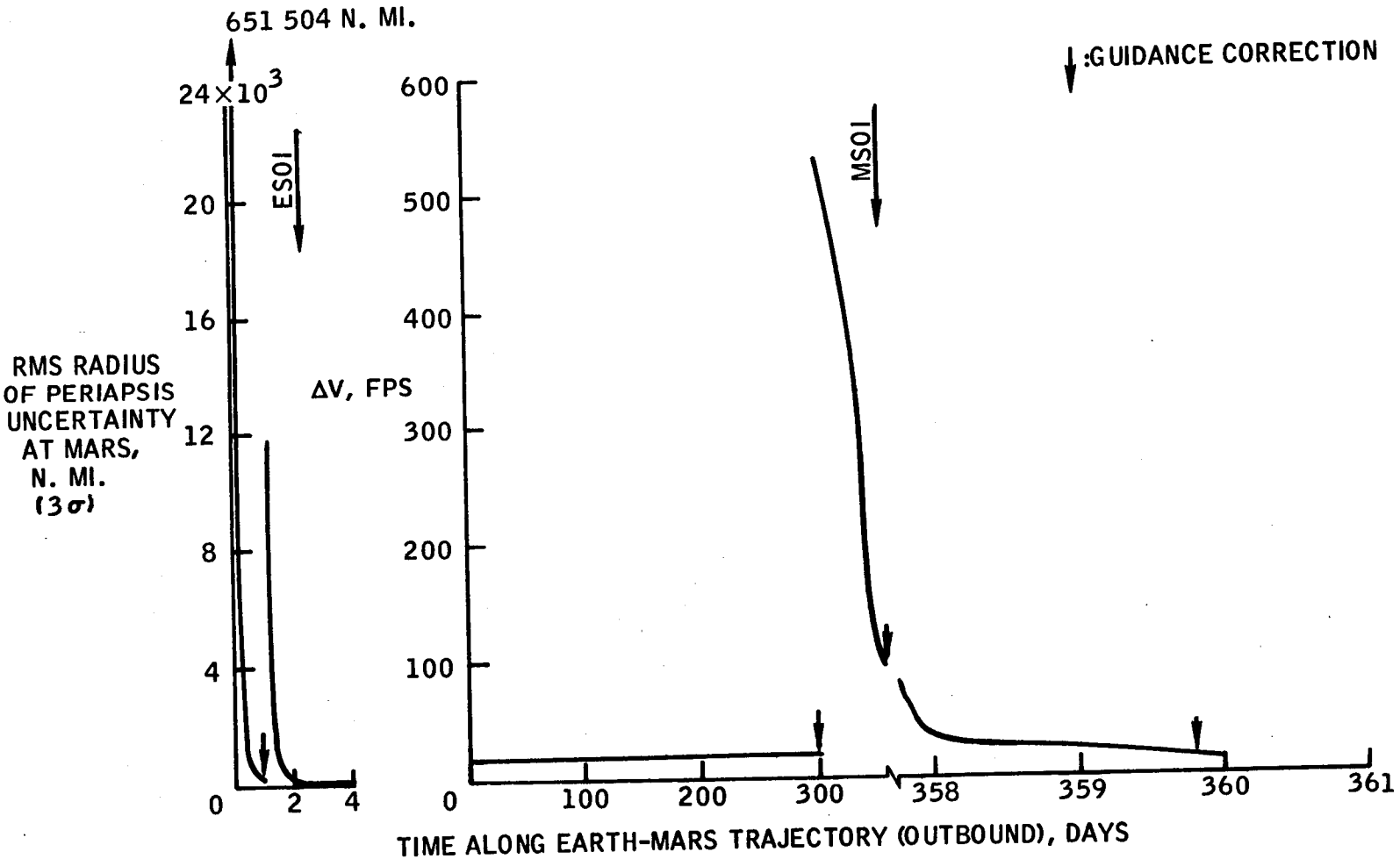

Figure 24-. RMS radius of periapsis uncertainty at Mars for the outbound phase of 1977 Mars stopover mission.

at Mars as a function of the outbound trajectory time. The breaks in the curve after each guidance maneuver show the degradation in estimation accuracy caused by the guidance system. The initially projected uncertainty is quite large but is effectively decreased early in the mission. During the heliocentric portion of the outbound phase the uncertainty remains almost static until it is affected by the second guidance correction. Within the MSOI, the navigation measurements rapidly decrease the estimation error until an end result of approximately 12 n. mi. is obtained.

Figure 25 shows the outbound midcourse ΔV as a function of spacecraft delivery accuracy. From this figure a total outbound ΔV budget can be chosen and the resulting periapsis radius dispersion determined, or vice versa depending on which choice is more critical. The obtainable corridor at Mars can also be seen in this figure by doubling the 3σ value of the root-mean-squared (RMS) dispersion. The last point on the curve on the right-hand side of figure 25 represents the third outbound correction at 60 hours from orbit deboost, resulting in a total ΔV of approximately 222 fps and a radius dispersion at Mars periapsis of almost 80 n. mi.

This dispersion value is a result of the navigation error which forms a lower bound for delivery accuracy. Referring back to figure 24, it can be seen that at this time along the trajectory, the estimation uncertainty of the navigation system is equally as large as the radius dispersion obtained by the third guidance maneuver. Thus, as the navigation estimation uncertainty decreases, the obtainable delivery accuracy increases. Since the dispersion is large, a fourth and final correction is needed and should be executed after the navigation has effectively reduced the estimation uncertainty to a required delivery level. The dashed line in figure 25 probably represents the best choice and the one made for this analysis. That is, for only 270-fps total ΔV, resulting from a fourth correction of 48 fps at 3.5 hours from orbit deboost, a periapsis radius dispersion of 12 n. mi. can be acquired. Also, by inspection of the curve, it is evident that the dispersion gets no better, but rather the required ΔV increases rapidly. As previously mentioned, the lower bound of the accuracy depends greatly on the navigation accuracy; thus, only by improving the navigation accuracy can a better corridor be obtained.

4.4 Outbound Phase (Unmanned Lander)

At approximately the MSOI on the outbound mission phase, an unmanned lander is deployed from the spacecraft to arrive at Mars at some prespecified time. The ΔV required for such a separation is a function of several constraints, such as entry speed, altitude, flight-path angle, and orbital inclination. For this analysis, these parameters were constrained so that a 100-fps deploy ΔV was obtained. With this deploy ΔV of 100 fps,

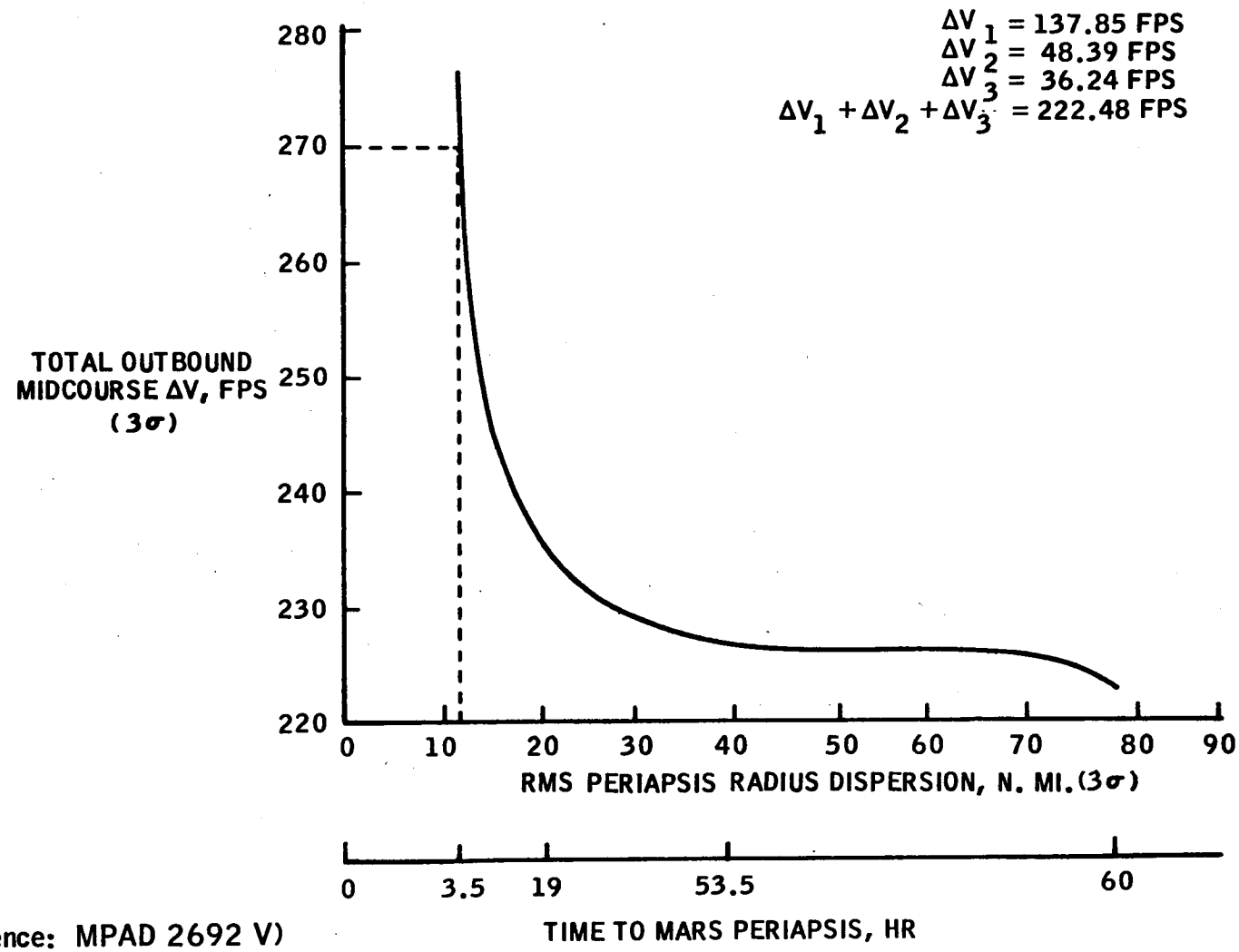

(Reference: MPAD 2692 V)

Figure 25.- Outbound midcourse ΔV as a function of spacecraft delivery accuracy at Mars.

the unmanned lander (or a probe) would reach vacuum periapsis at Mars approximately 40 minutes before spacecraft deboost to orbit. An onboard radar system was postulated for tracking the lander from the spacecraft during the lander delivery. It was assumed that this radar was capable of measuring the relative range and range-rate between the manned spacecraft and the unmanned lander. Note that, since the lander is released from and tracked by the spacecraft, the accuracy of lander delivery is constrained by the spacecraft navigation errors; i.e., delivery accuracies for the lander can never be better than those for the spacecraft.

Figure 26 contains information for the unmanned lander similar to that for the spacecraft in figure 25. In figure 26, the unmanned lander delivery accuracy, given in terms of RMS vacuum periapsis radius dispersion, is plotted as a function of midcourse ΔV. It is obvious that a midcourse correction must be implemented since the delivery accuracy at separation is approximately 80 n. mi. By inspection of the curve, a midcourse correction ΔV can be determined for the lander to achieve a specific vacuum periapsis radius dispersion. In order to obtain a desirable delivery accuracy, it is necessary to wait until 0.8 hour from vacuum periapsis to initiate a midcourse correction. Nothing is gained by waiting longer since the cost is rising sharply and the delivery accuracy does not appear to improve. Thus, by making a midcourse correction at 0.8 hour from vacuum periapsis for the cost of approximately 150 fps, a delivery accuracy of 15 n. mi. can be obtained. The accuracy is somewhat less than that obtained for the spacecraft for the outbound leg; however, it is reasonable to expect a higher ΔV cost for a lander delivery accuracy equal to that for the spacecraft or a slight decrease in accuracy for less ΔV cost because of the effect of separation errors. As pointed out previously, the spacecraft navigation significantly affects the achieved accuracy. Thus, improvements in the navigation system as well as in the manipulation of the measurement schedule should result in improved delivery accuracy for less cost.

4.5 Orbit Phase

When considering an orbit about Mars for the time length of 300 days, questions arise about the type of navigation to use and size of velocity budget needed. For this analysis, the star-horizon included angle measurement was used for navigating the spacecraft in orbit about Mars. Since the orbit in consideration has an apoapsis altitude of approximately 10 000 n. mi. and a period of 12 hours, the star-horizon measurement should prove applicable. However, since the deployment of unmanned landers containing beacons or transponders is also being considered for this mission, two other types of orbital navigation for further study are the known landmark and the unknown landmark techniques utilizing the surfaced beacons and transponders. Techniques for tracking known and unknown landmarks are discussed in reference 17.

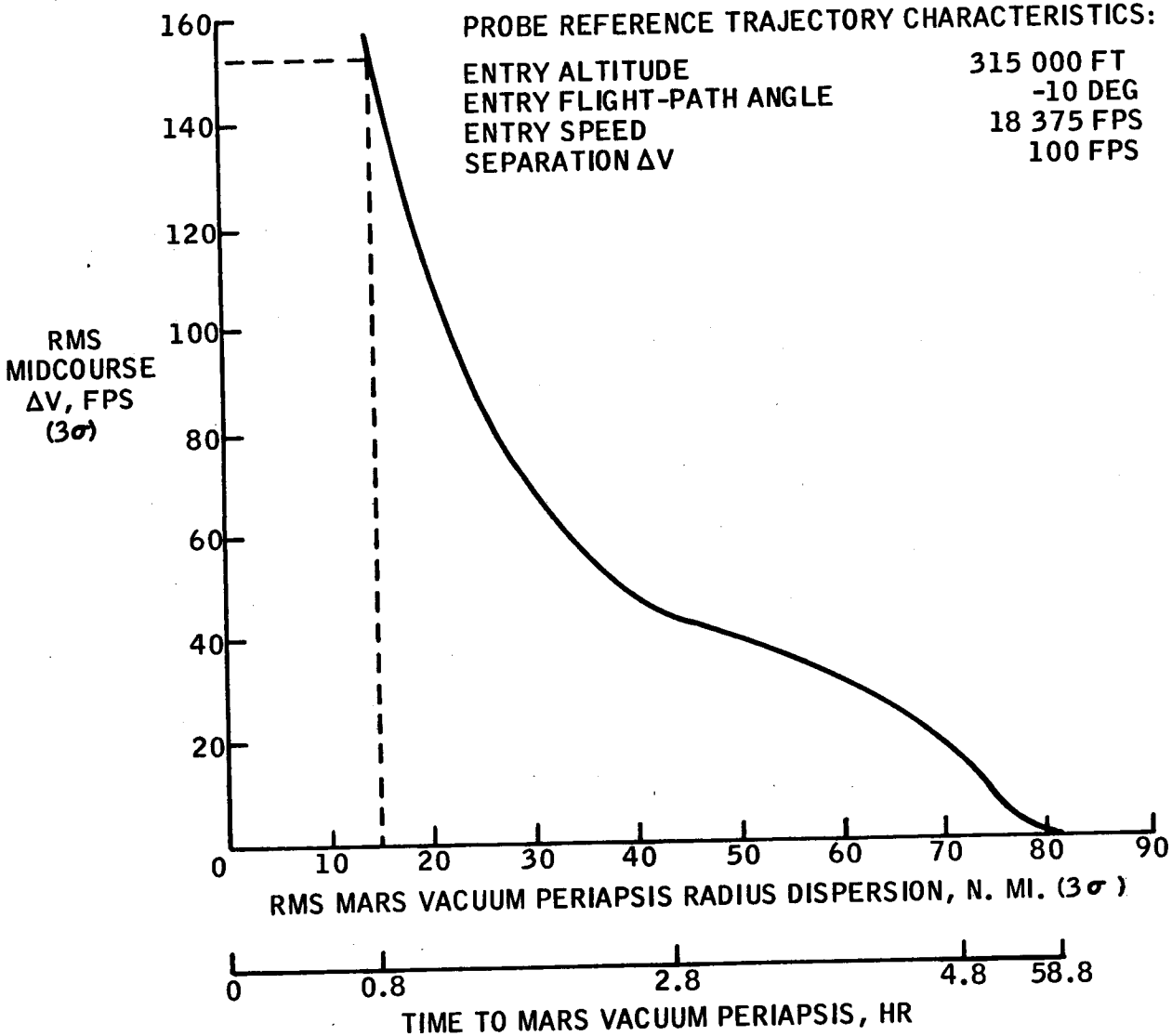

Figure 26.- Unmanned lander (probe) delivery accuracy at Mars.

Figure 27 contains the orbit navigation accuracy when using star-horizon measurements at 1-hour intervals for a 300-day stay time. The RMS position uncertainty is plotted against time in orbit. The most outstanding feature of this figure is the oscillatory effect of the estimated position uncertainty. This effect is probably caused by the geometry of the orbit and the asphericity of Mars, but no specific reason has yet been found. The position uncertainty ranges between approximately 2 and 9 n. mi. (3σ); the mean is approximately 4 n. mi. The principal conclusion which can be drawn from this figure is that the spacecraft can maintain a status quo in orbit using the star-horizon measurement for navigation. The bottom envelope of the curve represents the type of curve one would get if only points at apoapsis were plotted, whereas the top envelope represents that for periapsis. Not shown in this figure, because of the scale, is the oscillation of the curve during one orbit. Thus, the seemingly high point at the end of the orbit stay time (time for TEI) might result in a much lower position uncertainty for a slight delay or another measurement.

Nothing is presented for the guidance during the orbit phase because of the inability to directly apply present guidance techniques for multiple orbits during the 300-day stay. More time is needed for this study. However, we might assume a ΔV budget no worse, and perhaps no better, than that for the outbound leg. It may be found that corrections can be incorporated in other maneuvers or at TEI to conserve fuel.

4.6 Return Phase

The time, navigation scheduling, and guidance corrections of the return phase of the mission are very similar to the outbound phase. Again refer to the mission profile in figure 23. For the navigation, star-Mars horizon included angle measurements were assumed to be made at 30-minute intervals while the spacecraft was within the MSOI. During the heliocentric phase, star-Mars measurements were made at 12-hour intervals until 240 days, when the Earth became the sighting body for the remainder of the return phase to the ESOI. Within the ESOI, all navigation was accomplished by an Earth-based tracking system. The four guidance corrections for the return phase were executed at the same relative times as those for the outbound phase.

Figure 28 contains a plot of the accuracy of spacecraft delivery to Earth as a function of total ΔV required for the return mission phase. This figure contains data for the return phase plotted in the same manner as that for the outbound phase in figure 24. Thus the total return ΔV and the placement of the fourth correction can be determined in a similar manner. No choice is denoted on the figure because of the lack of space. However, by inspection, one can see that the most probable choice would be a fourth correction of 60 fps at 2.5 hours from Earth periapsis,

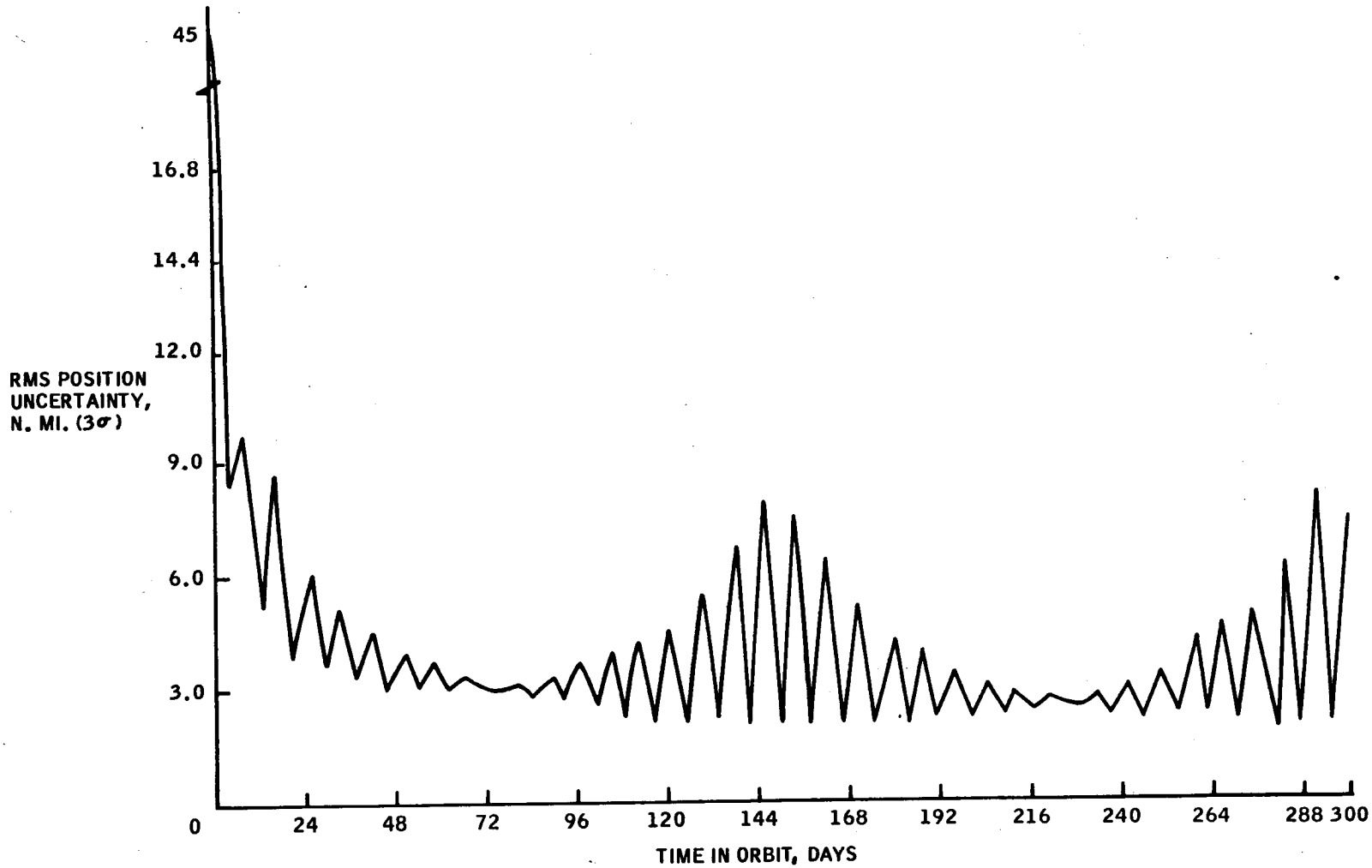

(Reference: MPAD 2695 V)

Figure 27.- Orbit navigation accuracy (3σ).

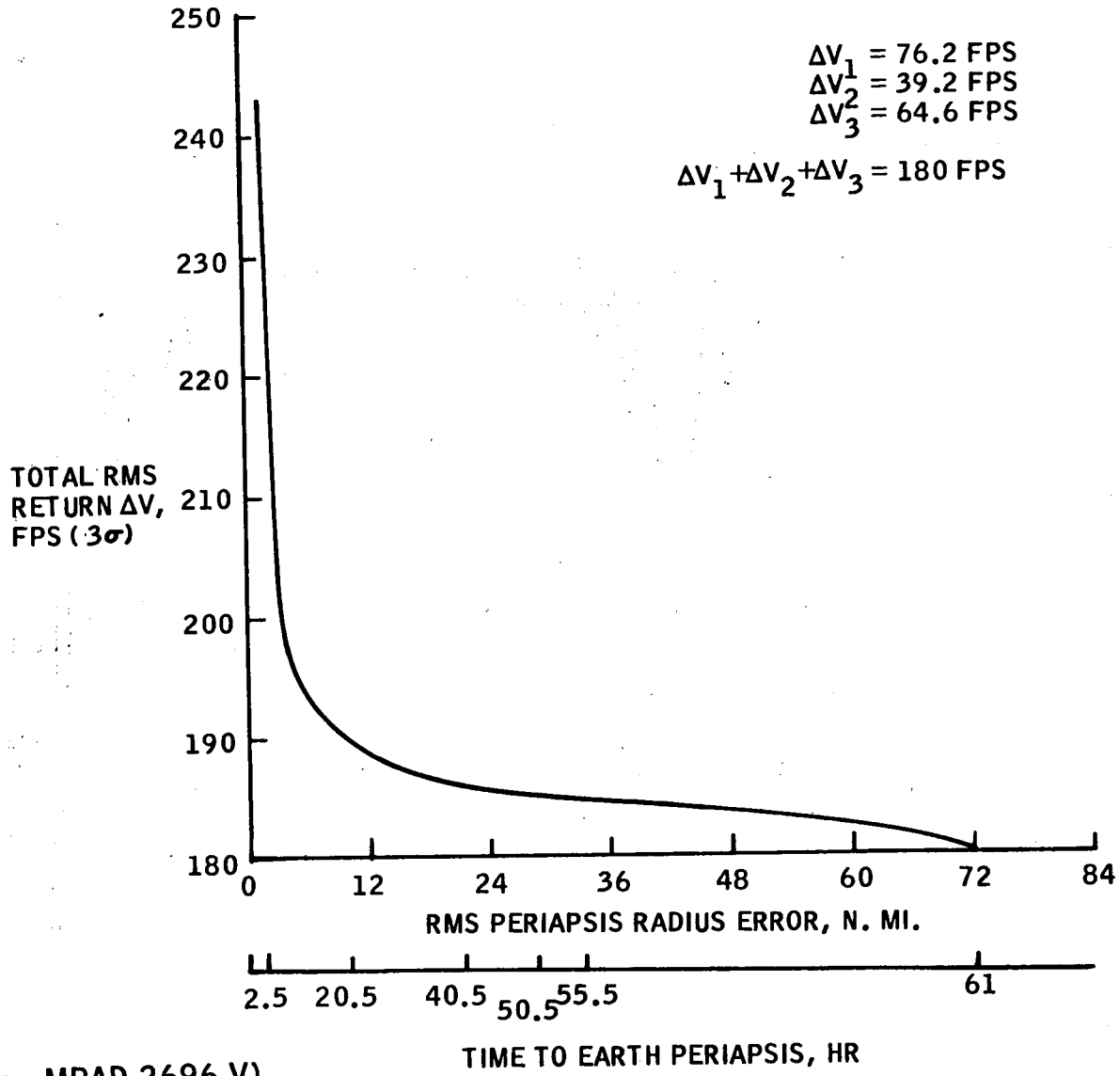

(Reference: MPAD 2696 V)

Figure 28.- Return midcourse ΔV as a function of spacecraft delivery accuracy at Earth.

resulting in a total return ΔV of 240 fps and a 1.8-n. mi. periapsis radius dispersion. The improvement of the dispersion at Earth on returning as compared to that at Mars for the outbound phase is a result of the improved navigation accuracy from the Earth-based tracking within the ESOI.

A summary of the midcourse ΔV costs for the Mars stopover mission is listed in table VIII. The costs represent 3σ delivery accuracies of approximately 12 n. mi., 15 n. mi., and 2 n. mi. for the spacecraft outbound, probe delivery at Mars, and spacecraft return-to-Earth phases, respectively.

TABLE VIII.- Midcourse ΔV SUMMARY (3σ)

Earth to Mars, fps	270
Hyperbolic entry of the unmanned lander	
Separation ΔV, fps	100
Midcourse ΔV, fps	150
Mars orbit operations, fps	
Mars to Earth, fps	243

5.0 SYSTEMS REQUIREMENTS

5.1 Introduction

This section outlines a system model capable of flying the low-energy Mars landing mission using current technology and as many modified Apollo systems as possible. This model is used to demonstrate the feasibility of the mission with current technology and to provide the systems model to be used for studying both the operational problems and the effect of the systems on abort and alternate mission modes.

The systems weights and performances presented are supported by studies in references 18 through 24.

5.2 Experiments and Probes

The experimental equipment and probes carried onboard the Mars orbiting spacecraft and the manned landing module (also called the Mars excursion module or MEM) are designed (1) to answer the major scientific questions about the target planet and the interplanetary medium, and (2) to obtain the mapping and atmospheric data required to support the manned landing operation.

The experiments, probes, and mapping equipment carried onboard and the support of Earth-based analysis of telemetered data are intended to provide a mission capability which requires no prior space flights to Mars. The low-energy requirements of the mission permit sufficient mapping and survey equipment to fulfill all the scientific objectives as well as provide atmospheric and soft-lander probes to support the landing operations. The long stay time in Mars orbit (i.e., 300 days or more) permits extensive surface mapping and landing site selection after the spacecraft arrives in orbit about Mars.

The probes and experimental equipment to be carried onboard the spacecraft can be divided into the following catergories:

1. Interplanetary research and orbit mapping and survey equipment (onboard the spacecraft).

2. Mars unmanned soft-lander probes.

3. Mars atmospheric sounding probes.

4. Manned Martian moon rendezvous module (MMRM).

5. Manned landing module.

A summary of the experimental equipment and probe weights for a single mission is shown in table IX. The experiments list is given in tables X and XI.

The experimental requirements, probe design, and weights for categories 1, 2, and 3 were obtained from the interplanetary flyby mission studies in reference 18. The results of these studies were found applicable to the orbiting and landing missions because the scientific objectives of exploration of the planet are unchanged and the atmospheric sounding probe and soft-lander designs of reference 18 are relatively insensitive to entry velocity. Therefore, these probe designs are applicable to orbiting missions. The manned landing module weight and preliminary configuration are based on reference 19. The two-man, 30-days version of the landing module which returns to a high elliptical orbit is used in this mission. The MMRM is based on the Apollo LM upperstage weights and dimensions.

5.3 Soft-Lander Probes

The configuration of a soft-lander probe is shown in figure 29. The soft lander has mission support requirements in addition to the scientific requirements. The soft lander is to land radar beacons on the surface of Mars to aid the spacecraft in navigation and guidance. Three landers are required for mission support; they are deployed about 120° longitude apart for good tracking coverage. The landers will transmit information on atmospheric characteristics during descent as well as provide Martian surface data and weather information over extended periods of time. These data will be used to support the manned landing operation. The experiments for the soft lander are given in table XI. The soft lander is designed for an entry speed of 20 000 fps so that, if necessary, one or more can be staged hyperbolically on approach of the planet. The design study of reference 18 shows very little change in entry weight. Entry velocity ranges from 20 000 to 42 000 fps. Extrapolation of this data to the orbit entry velocity of 16 000 fps indicates no reduction in weight. The design entry velocity for the soft-lander probe is 20 000 fps and provides for the operational flexibility of probe delivery on planetary approach as well as from planetary orbit.

The soft lander is 10.4 ft in diameter and has a ballistic number of 0.512 slug/ft^2. The entry corridor is 90 n. mi. for the VM-8 Martian atmosphere (ref. 18). The total weight of each lander is 2760 lb, of which 235 lb is scientific and engineering instrumentation. Electrical power is supplied by the radioisotope thermal generator with battery supply for landing and deploying the experiments. The telecommunications system uses a high-gain antenna capable of tracking the orbiting spacecraft.

The atmospheric sounding probe is shown in figure 30. In addition to collecting scientific data, this probe supports the mission by

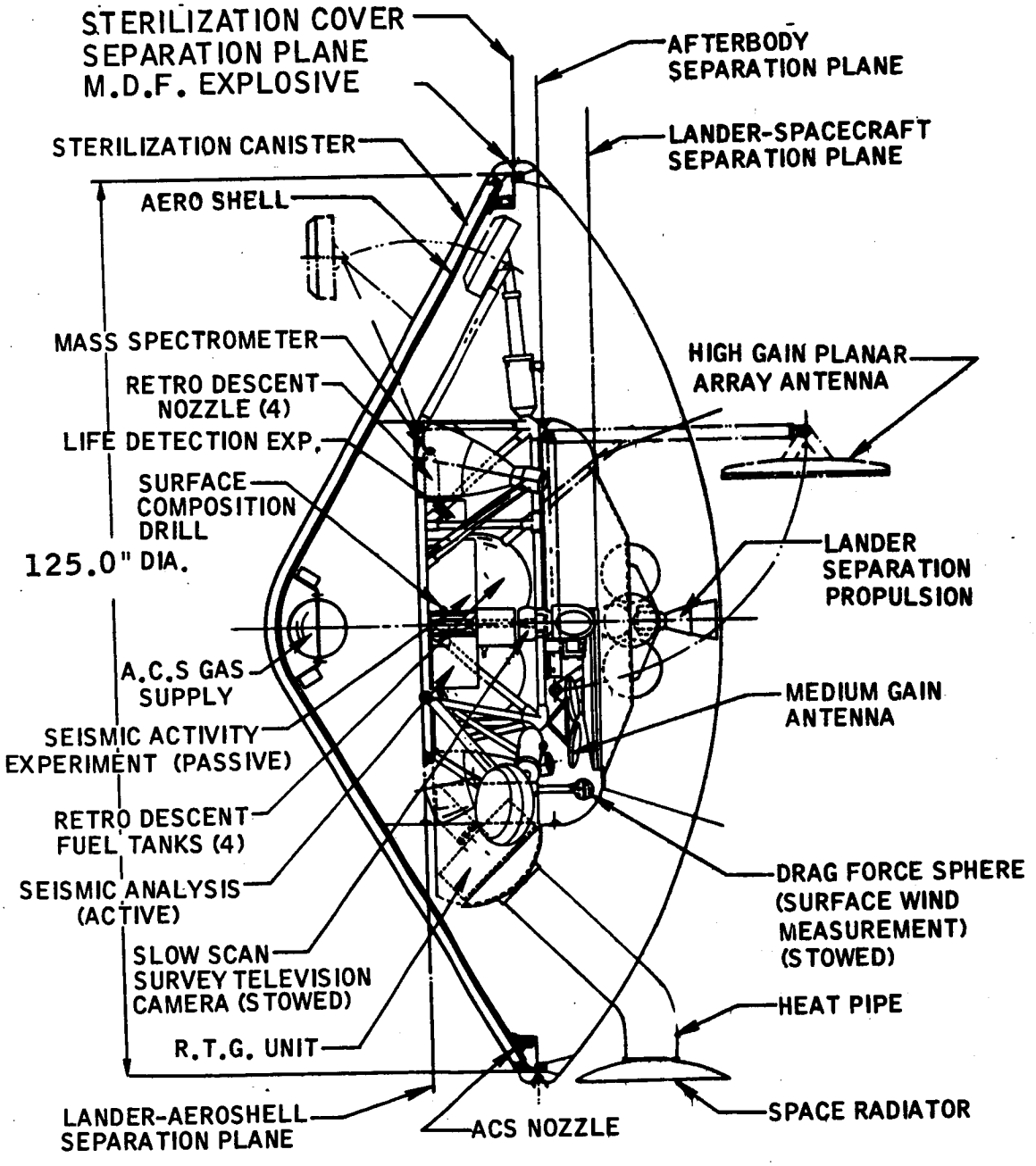

(Reference: MPAD 2701 V) Figure 29.- Mars soft lander.

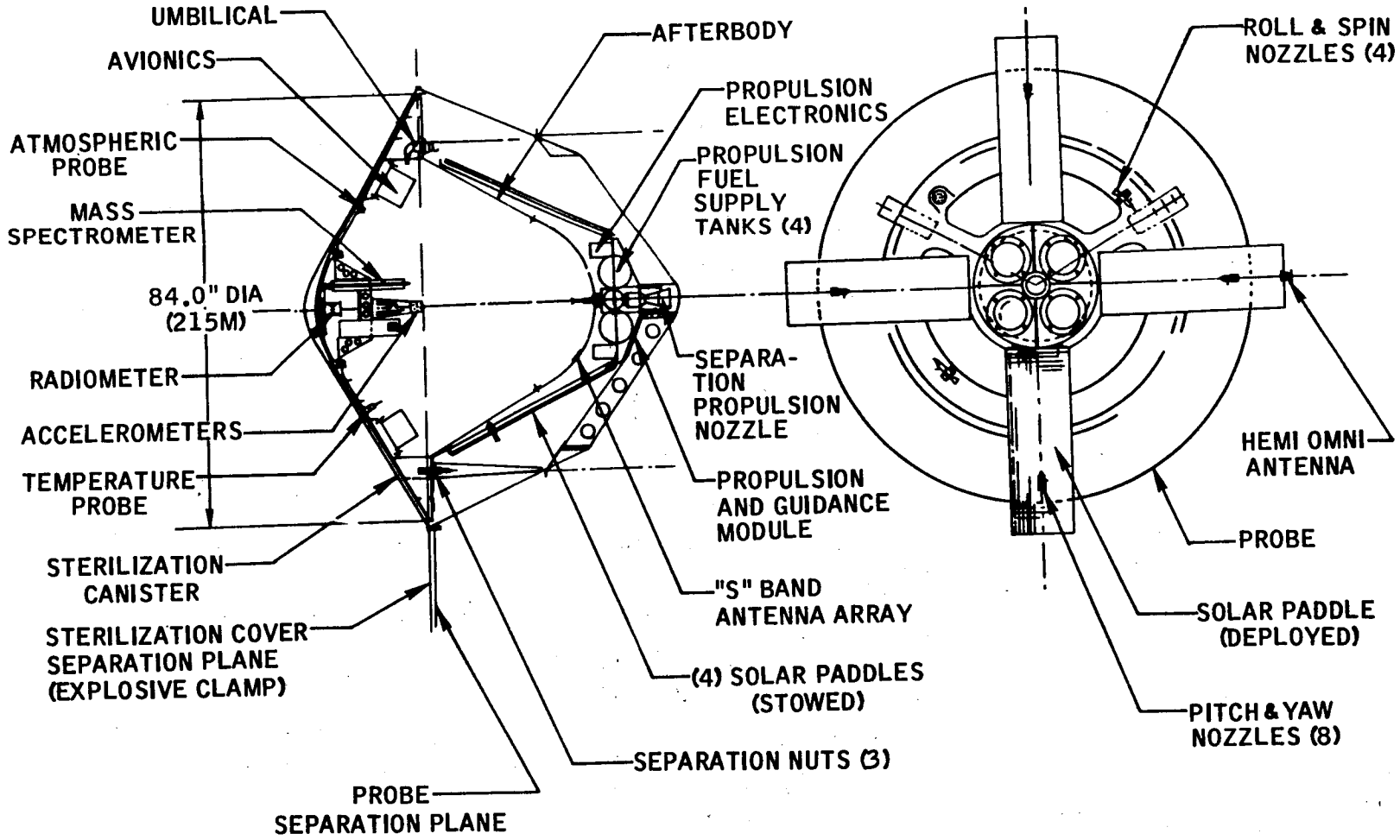

(Reference: MPAD 2702 V)

Figure 30.- Mars atmospheric probe.

TABLE IX.- EXPERIMENTAL PAYLOAD AND PROBE WEIGHTS

	Number of probes	Weight, lb
Mars soft-lander	3	8 300
Atmospheric probes	7	2 040
Onboard spacecraft		6 360
Orbit survey and mapping		2 000
Interplanetary		4 360
Total probes and experiments		16 700
Mars manned lander	1	91 700
Martian moon rendezvous manned probe	1	11 500
Total manned excursion modules		103 200

TABLE X.- ORBITAL AND INTERPLANETARY SPACECRAFT EXPERIMENTS LIST

(a) High priority experiments

Radiation and meteoroid effects on optical thickness
Meteoroid penetrating flux versus thickness
Spacecraft attitude control, holding, and vibration limit
Structures temperature on spacecraft and probes
Subsystem pressures on spacecraft and probes
Cardiovascular reflex activity (orthostatic tolerance)
Exercise tolerance
Thermal regulation
Urine studies
Cardiovascular function
Metabolic studies
Muscular system function
Mineral metabolism
Body fluid balance studies
Incubation of returned samples in C-14 substrates (wet gulliver)
Evolution of radioactive gas (dry gulliver) for life detection
Phosphatase assay of returned samples
Samples - microbiological cultures
Solar radio noise measurements
Stereoheliograph
Solar flare x-ray patrol
Asteroid rotation periods and figures
Meteoroid flux versus mass and velocity
Meteoroid penetration flux
Solar high energy charged particle environment
Figure of planet Mars
Mars surface mapping, high resolution
Mars surface mapping, medium resolution with relief
Mars surface mapping, wide angle

TABLE X.- ORBITAL AND INTERPLANETARY SPACECRAFT

EXPERIMENTS LIST - Continued

(a) High priority experiments - Concluded

RF transmission through Mars atmosphere
Roughness of Mars surface
Radio reflectivity/absorptivity of Mars ionosphere
Mars solar ultraviolet occultation (200 to 3000A)
Engineering flight qualification measurements

(b) Additional balanced objective experiments

Thermal control experiments in deep space
Degradation of thermal coatings and paints in solar plasma
Space environment effects on electronic components
Plastic and electronic materials degradation in space
Structural strain measurements
Spacecraft puncture and crack search detection and repair
High data rate laser communications experiment
Space accumulation of charges on space vehicles
Electrical charge flow along insulating surfaces in space
Gas layer atomic density along space vehicle surfaces
Pulmonary function
Blood studies and hemostasis
Bone demineralization
Visual studies and otilith sensitivity
Mass spectrometry of returned MSSR samples
Gas chromatographic analysis of returned MSSR samples
radiowave passage through solar corona
Gravitational space curvature near Sun
Solar magnetograms
Stereocoronagraph

TABLE X.- ORBITAL AND INTERPLANETARY SPACECRAFT

EXPERIMENTS LIST - Concluded

(b) Additional balanced objective experiments - Concluded

X-ray and ultraviolet coronograph
Ultraviolet spectra of variable stars
Cosmic dust
Zodiacal light
Planetary transits
Stellar parallaxes
Jupiter radio emission
Galactic charged particle environment
Interplanetary magnetic field
Solar wind charged particle environment
Altitude and thickness of clouds in Martian atmosphere
Lander rocket trail photography for wind profile (Mars)
Infrared mapping of Mars atmosphere and surface
Magnetic field of Mars (intrinsic)
Mars magnitudally trapped radiation environment
Solar plasma measurement in vicinity of Mars
Meteoroid flux versus mars and velocity
Survey of Mars meteor trails
Microwave radiomatric study of atmosphere and surface temperature
Atmospheric glow, aurorae at Mars
Photography of Mars satellites
Engineering flight qualification measurements

TABLE XI.- MARS SOFT-LANDER EXPERIMENTAL LIST

Radar beacon for orbit navigation
Mars wind velocity and direction on surface
Mars surface atmospheric density
Mars surface atmospheric pressure
Mars surface temperature and thermal conductivity
Mars atmospheric temperature versus time and altitude
Mars atmospheric composition versus altitude
Mars atmospheric density profile from acceleration measurements
Mars atmospheric density translunar measurements
Mars atmospheric pressure translunar measurements
Mars surface bearing strength and soil penetrability
Detection of extraterrestrial life by bioluminescence
Detection of extraterrestrial life by chemiluminescence
Multivator life detection experiment
Wolf trap life detection experiment
Pyrolysic gas chromatograph - Mars spectrometer
Soil Sample and dust vidicon microscope
Scanning vidicon camera

collecting data on the atmosphere for the landing. Seven probes are carried onboard the spacecraft. Two are to be deployed as the spacecraft approaches the planet to obtain atmospheric data for aerobraking the lander into orbit. Three are used to obtain data just prior to the landing operation. The remaining two probes can be deployed for optional purpose such as sounding at other latitudes.

Each probe weighs 292 lb, which includes a 100-lb sterilization canister. The diameter of each probe is 6 ft, and the ballistic number is 0.128 slug/ft^2. The probe is designed for a maximum entry velocity of 20 000 fps so that it can be staged hyperbolically.

5.4 Martian Moon Rendezvous Module (MMRM)

The Martian moon rendezvous experiment is to be performed by a manned excursion vehicle (i.e., the MMRM) rather than the orbiting spacecraft. The ΔV required for the rendezvous and return is 6500 fps, and the required mission time is 5 days. The Apollo lunar module upperstage weighs 10 000 lb and is capable of a ΔV of 7000 fps. The MMRM can be a modified Apollo lunar module upperstage. The required modifications are as follows:

1. Add adequate storage for two years.

2. Add adequate life systems for a 5-day mission.

3. Add sufficient power supply for a 5-day mission.

4. Add a moon docking bumper.

The estimated weight increases for these modifications are as follows:

1. Seals, heaters and changes to valves - 100 lb

2. Life systems and power - 600 lb

3. Moon docking bumper - 100 lb

4. Increased fuel - 618 lb

In addition to the above modifications, it is desirable to have the MMRM use the same type fuel as the main spacecraft so that the MMRM can be fueled and resupplied from the main spacecraft. This allows more than one excursion of the MMRM for those mission opportunities with fuel reserves in the main spacecraft tanks. For the 1977 and 1979 missions, the fuel reserves would allow three or more excursions of the MMRM. This would permit a visit to both moons and a low orbit about Mars for high resolution photography.

The total weight of the MMRM is 11 500 lb. The inert weight is 6180 lb, and the fuel is 5320 lb and has a specific impulse of 400 seconds. The available mission profile ΔV is 8000 fps, which is adequate to fly rendezvous missions to either moon.

The MMRM configuration is shown in figure 31. The dimensions of the MMRM stored is 16.75 ft by 15.0 ft by 16 ft.

The scientific experimental payload for the moon rendezvous experiment is 150 lb. The experiments to be performed are as follows:

1. Photograph the surface.
2. Determine the gravitational attraction of the moons.
3. Determine the moon rotation rate.
4. Test surface hardness.
5. Sample the soil.

The gravitational attraction of the Martian moons is so small that photography is possible at any altitude.

A small commerical-type, 120-mm camera equipped with several lenses would be satisfactory for this mission. The weight of camera, film, and mount would be 25 lb or less. The gravitational attraction experiment can be performed using the MMRM IMU accelerometers. No additional instrumentation is required. Rotation rate can probably be measured using optical observation from the MMRM without additional equipment so that 120 lb can be devoted to surface hardness test, soil samples, and other experiments.

5.5 Manned Landing Module

The manned landing module (or MEM) configuration is shown in figure 32. The total weight for a two-man vehicle is 91 700 lb at separation from the spacecraft and prior to aerobraking into orbit about Mars. The landing module is designed for a lifting reentry lift-to-drag ratio of 0.5. Obstacle avoidance, hover, and soft landing are obtained by a retrograde-propulsion engine that has 140 000-lb thrust and enough fuel for 2 minutes of hover time. The fuel for the soft landing and ascent is FLOX/CH_4. Both plug and bell nozzle engine designs are possible. To reduce the volume, extendable skirts are necessary for the bell engines to obtain the expansion ratio required for a specific impulse of 390 seconds.

The diameter of the entry vehicle is 30 ft and the height is 25 ft. The landing module is designed for a 30-day stay on the surface of Mars.

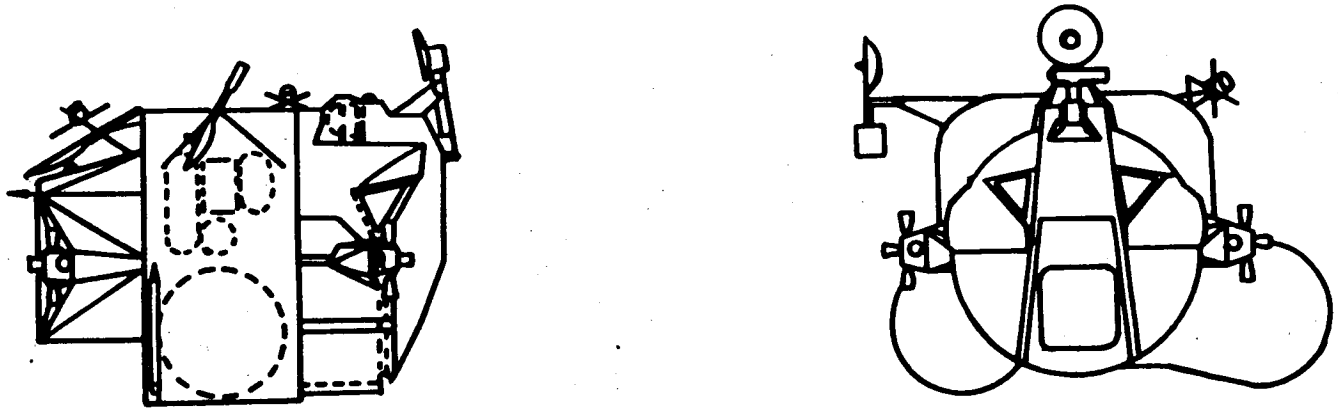

Figure 31.- Mars moon rendezvous module.

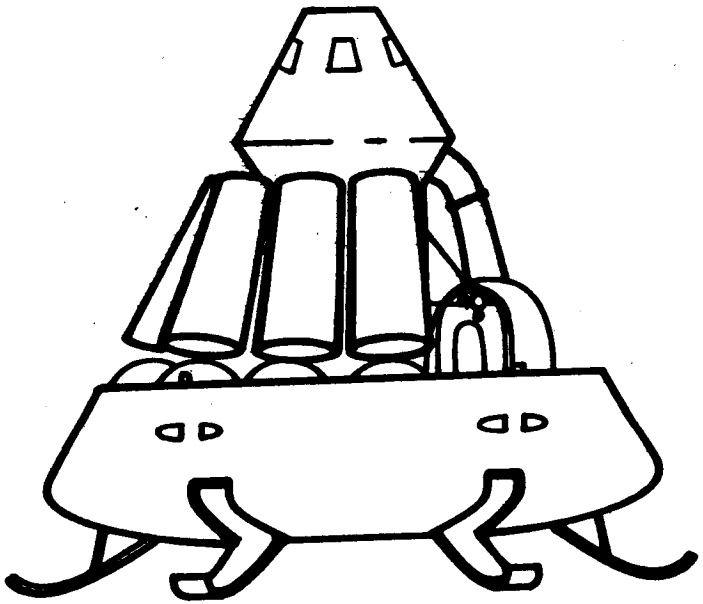

2 MAN CREW
L/D = 0.5
TOTAL WEIGHT = 75 000 LB
SURFACE EXPERIMENTS = 4 500 LB

(Reference: MPAD 2700 V)

Figure 32.- Mars landing module (i.e., the MEM).

The landing module carries a 4500-lb payload to the surface to be used in scientific exploration during the 30-day visit. The Mars roving vehicle can be the same as the lunar roving vehicle shown in figure 33. The performance characteristics of this vehicle are shown in table XII.

5.6 Mars Orbiting Spacecraft

A possible configuration for the Mars orbiting spacecraft is shown in figure 34. The spacecraft consists of five main parts: a mission module which houses the crew quarters and spacecraft control rooms, a gravity spacer, Earth entry module, TEI propulsion stage, and MOI stage. Because of the long mission duration of 2 3/4 years, the spacecraft is configured for artificial gravity. The gravity arm is obtained by a rigid structure between the mission module and the propulsion modules. In addition to shifting the center of gravity away from the mission module to increase the swing arm for artificial gravity, the gravity spacer serves a variety of purposes. For example, the gravity spacer serves as a structure to support the solar cell power source. This eliminates most of the objectionable features of the solar cell power supplies given in reference 18. The dynamic stability of the large solar array mounted as indicated in figure 35 should be good, even during the TMI maneuver when the solar array is in the extended position. Easy retraction and extension of the solar array for thrusting maneuvers is possible with this configuration. The configuration presents no particular problem when the solar array is operating in either a rotation or zero-gravity mode. The solar array is available as a power source in both Mars orbit and in the Earth assembly orbit.

The configuration provides for easy retraction and storage of the two 16-ft communications antennae during thrusting maneuvers. The probes, experimental equipment, and MMRM are installed in the gravity spacer for easy deployment.

The 50-ft gravity spacer weight of 3000 lb is for the structure and does not include the weight required for installation of the probes and systems housed in the spacer. These are included in the system weights of the specific systems. The maximum load factor both for thrusting maneuvers and for tension during spacecraft spin is 1g. Additional structure is added to take the higher loads for the Earth orbit launch phase, which is jettisoned in Earth orbit. This structure also protects the solar array and provides aerodynamic fairing.

The complete weight statement for the spacecraft is presented in table XIII. The mission module weight includes all spacecraft systems except propulsion, probes, and meteoroid protection. This weight is based on references 18 and 19. The propulsion module weights were obtained from reference 22 and include meteoroid protection for a 3-year mission for the TEI stage and 1 year for the MOI stage.

TABLE XII.- MARS SURFACE VEHICLE PERFORMANCE CHARACTERISTICS

Mass of an empty vehicle, lbm	653
Maximum speed on a firm, level, smooth surface, mph	10
Obstacle negotiability, ft	1.0
Crevice negotiability, ft	2.5
Slope negotiability, deg	30
Operational period	day only
Operational radius, n. mi.	10
Total range without recharge, n. mi.	30
Cargo capability, lbm	200

TABLE XIII.- SPACECRAFT WEIGHTS

Components	Weight, lb	
Dry MM for a 4-man crew	35 000	
MM expendables for 1300 days	26 000	
Meteoroid protection	5 740	
Earth entry M	15 100	
Onboard experiments	6 360	
Probes	10 340	
MMRM	11 500	
Installation for MMR and probes	5 000	
Gravity tube	3 000	
Total		118 000
TEI fuel (I_{sp} = 400 sec)	67 300	
TEI stage dry	14 700	
MOI fuel (I_{sp} = 400 sec)	140 000	
MOI stage dry	20 000	
Total		242 000
CM crew transport	20 000	
Grand Total		380 000

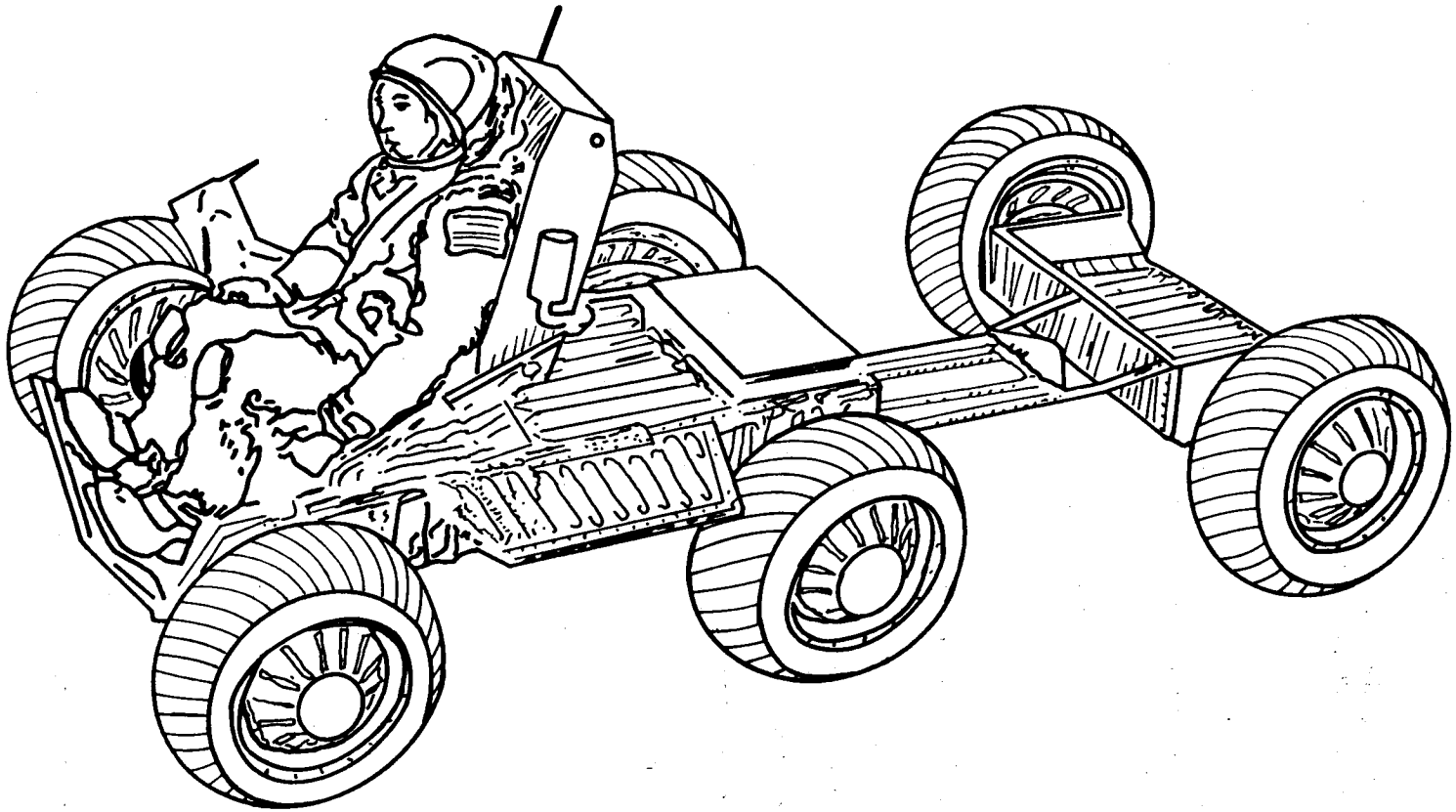

Figure 33.- Mars surface vehicle high mobility concept.

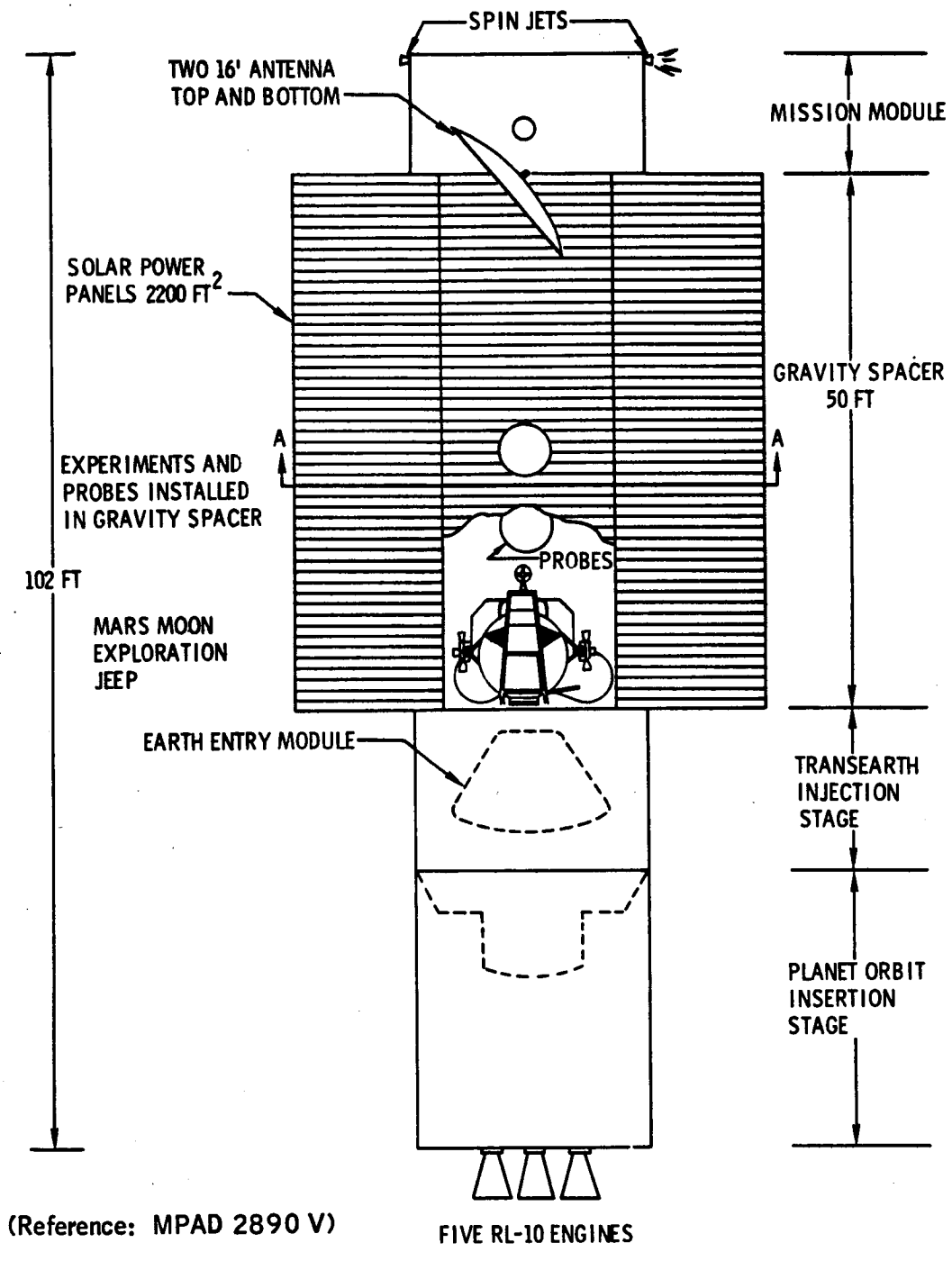

Figure 34.- A possible Mars orbiting spacecraft configuration.

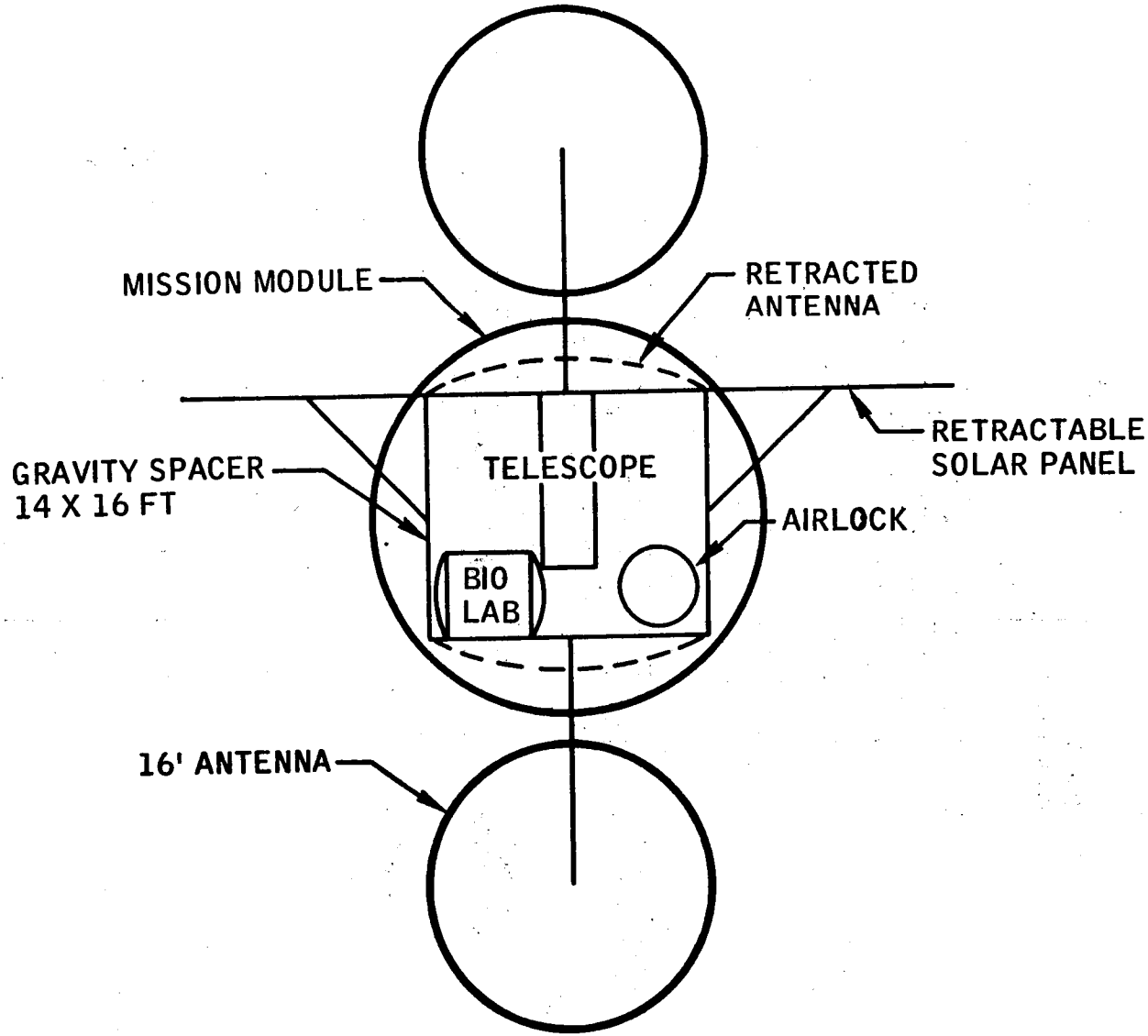

(Reference: MPAD 2705 V)

Figure 35.- Cross-section AA of a possible Mars orbiting spacecraft configuration.

The rotational characteristics of the gravity spacecraft for various mission phases is shown in table XIV. The rotation rate for a 1g operation, and the fuel required for a 1g spin-up at an I_{sp} of 300 seconds are shown.

Reference 21 indicates that the maximum spin-rate for crew comfort is 6 rpm. Thus the maximum g on the trans-Earth phase is 0.41. This increases to 0.63 in Mars orbit and 0.82 on the outbound leg of the mission. In Earth orbit with the TMI stages attached, up to 1g is possible.

A representative spin hisotry and the fuel requirements for spinning the spacecraft to a maximum of 6 rpm during all mission phases are shown in table XV. The fuel used to spin the spacecraft is contained in the midcourse ΔV budget. The fuel shown in table XV corresponds to 121 fps on the trans-Mars leg, 230 fps in Mars orbit, and 188 fps on the return leg.

The performance of the spacecraft for the various primary and alternate mission maneuvers is shown in table XVI for a fuel specific impulse of 400 seconds. The total capability of 6500 fps for MOI and 6500 fps for TEI, or 13 000 fps for MOI and TEI, exceeds the maximum mission requirements of 11 000 fps in 1983. (See table III and page 23.) Thus the capability of the spacecraft provides a mission performance margin of 2000 fps for the worst mission and greater performance margin for the earlier missions. The velocity requirements shown in figure 5 include midcourse correction and spacecraft spin fuel. At TMI 6430 fps are available from the MOI stage for abort and 5275 fps from the TEI. The capability of these stages to abort for the TMI is discussed in section 6. The capability of the spacecraft to return without going into orbit and return early from orbit are also discussed in section 6.

5.7 Launch Vehicle

The minimum requirement for the launch vehicle of the Mars landing mission is that it be capable of launching the largest module that must be placed in orbit. A second requirement is that the total number of launches be within the feasibility of the launch site to launch and the vehicles to assemble in a reasonable time. Reference 23 presents a study of increasing the payload to Earth orbit of the Saturn V launch vehicle by adding solid rockets to the first stage and increasing the tank size. This and other studies have resulted in several alternate concepts of improving the payload to Earth orbit, as shown in figure 36. Three possible payload capabilities to Earth orbit are available by uprating the Saturn V: 332 000 lb with the product improved version, 400 000 lb by the addition of four 120-in. solids (model 4S-B), and 500 000 lb by the addition of four 156-in. solids (model 25-S).

TABLE XIV.- SPACECRAFT SPIN CHARACTERISTICS

Mission phase	Weight, lb	Moment of inertia, slug-ft^2	Center of gravity, ft (a)	Spin, rpm (b)	Fuel, lb (b)
Trans-Earth	101 820	2 911 000	33.1	9.43	290
Mars orbit	213 500	6 647 000	51.5	7.56	341
Trans-Mars					
with lander	456 700	19 724 000	78.5	6.11	536
without lander	360 000	12 098 000	66.9	6.63	418
Earth orbit					
with OLV III	720 000	58 112 000	109.1	5.19	965
with OLV III and II	1 080 000	140 182 000	143.4	4.52	1544
with OLV III, II and I	1 440 000	261 268 000	173.0	4.12	2171

[a]Measured from the floor of the mission module.

[b]For 1g operation, fuel varies directly with RPM and the square root of the gravity level.

TABLE XV.- FUEL REQUIREMENTS FOR ARTIFICIAL GRAVITY

[I_{sp} = 300 sec]

Mission phase		Gravity level[a], earth g	Fuel, lb	Total fuel, fps
Earth orbit	SC checkout to docking OLV I	1.0	840	
	Between docking OLV I and II	1.0	1930	
	Between docking OLV II and III	1.0	3090	
	Between docking OLV III and TMI	1.0	4340	
				10 200
Trans-Mars	TMI to MCC I	1.0	1072	
	MCC 1 and 2	1.0	1072	
	MCC 2 to 3	1.0	1072	
	MCC 3 to 4	1.0	1072	
	MCC 4 to MOI	0	0	
				4 288
Mars orbit	Lander docking to midcourse 1	0.63	542	
	MCC to MMRM staging	0.63	542	
	MMRM staging to MMRM return	0.63	542	
	MMRM return to MCC 1	0.63	542	
	MCC 2 to lander staging	0.63	542	
	Lander staging to return	0.63	542	
	Lander return to TEI	0.63	542	
				3 794
Trans-Earth	TEI to MCC 1	0.40	370	
	MCC 1 to 2	0.40	370	
	MCC 1 to 3	0.40	370	
	MCC 3 to 4	0.40	370	
	MCC 4 to Earth entry	0	0	1 480

[a]The maximum spin rate is G rpm.

TABLE XVI.- SPACECRAFT PERFORMANCE CAPABILITY

[I_{sp} = 400 sec]

Stage	Event	ΔV, fps
MOI	Nominal MOI and powered turn	6 500
	TMI	6 430
TEI	Nominal stay	6 500
	1-day stay	6 155
	Powered turn	5 426
	TMI	5 275
MOI and TEI	Powered turn	11 926
	TMI	11 705

PRODUCT IMPROVED
F-1 THRUST 1.8M LB
EXTEND S-IC 20 FT
J-2S ENGINE ON S-II
PAYLOAD 332 000 LB

4 S-B
4 120 INCH SOLIDS
EXTEND S-IC 28 FT
J-2S ENGINE ON S-II
PAYLOAD 400 000 LB

25S
4 156 INCH SOLIDS
EXTEND S-IC 41.5 FT
J-2S ON S-II
PAYLOAD 500 000 LB

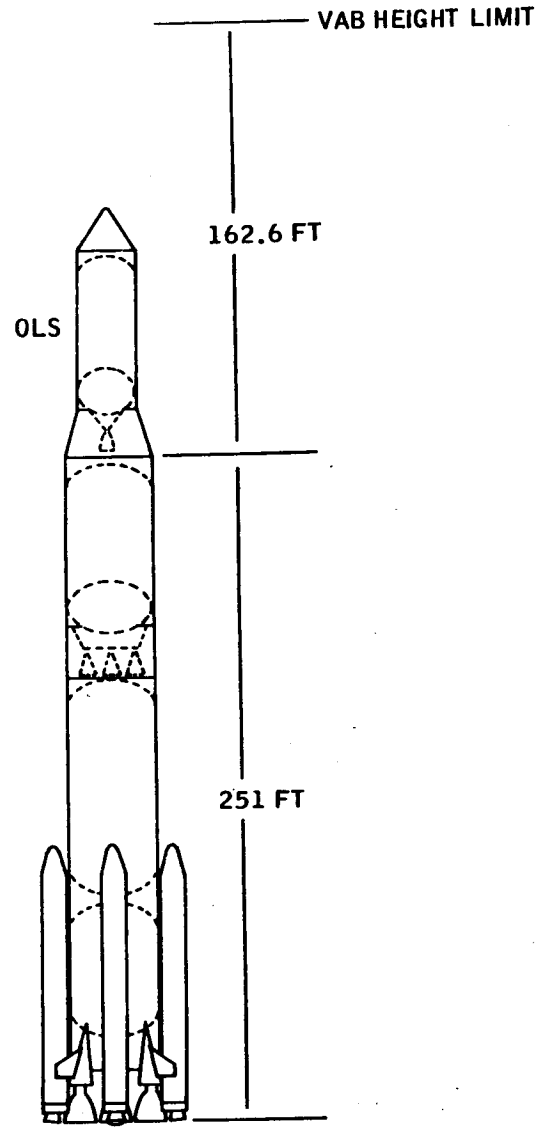

(Reference: MPAD 2889 V)

Figure 36.- Launch booster configuration.

The spacecraft weight is 360 000 lb, and it is desired to build and launch it as one unit. Additional weight of 40 000 lb is required for such items as interstage, instrument units, docking structures, and crew transport so that the total launch payload for a single launch is matched to the S-V model 4S-B. This payload is for two-stages-to-orbit. The third stage is either the spacecraft or a propulsion unit for trans-Mars injection. The number of launches required, therefore, will depend on the TMI velocity requirement for the mission and the type of orbital launch stage.

Reference 24 presents a preliminary design study of an orbital launch stage based on chemical fuels. The weight statement for the stage (S-IVC) is shown in table XVII. The S-IVC stage is designed for a total lifetime in Earth orbit of 30 days before the hydrogen boiloff becomes large enough to affect the performance.

Four launches are required to assemble the orbital launch vehicle in Earth orbit. The configuration of the Earth orbit payload for each launch is shown in figure 37. The first launch is the spacecraft. The second launch is an S-IVC OLV topped with the Mars lander and docking structure. The S-IVC is off-loaded 95 000 lb of fuel so that the lander and its interstage can be carried on this launch. The second and third launches are fully-loaded OLV's. The TMI velocity capability is shown for each stage. The total velocity capability of the four launches is 13 575 fps, which is 75 fps greater than the maximum TMI velocity of 13 500 fps in 1983.

TABLE XVII.- ORBITAL LAUNCH STAGE WEIGHT SUMMARY

Component	Weight, lb
Dry stage	33 000
Residuals	2 500
Aft interstage	6 300
Instrumentation unit	6 000
APS modules - forward	1 700
APS modules - aft	2 900
Main propellant	322 700
APS propellant - forward	1 300
APS propellant - aft	5 000
Propellant vented	16 000
Nose fairing	2 600
Total launch weight	400 000
Stage weight total	44 500
Total weight lost in orbit	32 800

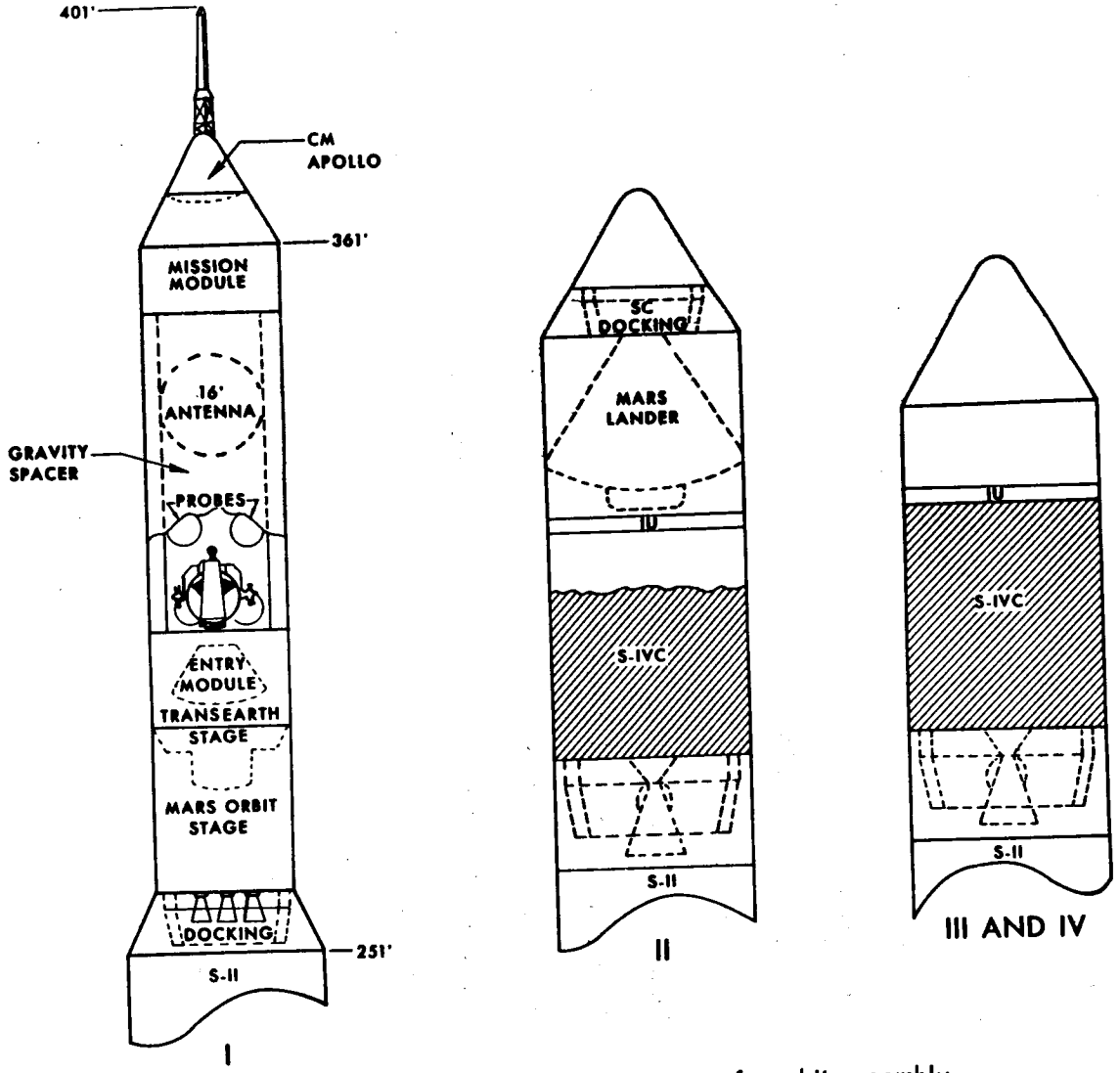

Figure 37.- Launch configuration for orbit assembly.

(Reference: MPAD 2911 V)

ENCL 13

6.0 ABORT AND ALTERNATE MISSIONS

6.1 Introduction

The preceding sections have defined a nominal mission profile and a spacecraft capable of performing a Mars mission. Therefore, the information necessary for an abort and alternate mission analysis is available, and the nominal mission trajectory and spacecraft parameters are known as a function of time. The parameters are the constraints which limit the number of abort and alternate mission possibilities to a finite group and make the analysis feasible. This study is a preliminary analysis of abort and alternate missions which are defined by the time of initiation in the nominal profile. For the purpose of this study, the only type of mission defined as an abort is one in which the spacecraft does not exit the Earth's sphere of influence (SOI) and the only objective is the safe return of the crew as soon as possible. If the spacecraft leaves the Earth's SOI, the minimum time required to return to Earth is 0.5 to 3 years (depending on the propulsion capability) and all such missions are considered alternates rather than aborts. Thus, the abort and alternate mission are:

1. Abort after trans-Mars injection (TMI) and early return from the heliocentric phase.

2. Powered turn flyby alternate.

3. Early return from Mars orbit alternate.

The second objective of an alternate mission would probably be a spacecraft checkout and systems qualification since a failure will have occurred to require the alternate mission. Depending on the nature and severity of the failure, as many nominal mission objectives as possible would be completed.

6.2 Abort After TMI

While the spacecraft is still within the Earth's SOI, a transfer can be made to a high-altitude, elliptical Earth orbit, as shown in figure 38. Depending on the propulsion capability of the spacecraft and the intended flight plan after abort, a synchronous elliptical or circular orbit might be achieved. All three possible modes for this abort maneuver place the entire spacecraft into the elliptical orbit. Mode I uses only the trans-Earth injection (TEI) stage which has a ΔV capability of 5275 fps. Mode II uses only the Mars orbit insertion (MOI) stage which has a ΔV capability of 6430 fps. Mode III uses both stages which have a combined ΔV capability of 11 705 fps. A comparison of these modes is shown in figure 39, which is a plot of the minimum period ellipse that can be achieved as a function of

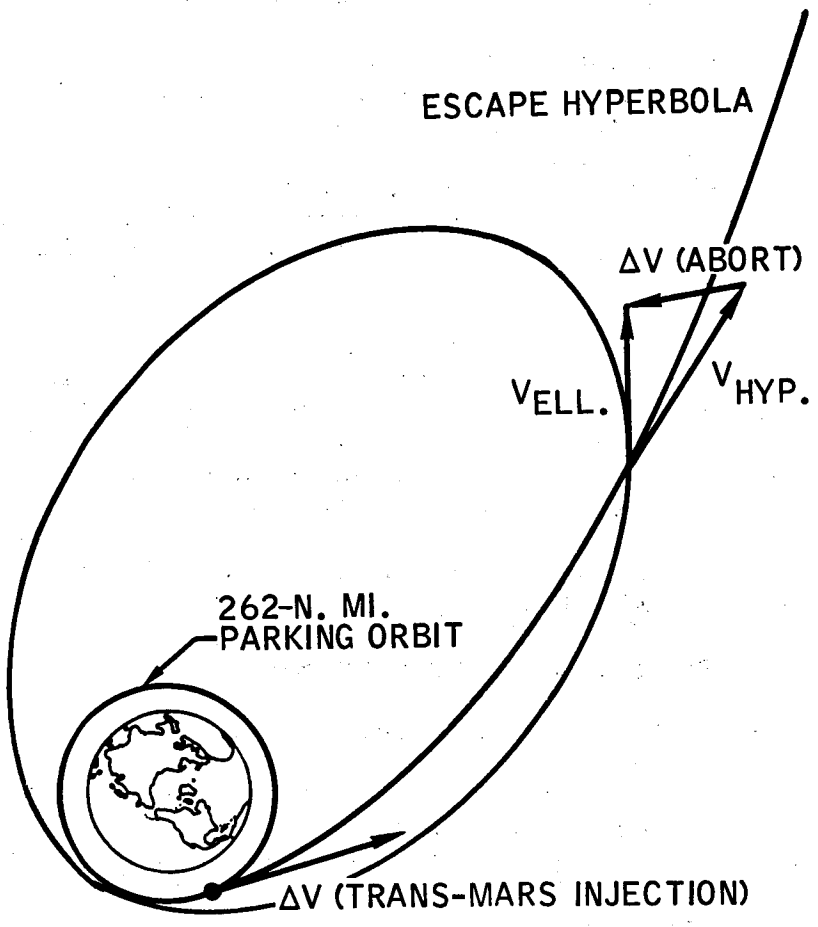

Figure 38.- Geometry of geocentric abort after trans-Mars injection.

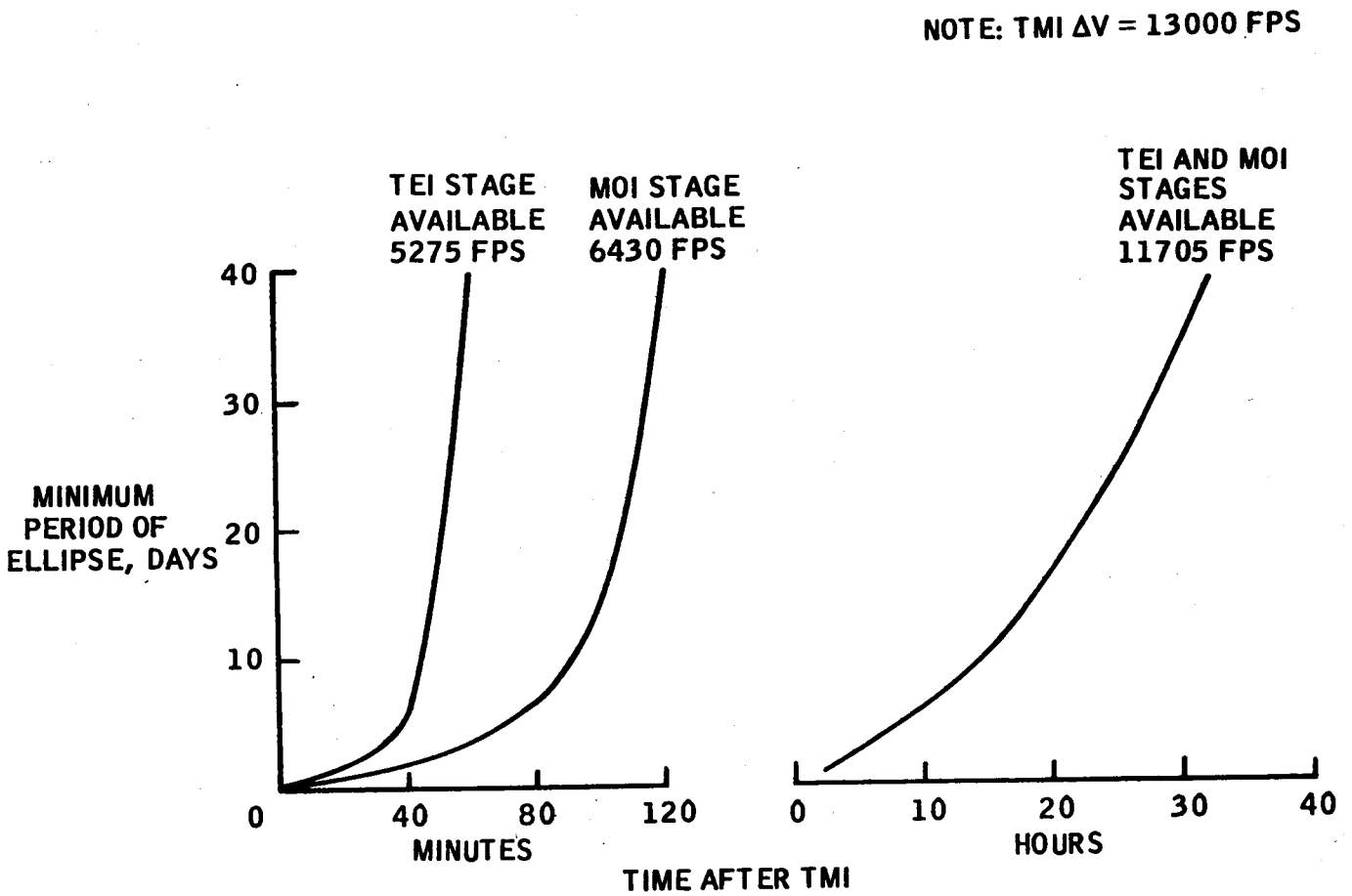

(Reference: MPAD 2714 V)

Figure 39.- Abort capability of spacecraft after trans-Mars injection.

time after TMI. If an arbitrary limit on the return-to-Earth time is set at 10 days, then abort is possible up until approximately 45 minutes after TMI using mode I, 90 minutes after TMI using mode II, and 14 hours after TMI using mode III. All three modes give ample time for ground tracking and an abort decision by mission control. This data was calculated assuming a single-impulse transfer between the escape hyperbola and the ellipse. The TMI ΔV used in calculating this data was 13 000 fps. This is over and above circular orbit velocity at 262 n. mi., and was the highest TMI ΔV encountered for any of the nominal missions.

If abort into a high Earth-centered ellipse is necessary, then consideration might be given to a practice mission in Earth orbit. Probably one of the first steps taken would be a checkout of the remaining systems since the condition of these systems would determine what could be accomplished in a practice mission. Possibilities for a practice mission might include the following:

1. Simulation of the Mars orbit phase of the nominal mission.

2. Onboard navigation simulation.

3. Extended lifetime check of systems.

If the spacecraft is near the Earth's SOI or if it is desired to go into heliocentric space as an alternate mission, then a 6-month or 1-year trajectory is a possibility. A change in both azimuth and flight-path angle appear necessary from a preliminary investigation. Figure 40 is a plot of the velocity required and indicates that the maneuver could be accomplished for approximately 11 000 fps during the first 60 days after leaving the Earth's SOI. This is within the capability of the spacecraft described in this study. The total mission times would be about 200 and 400 days for the two types of trajectories. Further investigation is needed in this area to properly assess its potential.

6.3 Powered Turn Flyby

If on arriving at Mars the decision is made not to orbit the planet, then a maneuver or series of maneuvers must be made to obtain a flyby trajectory for return to Earth. It has been found that the first maneuver must be made very near the Mars SOI on the approach hyperbola. If the first impulse is not made at this time, except for unusual cases, it will be virtually impossible to obtain a desirable inbound trajectory using only the MOI or TEI stage. A second and perhaps third impulse, made inside the Mars SOI, will reduce the total velocity increment. Multiple revolution trajectories about the Sun are also necessary as they reduce both the velocity required for the powered turn and the Earth entry velocity. The geometry of the multirevolution return trajectory is shown in figure 41. The two

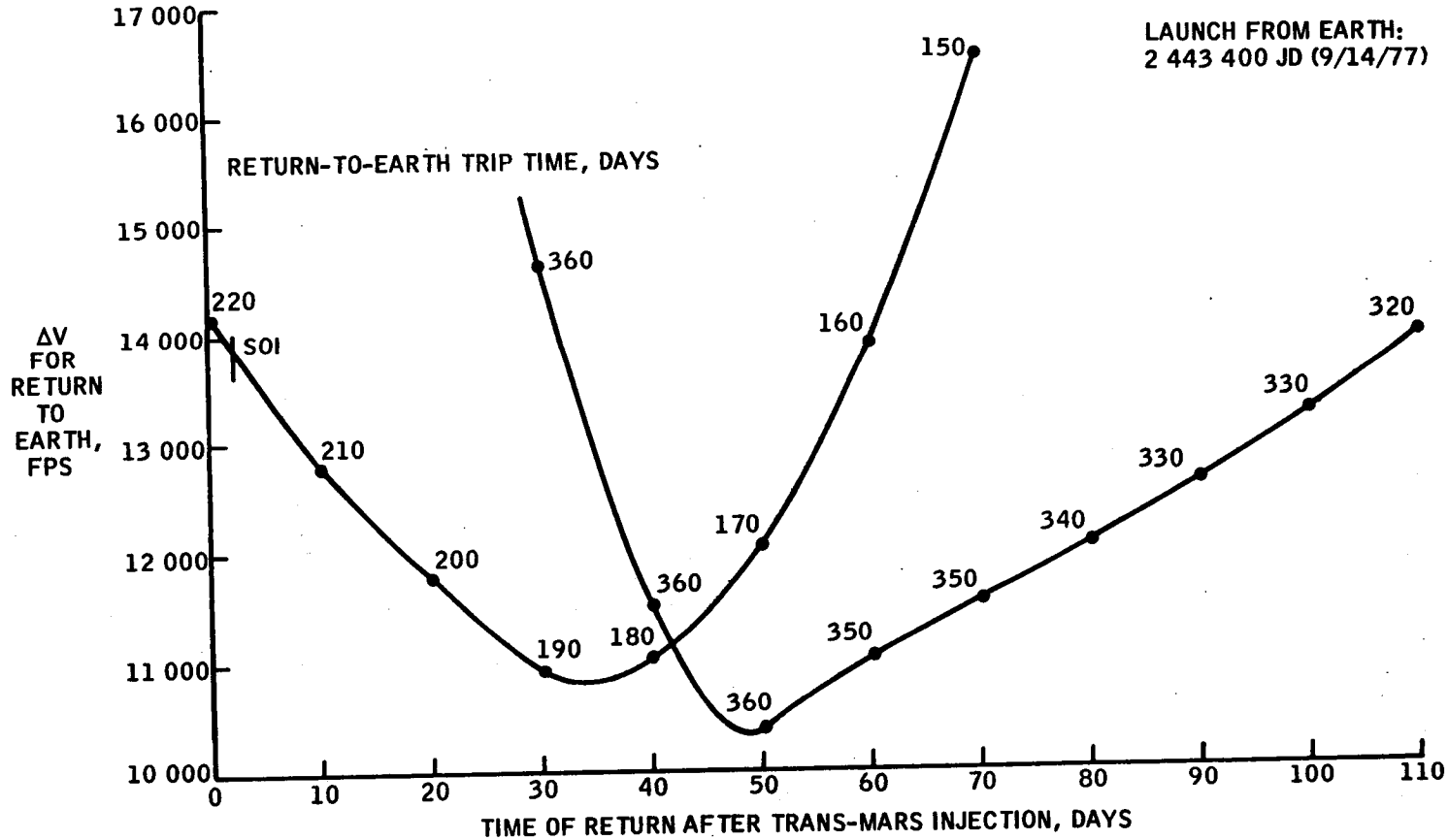

Figure 40.- Velocity required for return to Earth after exiting the sphere of influence.

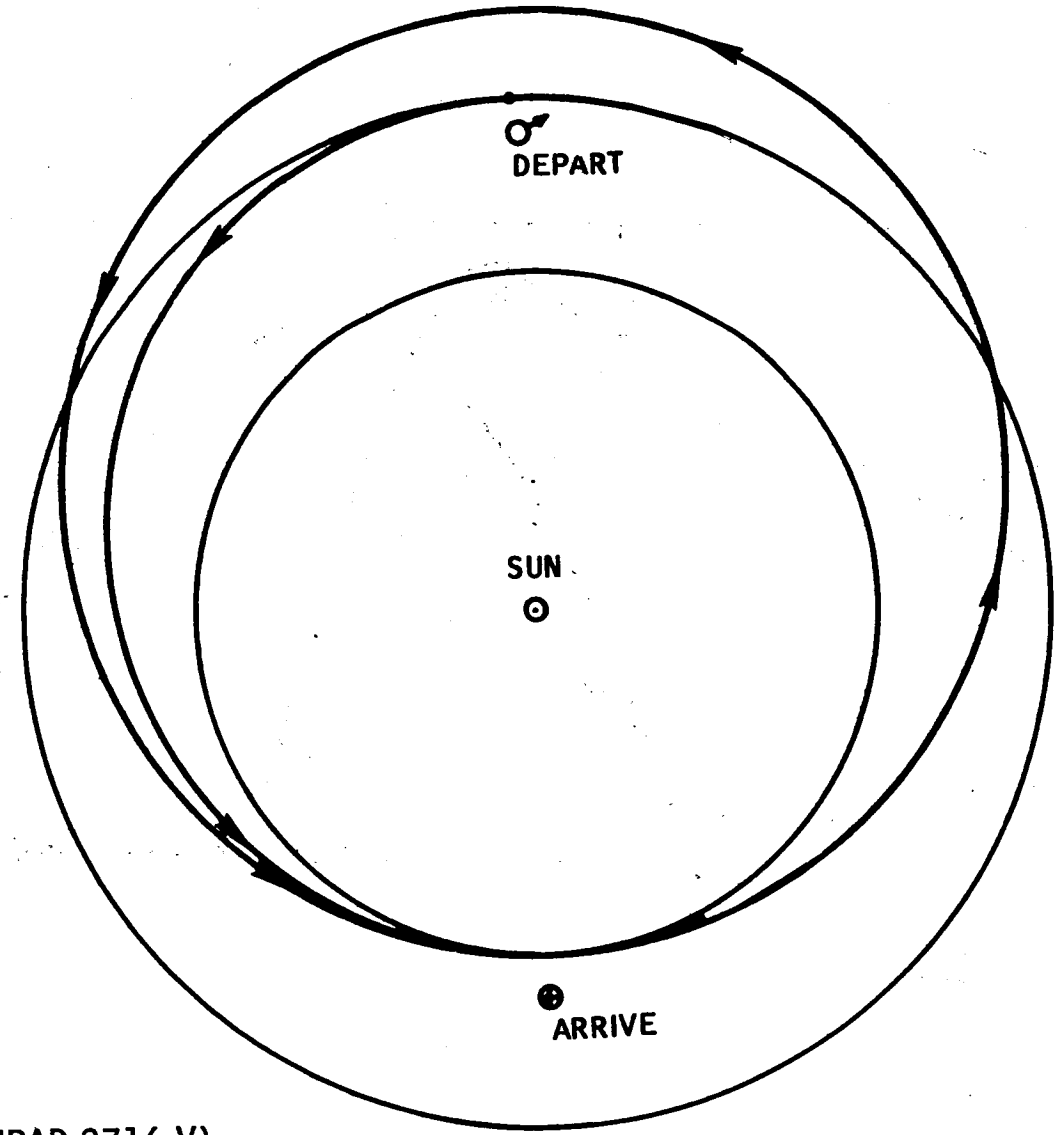

(Reference: MPAD 2716 V)

Figure 41.- Geometry of the powered-turn flyby alternate.

concentric circles represent the orbits of Mars and the Earth. The spacecraft will follow a trajectory similar to that indicated by the arrows and will depart Mars at the point marked "Mars depart." This is a near-Hohmann transfer with perihelion being close to Earth's orbit. The Earth will not be in the vicinity, however, and an additional full revolution is required to intercept the Earth. In most cases, a maneuver is required at perihelion to phase properly and return to Earth at the point marked "Earth return." Table XVIII summarizes the velocity requirements for the powered turn flyby alternate. The maneuver at the planet is cheapest during the 1977 mission, and there is no requirement for a perihelion maneuver. The requirements increase for each successive mission until 1983, which is the worst mission from almost every standpoint. The total trip times for the flyby alternates are about 150 days greater than those for the nominal missions. The velocity requirements listed in the table have not been minimized for lack of a complete computer program. Even so, these numbers indicate that the flyby alternate can be accomplished in 1977 and 1979 using only the MOI or TEI stage. Other minimization techniques are required, however, in order to bring the 1981 and 1983 flyby alternate velocity requirements within the spacecraft's capability.

6.4 Early Return From Mars Orbit

Unlike the situations of abort after TMI and the powered turn flyby alternate, only the TEI stage is available for early return from Mars orbit. The TEI stage has a velocity capability of 6500 fps at the time of nominal departure. Because of unused consumables, however, this capability drops to 6155 fps for an orbit stay time of only a few days. The geometry of the early return from Mars orbit alternate is shown in figure 42. The dashed portion represents the nominal stay in Mars orbit. The relative positions of the planets at times of departure and arrival are indicated in the figure. The notes, "return on multirevolution" and "return on single revolution," indicate the regions where it is cheaper to use the two different types of return trajectories. For example, in the case of the 1977 mission, the TEI velocity required for a single revolution return trajectory is about 22 000 fps; the TEI velocity required for a multiple revolution return trajectory is approximately 5000 fps. These two types of trajectories are essentially the same as those described in the powered turn flyby section.

After going into the nominal mission orbit about Mars, except for the nominal departure, the vehicle cannot leave for Earth without making a plane-change maneuver. Also, certain steering and gravity losses are incurred. All of these losses are reflected in the curves of figure 43 which shows the TEI velocity using finite thrusting and cross-product steering. However, all plane-change requirements have been taken care of by impulsive maneuvers at apoapsis of the ellipse just prior to TEI. Orbit "A" is characterized by no plane changes when entering or leaving Mars orbit

TABLE XVIII.- SUMMARY OF VELOCITY REQUIREMENTS FOR POWERED-TURN FLYBY ALTERNATE

Launch opportunity	Powered turn at mars, fps	Preihelion maneuver, fps	Total ΔV, fps	Total mission time, days
1977	1850	0	1850	1153
1979	2592	2194	4786	1154
1981	2412	4251	6663	1158
1983	2950	5938	8888	1143

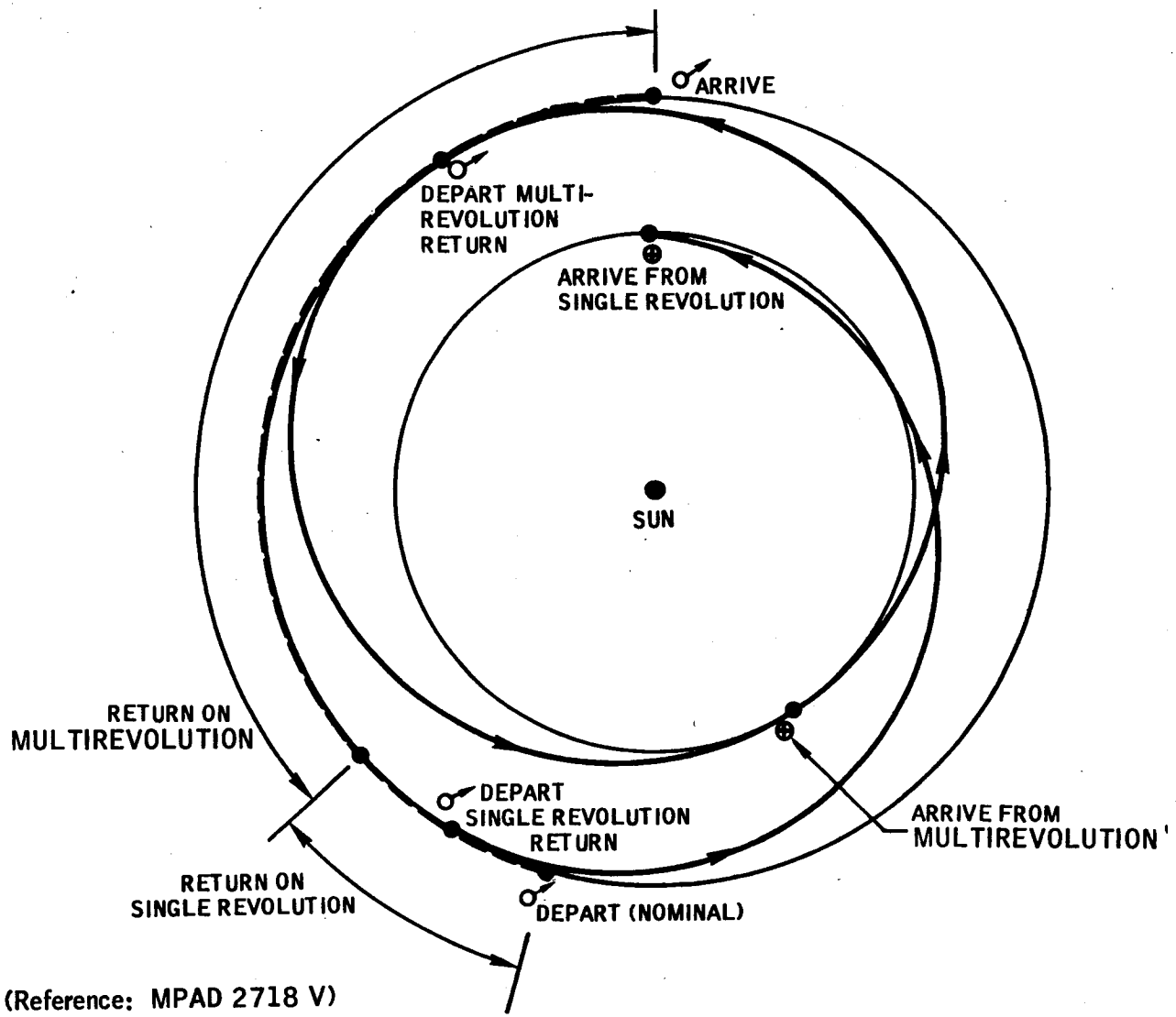

(Reference: MPAD 2718 V)

Figure 42.- Geometry of the early return from orbit alternate.

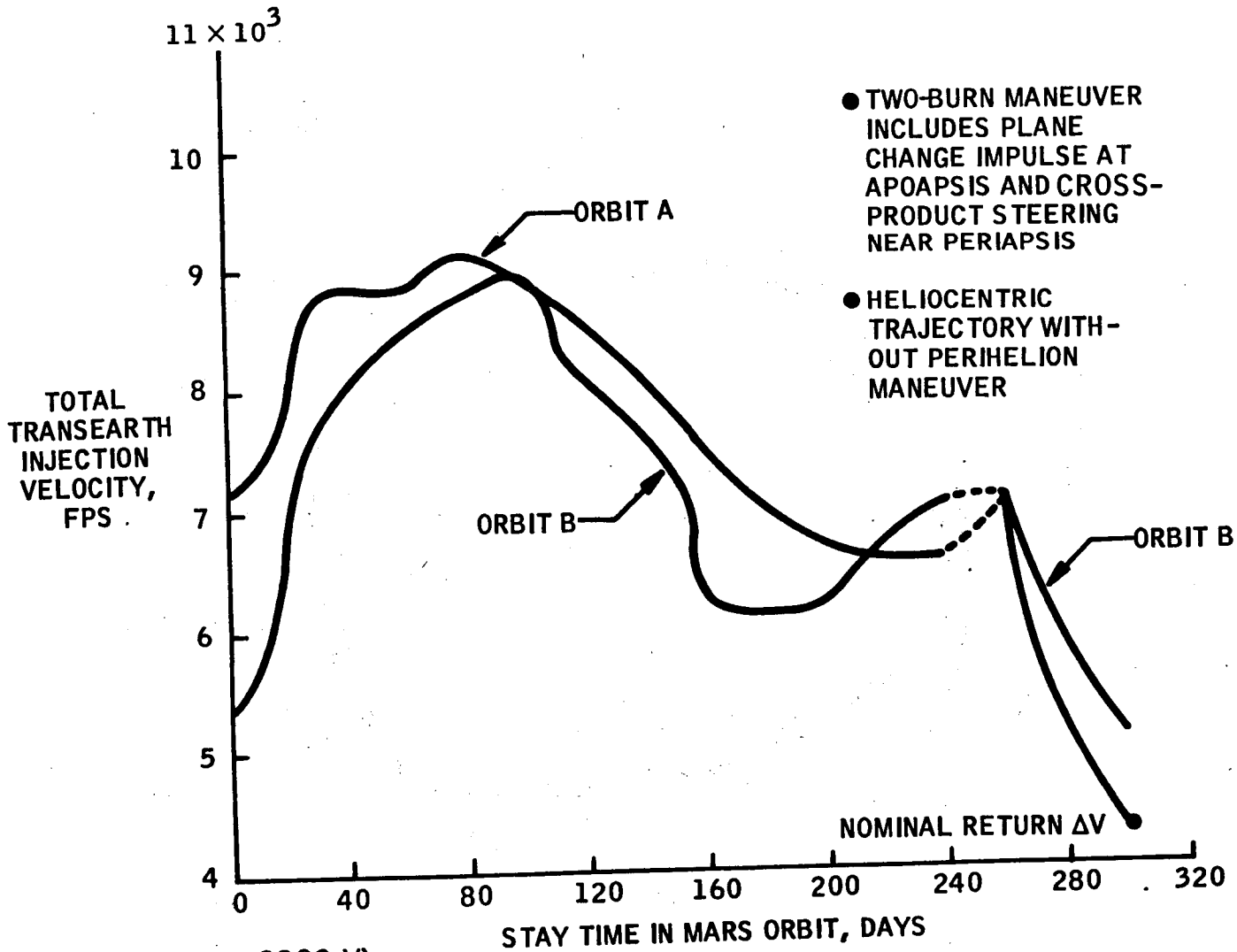

(Reference: MPAD 2893 V)

Figure 43.- Transearth injection velocity - finite thrusting with cross-product steering.

at the nominal times. Also, the periapsides of the approach and departure hyperbolas are coincident with the periapsis of the elliptical orbit at the times of arrival and departure, respectively. Orbit "B" is very similar to orbit "A" except that the initial node position is different, and there is a small plane-change requirement when leaving Mars after the nominal stay time. The dashed portion of the curve shows the slight discontinuity between the multirevolution and single-revolution return trajectories. Using this technique for return to Earth, the spacecraft is committed to stay in Mars orbit for a large portion of the planned stay time.

A very useful technique that can be employed to reduce the total TEI velocity required for a multiple-revolution return to Earth is the perihelion maneuver. If this maneuver is not made, the velocity required for a multiple-revolution trajectory increases rapidly as the transfer angle changes from 540° (1.5 revolutions). That is the reason for the hump in the curves of figure 43. The multiple-impulse TEI velocity is shown as a function of Mars orbit stay time in figure 44. This figure covers the same time interval of the 1977 mission as figure 43. However, the steering and gravity losses and plane-change requirements have not been considered because of insufficient V_∞ data. If these numbers are in any way representative, the perihelion maneuver may be a very useful technique in reducing the TEI velocity. Further investigation is needed in this area to determine its full value.

The Earth entry velocity is shown in figure 45 as a function of Mars orbit stay time. This plot is for the 1977 mission which departs Earth on September 14, 1977 and is very representative of the other missions. The multiple-revolution curve turns up sharply at about 240-days orbit stay time. However, this is about the point at which the single-revolution return becomes possible from the standpoint of ΔV. The Earth entry velocity never exceeds 39 000 fps in the case of the multiple-impulse, multiple-revolution return trajectory. Even so, there is a great reduction in total trip time any time the single-revolution return is used. In the case of the single-revolution return during the 1977, 1979, and 1981 missions, the Earth entry velocity is below 39 000 fps for orbit stay times over 200 days and less than or equal to the nominal. This figure is 40 000 fps for the 1983 missions.

The total trip times for the 1977 mission are shown as functions of Mars orbit stay time in figure 46. Both the single-revolution return and the multiple-revolution return are plotted. Imposing the constraints of any-time return from Mars orbit and 6500 fps or less TEI velocity results in total mission times of approximately 1300 days.

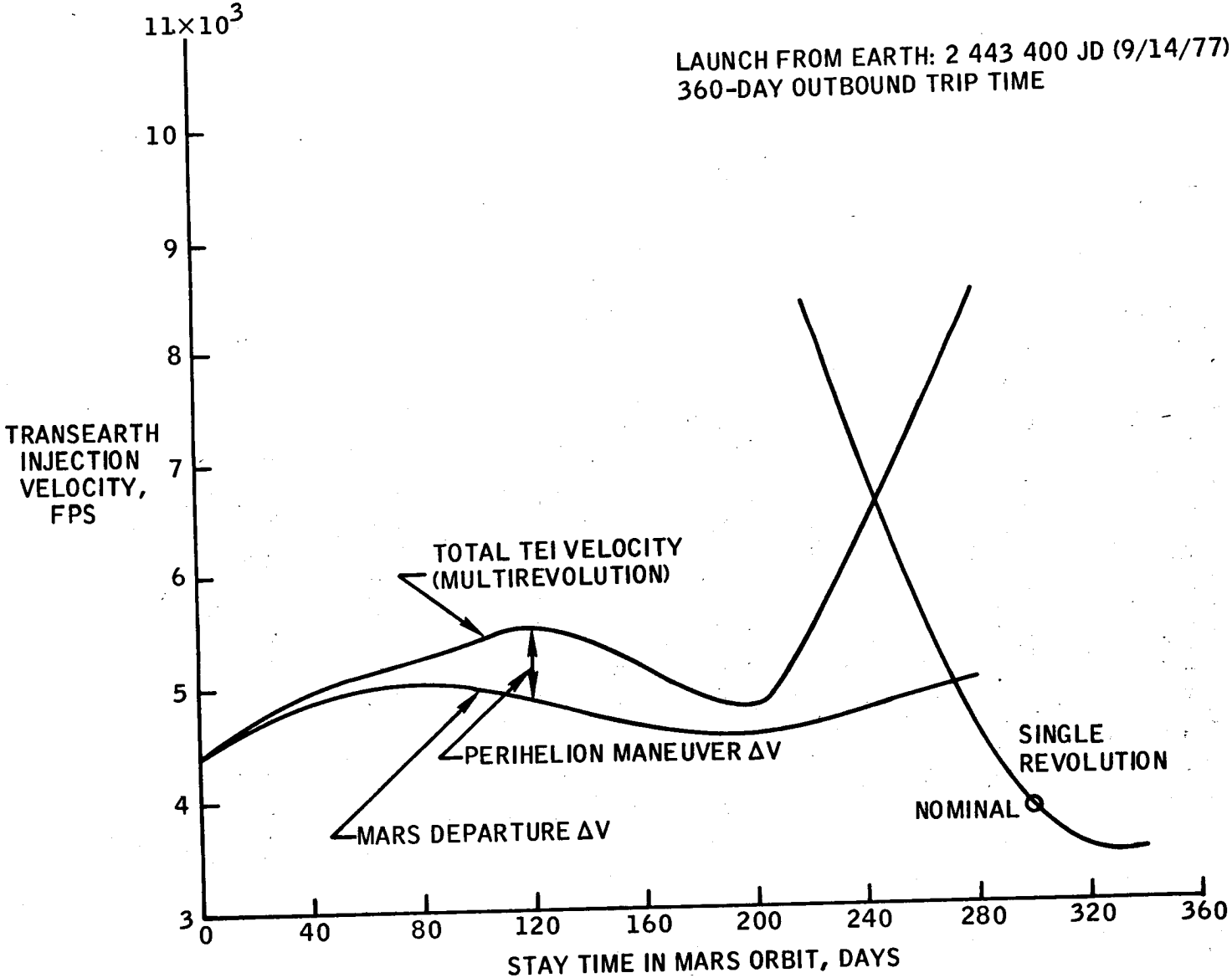

Figure 44.- Multiple impulse trans-Earth injection velocity for 1977 Mars mission.

LAUNCH FROM EARTH: 2 443 400 JD (9/14/77)
360-DAY OUTBOUND TRIP TIME

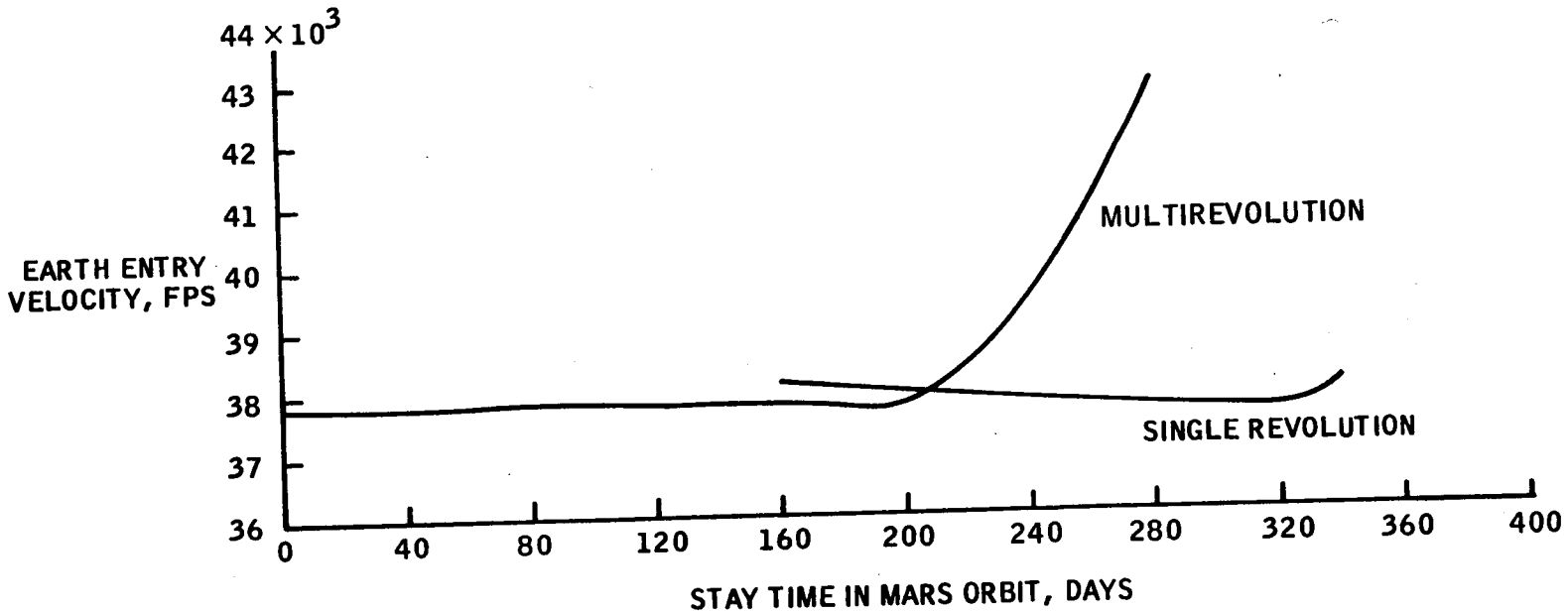

(Reference: MPAD 2721 V)

Figure 45.- Earth entry velocity for 1977 Mars mission.

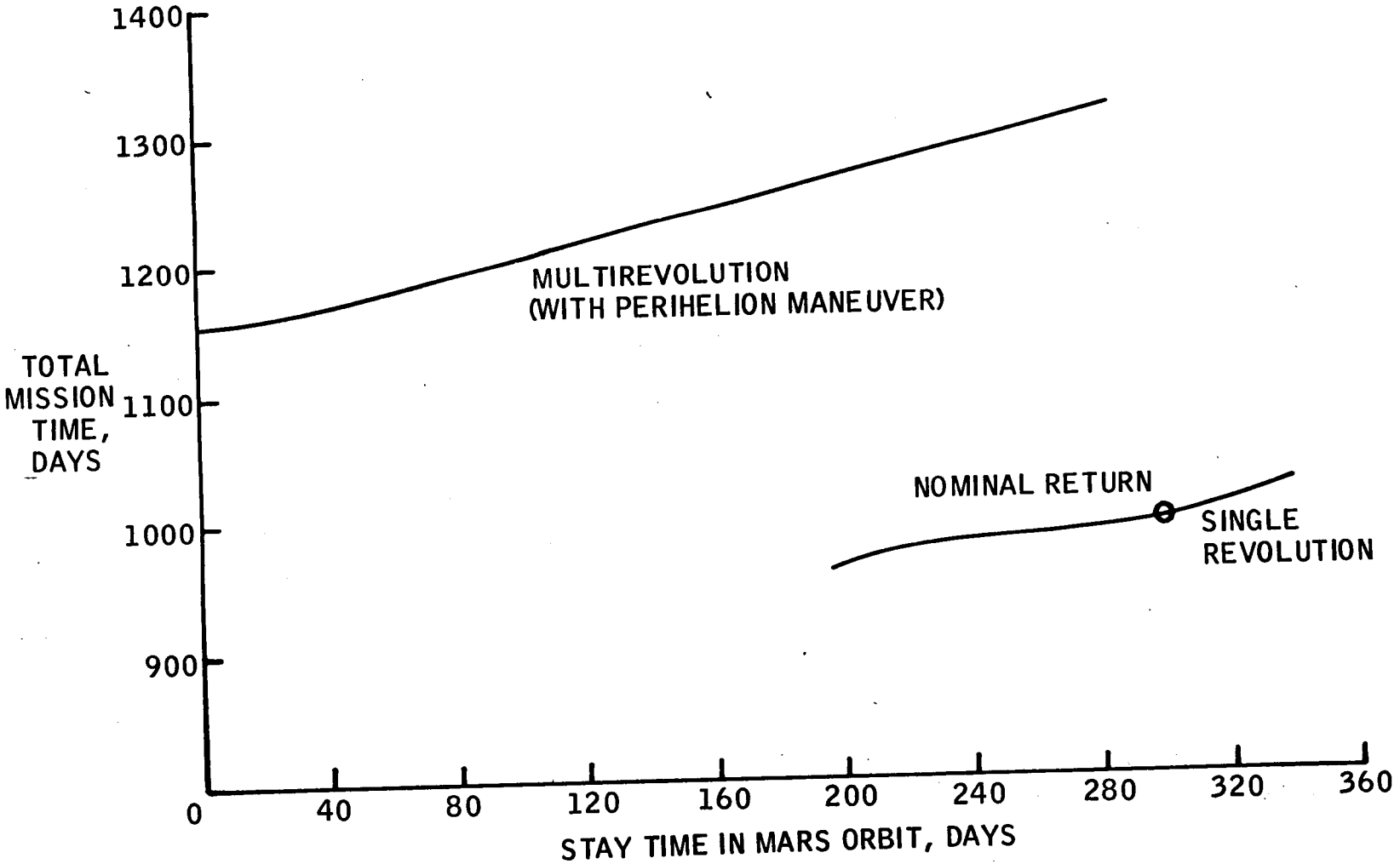

Figure 46.- Total mission time for 1977 Mars mission.

REFERENCES

1. Deerwester, Jerry M.; and Norman, Susan M.: Reference System Characteristics for Manned Stopover Mission to Mars and Venus. Working Paper MS-67-4, MASA, OART, Mission Analysis Division, Moffett Field, California, July 10, 1967.

2. Garland, Benjamine J.: Three-Dimensional Trajectory Analysis of Non-Stop Round-Trip Mars Missions Between 1970 and 1988 Using Propulsive Gravity Turns with Atmospheric Effects. TM X-1122, August, 1965.

3. Garland, Benjamine J.: Free-Return Trajectories to Mars Between 1975 and 1982. MSC Internal Note 66-FM-141, November 25, 1966.

4. Garland, Benjamine J.: Three-Year, Free-Return Trajectories to Mars Between 1975 and 1980. MSC Internal Note 67-FM-123, August 25, 1967.

5. Gobetz, F. W.: How to Open a Launch Window. United Aircraft Research Laboratories Report F-110058-27, November, 1967.

6. Planetary Flight Handbook, Part 1.-Speed Contours and Auxiliary Graphs for Manned Missions to Mars and Venus. NASA SP-35 (Lockheed Study for MSFC). Distributed by NASA, U.S. GPO, Washington, D.C., 1963.

7. Wilson, S. W.: Analysis of Planetary Hyperbolic Departure Techniques. TRW Note Number 67-FMT-591, December 22, 1967.

8. Bird, John D.; Thomas, David F.; and Collins, Robert L.: An Investigation of a Manned Mission to Mars. Given at Manned Planetary Mission Technology Conference, Lewis Research Center, May 21-23, 1963.

9. Bird, John D.; Thomas, David F.: Orbital Rendezvous Considerations for a Mars Mission. Paper presented at AAS Symposium on Space Rendezvous, Rescue, and Recovery, September 10-12, 1963. Advances in the Astronautical Sciences, Volume 16, Part 1, p. 219.

10. Luiden, Roger W.; and Miller, Brent A.: Efficient Planetary Parking Orbits With Examples for Mars. NASA TN D-3220, January, 1966.

11. Thibodeau, Joseph R. III: Use of Planetary Oblateness for Parking Orbit Operations for Interplanetary Missions. MSC Internal Note No. 67-FM-87, June 30, 1967.

12. Ehricke, Krafft A.: Space Flight-Volume I-Environment and Celestial Mechanics. deVan Nostrand Co., Inc, 1960, pp. 124-125.

13. Murtagh, Thomas B.; Lowes, Flora B.; and Bond, Victor R.: Navigation and Guidance Analysis of a Mars Probe Launched From a Manned Flyby Spacecraft. Pre-print volume of technical papers presented at AIAA Guidance, Control, and Flight Dynamics Conference. Paper No. 67-546. August 14-16, 1967.

14. Cicolani, Luigi S.: Interplanetary Midcourse Guidance Using Radar Tracking and Onboard Observation Data. NASA TN D-3623, September, 1966.

15. White, John S.; Callas, George P.; and Cicolani, Luigi S.: Application of Statistical Filter Theory to the Interplanetary Navigation and Guidance Problems. NASA TN D-2697, March, 1965.

16. Lowes, Flora B.; and Murtagh, Thomas B.: Navigation and Guidance Systems Performance for Manned Missions to Mars and Venus Between 1972 and 1980. MSC Internal Note 68-FM-50, February 23, 1968.

17. Baker, D. S.; Sears, N. E.; and White, R. L.: Lunar Orbit Navigation Performance With Various Random and Systematic Errors. MIT IL Document E-1983, July, 1966.

18. Manned Planetary Flyby Mission Based on Saturn/Apollo Systems. NAA Report SID 67-549, August, 1967.

19. Definition of Experimental Tests for a Manned Mars Excursion Module. NAA SID 67-755, November, 1967.

20. Planetary Missions Study: Task T2A600 - Mars/Venus Manned Missions (Phase II) Advanced Spacecraft Technology Division Report, February 24, 1967.

21. Preliminary Technical Data for Earth Orbiting Space Station. MSC-EA-R-66-1, November, 1966. Volume III.

22. Tradeoff Study of a New Cryogenic Stage for Manned Planetary Exploration. Douglas Aircraft Report DAC-58053, September, 1967.

23. Saturn V Improvement Study-Liquid/Solid System Integration. The Boeing Company, D5-13087, April, 1965.

24. Feasibility of Modifying the S-IVB Stage as an Injection Stage for Manned Planetary Flyby Missions. Douglas Missile and Space Systems Division Report DAC-56524, February, 1967.